

FABRICS FOR IMPROVED DEWATERING

A Dissertation
Presented to
The Academic Faculty

by

Sumner Dudick

In Partial Fulfillment
of the Requirements for the Degree
Doctor of Philosophy in the
School of Chemical and Biomolecular Engineering

Georgia Institute of Technology
December 2022

COPYRIGHT © 2022 BY SUMNER DUDICK

FABRICS FOR IMPROVED DEWATERING

Approved by:

Dr. Victor Breedveld, Advisor
School of Chemical and Biomolecular
Engineering
Georgia Institute of Technology

Dr. Saad Bhamla
School of Chemical and Biomolecular
Engineering
Georgia Institute of Technology

Dr. Dennis W. Hess
School of Chemical and Biomolecular
Engineering
Georgia Institute of Technology

Dr. Youjiang Wang
School of Materials Science and
Engineering
Georgia Institute of Technology

Dr. Chris Luetzgen
School of Chemical and Biomolecular
Engineering
Georgia Institute of Technology

Mr. Daniel Hedou
AstenJohnson

Date Approved: September 02, 2022

non secus ac liquidus Phrygiis Maeandros in arvis
ludit et ambiguo lapsu refluitque fluitque

—Metamorphoses VIII. 162-163

For my friends and family

ACKNOWLEDGEMENTS

For all the help and guidance I've received throughout this thesis project, many thanks to my advisors Dr. Victor Breedveld and Dr. Dennis W. Hess. Your insights and suggestions were essential in ultimately succeeding in this work and in my growth as a scientist. Without your direction and support, this thesis simply would not exist. I would also like to recognize previous members of the Breedveld group for their contributions including: Dr. Maritza Mujica for all her help with SEM, Dr. Jianshan Liao for always asking the right questions, and Dr. Nikhil Raj for his mentorship. From training me on the plasma reactor, to helping me navigate the first years of PhD life, late-night conversations, and many a challenging game of chess, Nikhil has been a core part of my doctoral journey.

There are so many others to acknowledge for their contributions to this thesis that any list would never be fully exhaustive. These include all my committee members, most especially Dr. Luetzgen and the team at AstenJohnson for helping me consider the practical aspects of applying insights from this project to the paper industry. To that point, I must thank previous papermaking professors from NC State, notably Dr. Pawlak, Dr. Jameel, and Dr. Byrd. The expertise I gained in your classes and research projects gave me an immense head start on this project. Special thanks are also due to my undergraduate mentor from NC State, Dr. Saad Khan. It was in your Transport I class that I first discovered a love for fluid mechanics, in your lab that I first explored a career in research, and in our conversations that I first considered pursuing this doctoral degree.

I have also received an enormous amount of direct, material help on this project. Thanks to Matt Addvensky for all his work on the transfer experiments covered in Chapter

3 (and many others that did not find their way into the thesis); mentoring you in your undergraduate research was an immensely enjoyable and rewarding experience. I also recognize Dr. Ashwini Sinha at Linde for donating the pentafluoroethane precursor used so much in my surface treatments, Arvind Ganesan for his help with SEM, Conrad Roos for his assistance with mercury porosimetry, Dr. Galfond for his help in collecting force measurements through LabView, AstenJohnson for providing all felts used in this study, Dr. Rallming Yang for letting me use his handsheet molds, and the Renewable Bioproducts Institute at Georgia Tech for funding this work.

Finally, no acknowledgement would be complete without recognizing the overwhelming personal support I received in my time here at Georgia Tech. Thank you to all my friends in the ChBE department. You made coursework bearable, research collegial, coffee hours enlightening, social events wholesome, camping trips an adventure, racquetball a thrill, and Home Park home. Unending thanks to my dear sister, my beloved parents, and my extended family. Your support has sustained me every step of the way. Thank you for always having my back.

TABLE OF CONTENTS

ACKNOWLEDGEMENTS	v
LIST OF TABLES	x
LIST OF FIGURES	xi
LIST OF SYMBOLS AND ABBREVIATIONS	xviii
SUMMARY	xxi
CHAPTER 1. Introduction	1
1.1 Project Motivation	2
1.2 Papermaking	3
1.3 Flow in a press section	6
1.3.1 Dewatering	6
1.3.2 Rewet	8
1.4 Thesis objective and structure	10
1.5 Technology review	12
1.5.1 Unidirectional flow strategies	12
1.5.2 Previous attempts at flow control felts in paper industry	17
1.6 Physics of wetting and flow in fibrous media	20
1.6.1 Surface wettability	20
1.6.2 Capillary forces in fibrous materials	21
1.6.3 Adhesion	26
1.6.4 Interfacial instability	28
CHAPTER 2. Liquid repellence of phobic fiber networks	31
2.1 Background and scope	31
2.2 Experimental methods	32
2.2.1 Materials	32
2.2.2 Plasma treatment	32
2.2.3 Contact angle	33
2.2.4 Breakthrough cell	33
2.2.5 Imaging	35
2.3 Results and Discussion	35
2.3.1 Track-etched membranes: cylindrical pores with stochastic variation	35
2.3.2 Metal meshes: regular, filamentous pores	38
2.3.3 Forced wetting of hydrophobized paper substrates	41
2.3.4 Application of wetting barriers to press fabrics	47
2.4 Conclusions	52
CHAPTER 3. Adhesive transfer of fluids between fiber networks	53
3.1 Background and scope	53
3.2 Experimental Methods	55

3.2.1	Surface treatment	55
3.2.2	Transfer experiments	57
3.3	Results and discussion	61
3.3.1	Effect of contact angle hysteresis on adhesion of droplets to paper substrates	61
3.3.2	Estimation of forces	67
3.3.3	Dynamic effects	69
3.3.4	Flux boundaries	71
3.4	Conclusions	73
CHAPTER 4. Instability enhanced dewatering		75
4.1	Background and scope	75
4.2	Experimental methods	77
4.3	Results and discussion	81
4.3.1	Effect of spacer parameters on enhanced dewatering	81
4.3.2	Mechanism of enhanced dewatering	84
4.3.3	Effect of spacer wettability	88
4.3.4	Effect of liquid properties	91
4.4	Discussion	94
4.4.1	Interfacial instability	94
4.4.2	Instability hypothesis falsification	99
4.5	Conclusions	100
CHAPTER 5. Rewet suppression through press felt engineering		103
5.1	Background and scope	103
5.2	Experimental methods	105
5.3	Results and discussion	106
5.3.1	Effect of spacer on dewatering of prepared handsheets	106
5.3.2	Effect of mesh size	108
5.3.3	Effect of basis weight	110
5.3.4	Nylon meshes	111
5.3.5	Compatibility of technology with different felts	114
5.4	Economic Impact	114
CHAPTER 6. Conclusions and future work		116
6.1	Contributions to the field	116
6.1.1	Capillary barriers in fibrous materials	116
6.1.2	Adhesion of fluids to fibrous materials	118
6.1.3	Instability-enhanced dewatering	119
6.1.4	Process applicability / feasibility	120
6.2	Future work	120
6.2.1	Geometry of spacer, custom pore profile	121
6.2.2	Dynamic process conditions	121
6.2.3	Multidimensional flow	122
6.2.4	Effect on sheet properties	123
6.2.5	Definition of stiffness	123
6.2.6	Introduction of air to the interface	124

APPENDIX A. Video analysis code	125
REFERENCES	127

LIST OF TABLES

Table 2.1	The breakthrough pressure of water on two hydrophobized papers was measured at different average pressurization rates to show that transport delays and flow resistance do not significantly affect the measurement	34
Table 2.2	Predicted wetting resistance of various liquids for the Q5 filter paper, compared to experimental values. The critical entry pressure for water serves as the basis for calculating predicted entry pressures via the cylindrical pore model. Predictions for the reentrant model were made using Equation 1.6, utilizing the structural parameters for Q5 filter found in earlier analysis.	47
Table 4.1	Static contact angle of water on each mesh and physical dimensions. 70+ and 70- refer to #70 meshes that were hydrophobized and hydrophilized, respectively.	79

LIST OF FIGURES

Figure 1.1	Distribution of energy usage in a paper mill. About half of energy used in papermaking allocated to drying [25], even though drying does less than 1% of water removal.	3
Figure 1.2	Simplified process schematic of a paper machine showing flows of water (blue) and energy use (red). All streams are reported on a one ton of dry fiber basis. Although the drying section accomplishes less than 1% of water removal, it consumes about half the energy of the entire papermaking process, when up and downstream processes are included.	4
Figure 1.3	Schematic of a press nip in a paper machine, with rewet illustrated at nip exit	10
Figure 1.4	3-D wetting gradients used to control flow of fluid in paper-based microfluidic circuit. Reproduced from Raj [58]	14
Figure 1.5	Adhesion used to control transport of water between two paper substrates. Reproduced from Balu [63]	14
Figure 1.6	Passive check valve which poses low resistance to flow in the biased direction (a, c) but retards reverse flow (b, d). Reproduced from Nguyen [67]	16
Figure 1.7	Schematic illustrating critical wetting pressure in fibrous media. At low pressures, capillary forces exclude the fluid. Higher applied pressures overcome this barrier, resulting in wetting.	23
Figure 1.8	Liquid bridge adhering to two surfaces. The adhesive forces and the physical parameters contributing to them are illustrated.	28
Figure 1.9	Deformations to the interface cause surface tension to create pressures that lead to self-correcting flow. Perturbations decrease with time, causing the interface to remain stable.	29
Figure 1.10	Schematic showing onset and growth of the Plateau-Rayleigh instability. Constriction of the column creates high pressure in the concavity of the disturbance, pushing fluid out and increasing the concavity. This process accelerates until droplet pinch-off. Figure reproduced from Rapp [108]	30
Figure 2.1	(a) Bcell: the apparatus used to directly measure the critical breakthrough pressure of hydrophobized porous media. A syringe pump increases the pressure above the probe liquid over	35

time. When critical pressure is reached, the wetting is observed in synchronized video. (b) Brightness sharply decreases when liquid penetrated to the bottom surface.

- Figure 2.2 SEM of track-etched membranes of nominal sizes 2 μm (a), 5 μm (b), and 12 μm (c). Note the nearly cylindrical pores which permeate the medium. The presence of multi-core pores (see red highlight in (a)) results in an effective pore size greater than the nominal pore size. 36
- Figure 2.3 (a) Critical breakthrough pressure of liquids through track-etched membranes with different pore sizes. Water (W), 35 wt.% water in ethylene glycol (W/EG), and ethylene glycol (EG) were used. (b) Deviation of effective pore size from nominal. Error shows spread in effective pore size across the three probe liquids tested, pooled standard deviation over 15 individual replicates per membrane. 37
- Figure 2.4 Optical microscope images of metal meshes, sized 37 μm (a) and 11 μm (b). Note the regular, well-defined structure and curved pore walls 38
- Figure 2.5 1:1 plot comparing the experimentally measured apparent contact angle on meshes (x -axis) to the apparent contact angle predicted by the Cassie-Baxter equation (y -axis). The line represents the relation $y = x$. Squares represent points for the 11 μm mesh, circles for 37 μm mesh. Colors represent droplets of different liquids: black (ethylene glycol), blue (diiodomethane), green (35 wt.% ethylene glycol in water), and purple (water). Experimental error lies within the data points. 40
- Figure 2.6 (a) Critical breakthrough pressure of various liquids through phobized metal meshes. (b) Effective cylindrical pore sizes of meshes for each liquid. Differences between liquids highlight a failure of the cylindrical pore model. 40
- Figure 2.7 1:1 plot of critical pressure predicted by reentrant model vs. those observed by direct measurements. Purple corresponds to water, green to W/EG mixture, and black to EG. Squares, circles and triangles correspond to 11 μm , 37 μm , and 74 μm meshes, respectively. The line represents the line $y = x$. Errors fall within the data points. 41
- Figure 2.8 SEM images of paper samples: chromatography paper (left), Q5 filter paper (center), Q2 filter paper (right) 42
- Figure 2.9 Apparent contact angle measurements on the paper surface agree with the assumption that liquid-solid interaction on a PFE coated 43

fiber is similar to the liquid-solid interaction on a flat, PFE coated silicon wafer. Shapes correspond to chromatography paper (circle), Q5 filter paper (square), and Q2 filter (triangle). Colors correspond to water (purple), 35 wt.% ethylene glycol in water (green), and ethylene glycol (black). The slope is not statistically different from 1 ($m = 1.08 \pm 0.11$) and the correlation is strong ($R^2 = 0.98$). Errors fall within the data points.

- Figure 2.10 (a) Cylindrical pore analysis and (b) reentrant pore analysis for three different paper substrates and three test fluids (water, water/ethylene glycol mixture, ethylene glycol). The underlying material structure cannot depend on entrant liquid, as is suggested by (a), highlighting the insufficiency of the cylindrical pore model; reentrant pore analysis, (b), shows consistent fiber spacing values for all liquids, with the dashed lines denoting the average pore size. (c) Fiber width distribution obtained from SEM image analysis. (d) Mercury porosimetry data for paper samples. Differential intrusion measurements show a greater average pore size for chromatography paper vs. the filter papers. The singular effective pore size for wetting resistance, found from direct breakthrough pressure measurement and analysis via the reentrant pore model (see (b)), lies in the upper tail of the distribution for each sample. 45
- Figure 2.11 (a) Optical micrograph of nylon non-woven fabric. (b) Effective pore size for phobized nylon non-woven, comparing two analytical models, the cylindrical pore model (Equation 1.5) and the reentrant pore model (Equation 1.6), for three test fluids (water, water/ethylene glycol mixture, ethylene glycol). 48
- Figure 2.12 The effectiveness of using wetting gradients to prevent rewet is assessed. Chromatography paper initially at $MR = 2$ was pressed at 10 MPa for these experiments. The unmodified press felt resulted in the worst dewatering as the sheet pressed with it had the highest moisture content after pressing. Blotters were used to simulate a press felt that completely prevents rewet. The hydrophobic barrier prevented some, but not all, rewet. 50
- Figure 3.1 The contact angle hysteresis (difference between advancing and receding contact angles) on a paper substrate can be controlled by oxygen etching prior to fluorocarbon deposition. High-adhesion paper (HAP) and Low-adhesion paper (LAP) have the same level of hydrophobicity (static contact angle) but very different interactions with liquids. 56
- Figure 3.2 Transfer cell (TCell) used to conduct transfer experiments. The linear actuator pushes on a control arm that moves the upper 58

surface down or up. The advantage of the control arm is that it trades down the length of the actuator's stroke for accuracy in the upper surface's displacement. The lower surface is fixed in place. A camera enables estimations of volume transferred. The figure inset highlights how the upper and lower surfaces are used to transfer droplets.

- Figure 3.3 (a) Geometry of a spherical cap and the equation of its volume. Note, this equation is valid even when $h > a$. (b) Droplet in its initial state resting on the surface of the paper. The two measurements needed to estimate its volume are shown. (c) The quantity of the droplet which has been transferred to the opposite surface is estimated using the same equation. Equation and geometric model referenced from Wolfram MathWorld [128] 58
- Figure 3.4 Frames taken from a transfer experiment. The droplet is squeezed between two surfaces that are subsequently pulled apart. This allows liquid to be transferred from its initial surface to another surface. 59
- Figure 3.5 Errors in conservation of volume across trials conducted for the experiments in Figure 3.6. Volume subscripts refer to the drops depicted in Figure 3.3. The majority of errors fall within $\pm 5\%$, and there is no trend in the errors. Thus, the optical method used to estimate volumes in the experiments is justified. 60
- Figure 3.6 The transfer behavior of water droplets from papers of high (HAP) vs. low (LAP) adhesion to surfaces that are hydrophilic (SiO_x) or hydrophobic (PFE – fluorocarbon film). $\text{TR} = 1$ shows that papers with low contact angle hysteresis transfer all their liquid to another surface. The outcomes for transfer from high-hysteresis papers are much more varied. Depending on how much the droplet is compressed prior to separation, different transfer behavior is observed. 63
- Figure 3.7 Profiles of contact angle and contact area of water droplets during compression and separation between high-hysteresis paper and a silicon oxide wafer. Arrows indicate the direction of compression or separation. Inflections around $H/H_{\text{drop}} = 0.4$ explain the transition in the open triangle series of Figure 3.6. 65
- Figure 3.8 Surface forces estimated from measurements made in Figure 3.4 and Equation 1.7. The good agreement in the force balance suggests that my methods are accurate and that Equation 1.7 is a good description of adhesive forces on fibrous substrates. 67

Figure 3.9	Dynamic transfer can be used to transfer liquids against the wetting gradient. By separating the surfaces quickly, 30% of a droplet initially on a silicon oxide surface can be transferred to a fluorocarbon deposited surface.	70
Figure 3.10	Flux into the boundary must be considered when the substrates area porous. (a) The rate of flux can be controlled by partially hydrophobizing the absorbent material. (b) Transport will tend to move liquid from the no-flux boundary to the flux boundary. (c, d) The effect of dynamics is visible for experiments involving flux into the boundary.	72
Figure 4.1	Screw press (foreground) used to exert a one-dimensional pressure gradient in dewatering experiments. A force sensor (readout in background) allows precise control of the applied stress.	80
Figure 4.2	(a) Effect of mesh number on final moisture ratio of chromatography papers pressed against a commercially available press felt. Various spacers were layered between the paper and the felt, as specified in the legend. No mesh series refers to a scenario where the paper is pressed directly against the press felt. To capture the limits of dewatering, with no reflux, a stack of blotters (Blotters series) was used. (b) The data points at the highest pressure tested in (a) are compared. Structural parameters of the meshes have a strong impact on enhanced dewatering, and the 70 mesh was the optimum of materials tested.	81
Figure 4.3	Frames from videos of paper being compressed. Fluorescent dye was added to the water to make the liquid phase more apparent. Higher brightness corresponds to more moisture. The breakup of liquid bridges is responsible for preventing reflux to the sheet.	84
Figure 4.4	Frames from the videos are analyzed. (a) The brightness distribution in the felt-web system is averaged row-wise to create a vector of the moisture content in the direction of flow (blue curve). The peak is fit to a Gaussian distribution, whose area corresponds roughly to the water content of the sheet (orange curve). (b) The area under the orange curve is normalized against the total brightness in the image and plotted against synchronized pressure data	87
Figure 4.5	Effect of mesh wetting properties on enhanced dewatering. Altering the wetting properties of the spacer changes pressed moisture of the sheet by about 10%, on average. Compare this to the effect of the spacer's presence. Removing the spacer increases the sheet's water moisture by 120%. At the highest	88

applied pressure, the hydrophobized mesh falls almost on top of the blotters, nearly eliminating reflux

- Figure 4.6 Effect of liquid surface tension on dewatering. Decreasing the surface tension of the liquid tends to improve dewatering with commercial fabrics and worsen the performance of the spacer. Even at extreme cases of surface tension for aqueous solutions (40 mN/m), the spacer-modified fabric still shows better dewatering than the conventional press fabric. 91
- Figure 4.7 Effect of temperature (viscosity) on paper pressed at 10^7 Pa with a number 70 mesh in between the web and felt. The trend in temperature suggests that better dewatering is attained at higher temperatures, although the effect is so minor as to be statistically insignificant. 93
- Figure 4.8 Dewatering with an included spacer that intentionally fails to meet the requirements dictated by the Plateau-Rayleigh criterion. In this case, dewatering is similar to the control, in which no spacer is used. 99
- Figure 5.1 Screw press used for dewatering trials. From bottom to top are seen: the bottom platen, paper, press felt, top platen, force sensor, and screw press. 106
- Figure 5.2 Pressed solids of 120 gsm SBSK handsheet vs. applied pressure for various pressing conditions: (blue squares) commercial tissue felt, (black circles) stack of dry blotters that represents limit of maximum drying and (red diamonds) tissue felt with metal #70 mesh. 107
- Figure 5.3 Still images from videos taken during the pressing of wet chromatography paper (initial solids 25%) up to maximum pressure of ~5 MPa with: (top) commercial felt, and (bottom) commercial felt + #30 mesh (wire thickness 165 μm ; openings 681 μm). Sideview image with fluorescently labeled water; greater brightness indicates larger amounts of water present. 108
- Figure 5.4 Effect of mesh size on press solids. The dimensions of the spacer layer have a significant impact on dewatering. A mid-size mesh balances tradeoffs between gap thickness, pressure distribution, and sheet contact. 109
- Figure 5.5 Sweet plot shows the effect of basis weight on dewatering. The intercept on each line indicated the minimum moisture content of the sheet during pressing. The slope of the line measures rewet. 111

The lines have the same intercept but different slopes, indicating that the spacer reduces rewet.

- Figure 5.6 Enhanced dewatering observed with nylon meshes. The medium size mesh (#61) performs best of the ones tested, for reasons previously discussed. Two of the mesh series, #30 and #168 fall on top of one another. 113
- Figure 5.7 Enhanced dewatering observed with new and used tissue felts 113

LIST OF SYMBOLS AND ABBREVIATIONS

Symbols

a	Radius of droplet's contact line on surface
Bo	Bond number
Ca	Capillary number
d	Fiber spacing
d_{eff}	Effective pore size
$d_{nominal}$	Nominal pore size
d_p	Pore size
F	Adhesive force
h	Height of droplet on surface
H	Vertical distance between surfaces
H_{min}	Minimum vertical distance between surfaces
\hat{K}	Nondimensional curvature
L	Length scale
m_{fiber}	Mass of fiber in the sheet
m_{water}	Mass of water in the sheet
n	Vector normal to liquid-air interface

P	Pressure
$P_{critical}$	Critical wetting pressure
r_p	Pore radius
t	Time
t_I	Inertial breakup timescale
t_V	Viscous breakup timescale
v	Velocity
\hat{v}	Nondimensional velocity
V	Droplet volume
We	Weber number
∇P	Pressure gradient
ΔP	Difference in pressure across interface
θ	Contact angle
θ_a	Advancing contact angle
θ_r	Receding contact angle
κ	Permeability
μ	Viscosity
σ	Surface tension

Abbreviations

ACA	Advancing contact angle
CA	Contact angle
CAH	Contact angle hysteresis
EG	Ethylene glycol
MR	Moisture ratio
PFE	Pentafluoroethane
RCA	Receding contact angle
RF	Radio frequency
SBSK	Southern bleached softwood Kraft
SCA	Static contact angle
SDS	Sodium dodecyl sulfate
SEM	Scanning electron microscope
TR	Transfer ratio
W	Water
W/EG	Water and ethylene glycol solution

SUMMARY

In 2021, the world consumed over 620 EJ of energy. Approximately 2.6 EJ, or about 0.4% of that total energy demand, was just used to dry paper during its manufacture. In a climate of growing energy costs and increasingly limited energy supplies, finding ways of improving the efficiency of this process are desperately needed. Even in state-of-the-art paper mills, the energy used to dry paper is well over twice as much as is theoretically needed. Clearly, there is a massive opportunity to make a major impact on global energy consumption.

This thesis develops a technology that reduces the need for energy-intensive drying. By creating a fabric with enhanced dewatering capability, more water can be squeezed from the paper sheet mechanically. Thus, there is about 40-50% reduction in the amount of water that has to be evaporated in the dryer section, cutting the energy requirements of drying paper in half. Arriving at the mechanism ultimately capable of achieving this followed a meandering path that wound through the fields of flow in porous media, surface chemistry and wettability, partitioning of liquid droplets, and the physics of interfacial instability.

The primary problem plaguing papermakers is that, after water is squeezed out of the paper sheet, the sheet resorbs water from the fabric that carried it through the press. Essentially, when pressure is released, the paper sucks water back out of the sink (the fabric) that was provided to remove it. No technology has yet been developed that can entirely avoid this rewetting tendency. Therefore, a fabric with one-way flow properties has been highly sought after in the industry for decades. Creating a fabric that lets water

in, but doesn't let it out, would drastically reduce the amount of water that has to be dried from the sheet later.

The first attempt I made at achieving this goal was to use capillary forces to trap water in the fabric. By creating a wetting gradient in the fabric, it is theoretically possible to allow water into the structure at high pressures, but prevent it from leaving at low pressures (i.e. during decompression). To accomplish this, the physics of forced wetting in fibrous materials (e.g. non-woven fabrics, paper) was studied in detail in the second chapter. I found that simplistic, but widely used, models for these wetting barriers in fibrous media were inaccurate and therefore inappropriate for informing design choices. One outcome of this study was that I developed a method for accurately predicting the wetting resistance of hydrophobic fiber networks. This helped me discover that it was not practical to use capillary forces alone to control flow in the press fabric. However, the approach I developed is useful in other applications where barrier properties of papers and fabrics are essential.

The second attempt to improve dewatering revolved around controlling the adhesion, or “stickiness” of the water to the press fabric. By making water more strongly adhere to the fabric, I reasoned, less water will go with the paper sheet when it is pulled away from the wet fabric. In this section, I indeed showed how altering adhesion can be used to control the transfer of water from two separating surfaces. I also illustrated the limits on using this approach, concluding that it is not a viable way of completely controlling flow in the press section.

The third and, thankfully, successful attempt at creating a fabric with improved dewatering ability required a radical change of perspective on the problem of rewet. This involved inducing an interfacial instability in the liquid lying between the paper sheet and the press fabric. The details of encouraging this instability and its effect on dewatering are explored in depth in the fourth chapter. Essentially, rupturing the liquid bridging the fabric and paper destroys all paths for flow. If this process is carefully implemented, full dewatering of the paper under pressure occurs, without any water returning to the sheet upon decompression.

With a successful and completely original method of controlling flow, I needed to determine the feasibility of implementing this technology in an industrial application. These preliminary studies occupy the focus of the fifth chapter. I find that the challenges associated with applying the insights of this thesis can largely be overcome with physically-informed design choices. However, there is a great deal of exciting work to be done in this area in the future.

In summary, this thesis investigates many aspects of wetting and flow in fibrous materials: a prospect enticing enough to command the attention of any reader. Amidst its twists and turns, a few paths are uncovered that lead nowhere, many more paths that lead to exciting applications for adjacent problems and fields, and one final path that leads to attaining this project's ultimate aim: fabrics for improved dewatering.

CHAPTER 1. INTRODUCTION

Understanding and controlling fluid flow in porous media is essential to many aspects of modern, industrialized life. Medical testing [1-3], bodily physiology [4-6], oil recovery [7-9], water management [10-12], industrial chemical production [13], function and comfort of apparel [14, 15], environmental impact mitigation [16-18], and numerous consumer products [19-21] all rely on manipulating the flow of fluids within and between porous materials to a desired end. For example, the healthy function of bodily tissue relies on blood flow through microscopic capillaries to deliver oxygen and nutrients, while carrying away waste. Exploring the physics of this process has enabled physicians to develop interventions that have saved countless lives.

Notably, flow in porous media is as complex as it is ubiquitous. In each of the scenarios alluded to, there are at least two, and often three, phases of matter interacting with each other simultaneously. A solid medium populated with holes (pores) serves as the matrix in which flow occurs. A liquid contacts the solid surface of these pores, flowing through their available voids. Often, the voids themselves are filled with air, resulting in a three-phase system. The interplay amongst solid, liquid, and gas is further complicated by the numerous forces acting on the system at once. These include: inertia, viscosity, gravity, surface tension, and applied mechanical stresses, to name just the most common. In more exotic applications, magnetic and electric fields, osmotic forces, buoyancy / temperature gradients, and viscoelasticity can also come into play. As is the nature of flow, such forces are rarely balanced in stasis. Rather, these multiphase systems, subject to all the forces acting on them, tend to exist in a state of dynamic flux.

Because of this complexity, challenging problems in the area of flow in porous media remain to be solved. Furthermore, the prevalence of such systems in large-scale industrial manufacture—as well as daily life—means that significant innovations have enormous potential. This thesis primarily focuses on solving one of the greatest current challenges in paper manufacturing. However, by focusing on fundamentals of the issue, insights developed here can hopefully be applied wherever manipulating the flow of fluids in, on, or between fibrous materials is desired.

1.1 Project Motivation

Every year, over 400 million tons of paper products are manufactured throughout the world [22]. To accomplish this, more than 8.9 EJ of energy are consumed, making pulp and paper the 4th largest industrial sector in terms of energy use [23, 24]. Economic and environmental concerns weigh heavily on paper manufacturers, and there is a constant push to develop more energy efficient processes. The increasing cost of energy, combined with a largely consumer-driven demand for greener materials, provides an enormous incentive for innovation in this field. As willing as manufacturers might be to realize the lofty aims of greener process design, the established nature of the industry can make implementing new approaches and concepts difficult. First, the age of the practice itself, which dates from the 2nd century in China, means that many potential ideas have already been tried, so creating technologies that have never been imagined is quite challenging. Second, the significant capital infrastructure of pulp and paper mills largely prohibits new designs that would greatly alter existing equipment configurations. With these challenges in mind, this body of work identifies the single aspect of papermaking that is currently in greatest need of effective solutions: drying.

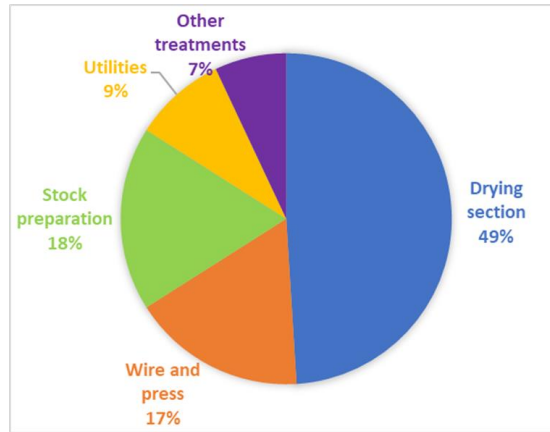


Figure 1.1 Distribution of energy usage in a paper mill. About half of energy used in papermaking allocated to drying [25], even though drying does less than 1% of water removal.

Given the scale of paper production, about 0.4% of all energy consumed in the world every year is dedicated solely to drying paper during its manufacturing. Allocating energy usage in a paper mill, about 50% is consumed in evaporative drying of the sheet, dwarfing any other single unit operation (Figure 1.1) [25]. This fact is even more astounding when one considers that drying does less than 1% of total water removal, compared to all prior steps (Figure 1.2). Thus, a technology that reduces the energy required to dry paper would have a measureable impact on global energy usage. To give some context for the approach that was taken in this project, the art of papermaking will briefly be reviewed.

1.2 Papermaking

Paper is made by suspending cellulose fibers in water at a ratio of about 200 parts water to fiber (0.5 wt.% solids) and then removing that water to create a consolidated web, also called the sheet, that contains 90-95 wt.% solids at the end of the process. Three serial sections of the paper machine are used to achieve this: forming, pressing, and drying (Figure 1.2) [26].

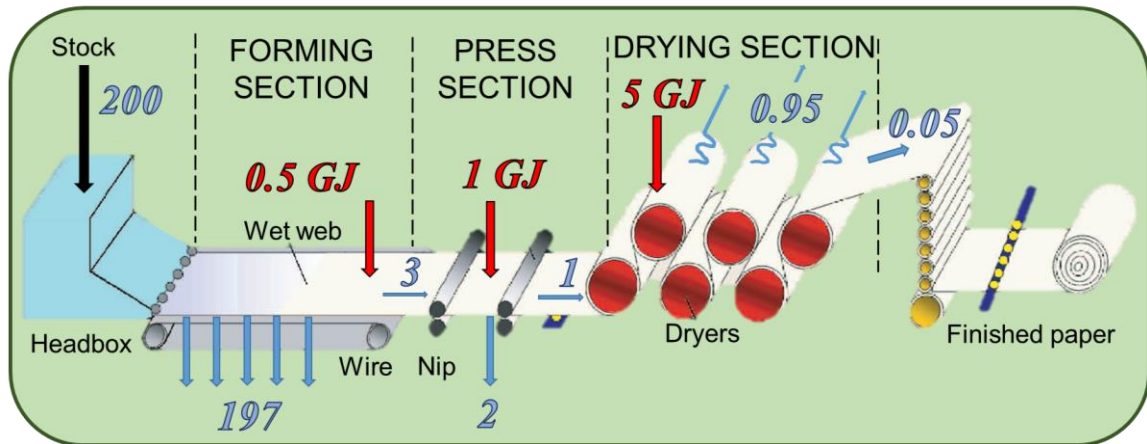


Figure 1.2 Simplified process schematic of a paper machine showing flows of water (blue) and energy use (red). All streams are reported on a one ton of dry fiber basis. Although the drying section accomplishes less than 1% of water removal, it consumes about half the energy of the entire papermaking process, when up and downstream processes are included.

First, the vast majority of water is removed by gravity-driven drainage in the forming section. During this stage, the dilute fiber suspension (stock) is pumped from a pressurized dispenser (the headbox) onto a forming fabric. The forming fabric is a woven cloth that serves as a filter—collecting the fibers into a mat while allowing water to pass through. The reason so much water has to be used in forming the sheet is that a dilute suspension prevents fiber aggregation, resulting in paper that is smoother and stronger. Although gravity is the primary force accomplishing water removal in the forming section, shear forces induced by hydrofoils and vacuums are used at the end of the forming section to further reduce the water content. At the end of forming, the paper sheet has taken shape, and its relative water content has reduced from a 200:1 slurry to a 3:1 pulpy mat.

Second, the press section applies mechanical work to squeeze more water from the paper web. This process may also be referred to as mechanical dewatering or wet pressing. In pressing, the paper sheet is supported by a fabric, known as the press felt, that carries

the damp sheet when it is too soft to be pulled by the machine, that provides a sink for the water during pressing, and that imparts a desired surface finish to the sheet [27, 28]. The press felt and paper web are fed into a tight gap (nip), where force applied on the press roll expels water from the sheet, much like dewatering a shirt with an old-fashioned clothes wringer. Nip configuration has a major impact on press section efficiency, with styles varying from the more conventional rolling nip (created by the gap between two rolling cylinders) to the current state of the art—extended nip presses. The nip is extended by complementing the cylindrical press roll with a concave shoe; this provides a crucial innovation in dewatering by increasing the dwell time over which pressure is applied [29]. Within an extended nip press, the ratio of water in the sheet can decrease to about 0.6:1 or even 0.5:1 for some pulp furnishes [30]. However, the relative water content of the sheet after leaving the press nip increases to about 1:1. This is because the sheet exiting the press typically reabsorbs water from the press fabric (rewet) [31]. This reabsorbed water must then be removed in the subsequent section—drying.

Finally, the sheet is heated to evaporatively dry the residual water remaining after pressing. The paper is contacted with steam-heated drums, which require a large amount of energy to run because of water's high latent heat. After drying, the relative mass of water in the sheet compared to fiber is about 0.05:1. Because drying is about ten times more energy intense compared to pressing [32], papermakers have long looked for ways to improve mechanical dewatering in the press section by eliminating rewet. Based on the rough numbers discussed earlier, improving the press section in such a way as to prevent rewet could reduce the energy demand of drying by about 40-50%. Working to mitigate or

even eliminate rewet, however, requires an understanding of the phenomena that cause this undesired reflux of water.

1.3 Flow in a press section

1.3.1 Dewatering

When the wet paper web enters the press nip, force applied by the press roll drives water out of the paper into the felt. By creating a region of high pressure in the paper, and low pressure in the felt, water is encouraged to flow from the former to the latter [33, 34]. The basic relationship between this driving force—the pressure gradient—and the rate of flow through a porous medium was first described by Darcy in his efforts to design a municipal water system [35]. Named in his honor, Darcy’s law applies to a wide range of applications including flow of fluids through soil, capillaries, membranes, fabrics, and paper:

$$v = -\frac{\kappa}{\mu}\nabla P \quad (1.1)$$

where v is the fluid velocity, κ the permeability, μ the fluid viscosity, and ∇P the pressure gradient. The permeability is a characteristic property of a porous medium that describes how easy it is for fluids to flow through (i.e. permeate) it. Permeability has units of area [m²], and for any given type of porous medium, permeability is proportional to the cross-sectional area of an individual pore. Thus, porous materials with very small holes present a large resistance to flow while media with larger pores are much more permeable, in general. The rate of dewatering in a press section, determined by the rate of flow (v), is

thus expected to depend strongly on the resistance to flow presented by the permeability of the paper and/or the press felt.

However, because the press felt has significantly larger pores than the paper sheet, fabrics used in dewatering do not pose significant hindrance to flow in the press section [36, 37]. The question of the wet paper's permeability, on the other hand, is both highly relevant and incredibly complex. The smaller pores in the paper mean that the majority of resistance to dewatering is posed by the paper itself [37, 38]. However, describing the permeability of the paper by a single number would be deceptive. The structure of the wet web consolidates during pressing, decreasing its permeability [39]. This diminishing permeability chiefly establishes the time-dependence of dewatering in the press section. If the (changing) permeability of the paper sheet is given, two techniques remain to accelerate dewatering in the press, according to Equation 1.1. The viscosity can be decreased (for example, by raising the temperature), or the pressure gradient increased (by applying more force).

Changing the applied force affects more than just the rate of dewatering; it changes the equilibrium moisture content of the pressed paper [40]. At any given applied pressure, water will flow from the sheet until a limit is reached and flow stops. At low pressures, this limit is determined by the extent to which the pore volume is collapsed, excluding free water. At high pressures, this limit is determined by the chemical thermodynamics of water-cellulose interactions on a molecular level (removing bound water). In industrial press sections, which operate at high pressures, water bound to the cellulose exerts an osmotic pressure that eventually opposes the pressure applied by the press roll. The balance

between these forces sets the equilibrium moisture as a theoretical limit of the maximum extent of dewatering [41].

Through the pressing process, the extent of dewatering is limited either by the rate-of-flow time-dependence resulting from Equation 1.1 or by the theoretical limit discussed in the previous paragraph. In the former case, pressing is said to be flow limited, whereas it is said to be pressure limited in the latter case [42]. Pressure limited dewatering is most common for lightweight grades of paper. Flow limited pressing is more common for heavy, thicker grades of paper, where a longer flow path must be traversed for complete dewatering. The implementation of extended nip presses, alluded to earlier, increase the time over which pressure is applied and dewatering can occur. This pushes many state-of-the-art press sections into the pressure limited regime [43]. Thus, on many machines, the best-possible dewatering (at a given pressure) is already attained. How can we possibly hope to get a drier sheet from the press section?

1.3.2 *Rewet*

Rewet—the main problem limiting papermakers’ ability to further decrease the moisture content of the sheet after pressing—has been a known problem since the 1960’s [44]. For over half a century, scientists have realized that the paper web tends to resorb water from the press felt *after* exiting the press section. In that time period, pressing technology advanced a considerable degree. Enhanced dewatering was obtained by use of extended nips, heated presses, and better press felt materials/designs. The chief accomplishment of these innovations is that modern press nips can achieve moisture content in the paper remarkably close to the thermodynamic equilibrium while pressure is

applied. That means that the theoretical limit of mechanical water removal has indeed largely already been realized, at least in state-of-the-art applications. However, as soon as the web-felt system undergoes decompression, water reflux from the press fabric to the paper undoes much of the progress made in water removal.

The driving force for this undesired transport is caused by two key properties of paper: its elasticity and hydrophilicity. When pressure is released, the paper web recovers some, but not all, of its original bulk. This expansion opens pores within the fiber matrix, which are highly hydrophilic due to the chemistry of cellulose. Thus, the pores exert strong capillary forces on the water, drawing it back into the paper. This phenomenon—desaturation providing a driving force for undesired reflux—is referred to as flow rewet. Because flow rewet is a time-dependent phenomenon according to the Lucas–Washburn equation (Equation 1.2) [45], papermakers have been able to reduce the extent to which flow rewet occurs by rapidly separating the paper from the felt after pressing.

$$L = \sqrt{\frac{\sigma r_p t \cos \theta}{2 \mu}} \quad (1.2)$$

L is the depth to which liquid penetrates into the medium, r_p the pore radius of the medium, t the exposure time of the porous medium to the liquid, θ the contact angle of liquid of the surface, and μ the liquid's viscosity. Reducing the time of contact thus decreases the extent to which reflux can occur.

In addition to flow rewet, there is another phenomenon which gives rise to undesired transport—separation rewet. Because both the paper and felt are rough surfaces, the interface between them is filled with spaces and voids. Water that collects in these

interstitial cavities between the two surfaces must then attach to one surface or the other when the two are pulled apart. Once again, the strong hydrophilicity of the paper web results in more of this interstitial water getting pulled with the paper, rather than remaining with the felt.

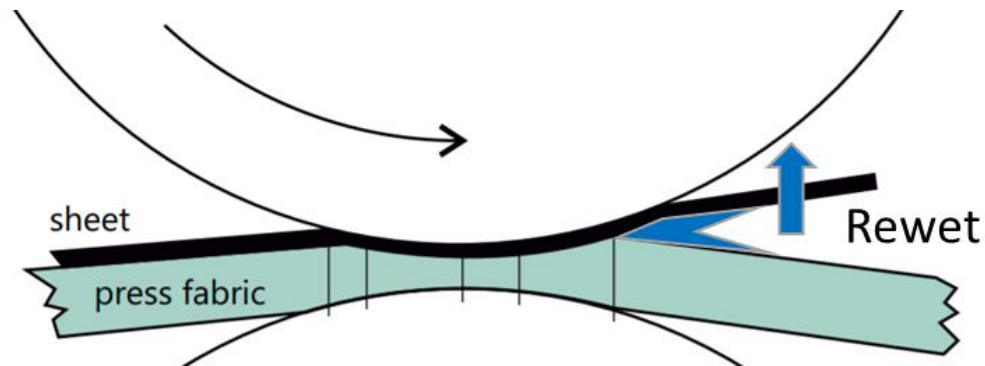


Figure 1.3 Schematic of a press nip in a paper machine, with rewet illustrated at nip exit

1.4 Thesis objective and structure

In this thesis, I aim to prevent rewet by designing a press fabric with unidirectional water transport properties. To accomplish this goal, various aspects of wetting and flow in porous media, particularly in examples of fibrous materials, will be explored.

In this first chapter of the thesis, existing strategies for controlling flow in porous materials and previous attempts at preventing rewet in the press section are reviewed. This discussion highlights some of the key physical concepts that are central to the work that was done in this thesis. Therefore, a modest summary of fundamental fluid physics relevant to each of the chapter's approaches is also included in the introduction.

The second chapter of the thesis focuses on preventing flow rewet by trapping water in the felt with a wetting barrier. This would prevent the paper sheet from resorbing water after the press. Because the effectiveness of this technique is pressure-dependent, precise knowledge of how this pressure dependence relates to the fundamental parameters of the system is essential. Developing a quantitatively predictive method for the strength of this wetting barrier constitutes the major scientific contribution of the chapter, as no one else has yet produced an accurate model—based only on fundamental parameters, without fit factors—for wetting barriers in phobic fiber networks.

The third chapter of the thesis investigates the possibility of reducing separation rewet by controlling the adhesion of a droplet to the fiber network. To accomplish this, liquid is squeezed between two surfaces before the surfaces are pulled apart. By observing what fraction of the liquid adheres to each surface, conclusions are reached about the effectiveness of strategies to control the fate of water when the press felt is pulled away from the paper.

The fourth chapter of the thesis develops a new approach to creating a fabric with one-way flow properties. Destabilization of water bridges lying between the felt and paper results in the breakup of channels necessary for backflow to the sheet during rewet. Appreciating the mechanism of this revolutionary dewatering concept requires an understanding of the physics of interfacial instability. Therefore, the reader should not disregard the subsection of this introduction dedicated to the Plateau-Rayleigh instability—even though its relevance to papermaking may not immediately seem obvious.

Finally, the fifth chapter deals with practical questions about implementing the technology developed in Chapter 4 to an industrial press section. The preliminary investigations of this latest phase of the project dovetail with conclusions about the impact of the thesis overall and directions future work on this project should consider.

1.5 Technology review

1.5.1 Unidirectional flow strategies

Due to the necessity of achieving unidirectional flow in many applications, several strategies have previously been developed [46-49]. These strategies are diverse in terms of the physical phenomena they exploit to attain the desired effect. In general, however, the approaches can broadly be categorized into either chemical or mechanical methods.

Changing the surface chemistry of a solid material alters its molecular interactions with a fluid substance. These molecular forces can either be favorable to liquid-solid contact or unfavorable. In cases where the solid's surface chemistry attracts the liquid, the liquid will tend to spread across the solid, which is referred to as "wetting." In cases where the solid's surface chemistry repels the liquid, the material is said to be "non-wetting." Thus, chemical potentials acting on the molecular level give rise to macroscopic forces that can push and pull fluid in a desired direction [50-52]. As a general term, forces associated with wetting and surface-interactions are referred to as "surface forces."

Surface forces acting on a liquid within the pores of a medium are, as mentioned earlier, capillary forces. One example of using capillary forces to create spontaneous, unidirectional, flow is in Janus membranes [53, 54]. Named after the two-faced Roman

god of beginnings and endings (thus, January ends one year and begins another), Janus membranes are so-called because one face of the membrane is hydrophobic (water repellent), while the obverse face is hydrophilic (water-attracting). This encourages one-way flow of water from the hydrophobic side to the hydrophilic side. Where some spectrum of wettability exists, rather than this simple binary, there is said to be a “wetting gradient.” The feasibility of this technology is attested to by specialty applications of Janus membranes in liquid-liquid separations, flow batteries, and for breaking emulsions [55-57]. A striking example of capillary forces being used to direct the flow of water can be seen in the work of Raj [58, 59]. There, structured wetting gradients within a porous paper sheet enabled manipulation of the flow of biological samples, creating a paper-based microfluidic assay for medical testing inside a porous medium.

Transport can occur not just within a certain material, but also between materials. In cases where two porous solids are brought into contact, then pulled apart, there is an opportunity to transfer fluid. Thus, there is a chance to use chemistry to achieve a desired outcome for transfer. Surface forces acting to hold fluid on the face of a material (or push it off) are called “adhesion.” Adhesion, which, as will be further elaborated upon, relies on more than just wettability, has previously been leveraged to control the transfer of fluid between paper substrates, for example in the work of Balu [60-62].

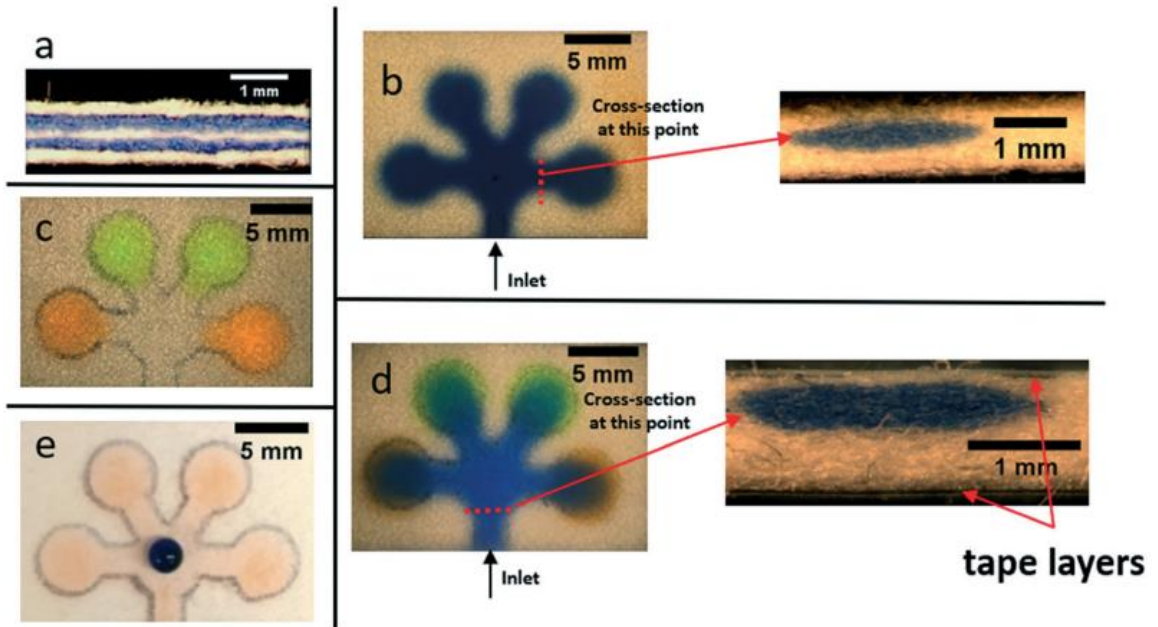


Figure 1.4 3-D wetting gradients used to control flow of fluid in paper-based microfluidic circuit. Reproduced from Raj [58]

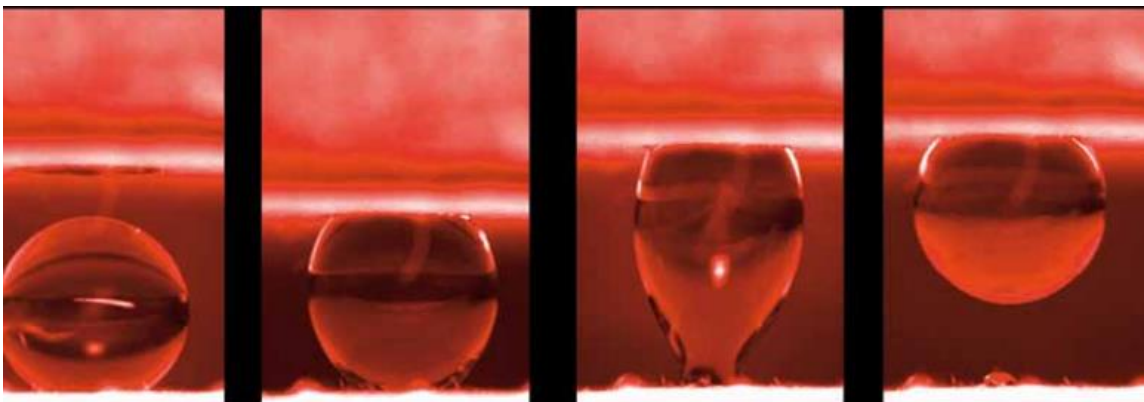


Figure 1.5 Adhesion used to control transport of water between two paper substrates. Reproduced from Balu [63]

Relying on wettability (i.e. chemistry alone) to ensure unidirectional flow comes with certain challenges. Although passive operation is highly advantageous, one major drawback is that surface forces are relatively weak on larger length scales. In order to create materials with significant surface forces, smaller (and thus greater surface-to-volume ratio) features are necessary. Eventually, this requirement can run afoul of practicality, as delicate, micro-structured materials may not withstand the harsh conditions of life. The messy reality of life compromises surface chemistry in other ways, too. To be effective, chemical surface modifications need to maintain their purity. However, when employed in an application, surface treatments can quickly become contaminated, losing their utility. Furthermore, mechanical abrasion and chemical corrosion can destroy or alter the chemistry of the surface, making wettability control ineffective [64].

In addition to chemical methods, mechanical strategies can be employed to achieve unidirectional flow. The most straightforward example on the macroscale is a check valve. While there are several mechanisms commonly used to create check valves, they all work on the same basic concept. Fluid flowing in the allowed direction pushes open a channel which is biased, in the opposition direction, to otherwise remain closed. As long as fluid continues to push in the right direction, the channel remains open, and flow occurs. When flow stops or reverses course, the force needed from the fluid to keep the opening clear disappears, causing the channel to automatically close. The counter-force that automatically closes the valve is usually provided by a spring of some sort.

Check valves can be scaled down to create mechanisms that ensure unidirectional flow in microfluidic applications. Many examples can be found which make use of microfabricated check valves. The main challenge associated with implementing this

strategy in a commercial, large-scale industrial application is that, once-again, materials with fine features are unlikely to withstand the wear and tear of harsh process conditions. Additionally, the time-scale of the mechanical closure response could limit the success of such designs when applied to processes with vanishingly short dwell times.

A final note on mechanical strategies to prevent backflow should mention the fascinating possibility of a passive, mechanical flow-control device that uses no moving parts. First described by Tesla in 1920, the eponymous Tesla valve has been successfully used to regulate microfluidic flows, as well as macroscopic ones. By creating labyrinthine, tortuous paths for flow in one direction—with a relatively straightforward path for flow in the other—a bias in flow resistance is created [65, 66]. Unfortunately, the physical complexity of such structures prohibits their implementation in a press felt application.

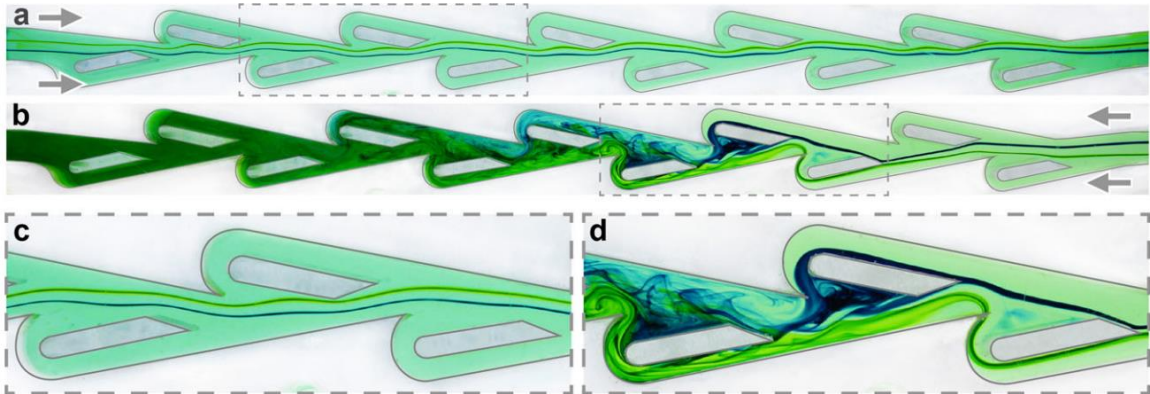


Figure 1.6 Passive check valve which poses low resistance to flow in the biased direction (a, c) but retards reverse flow (b, d). Reproduced from Nguyen [67]

1.5.2 Previous attempts at flow control felts in paper industry

Various embodiments of the basic flow-control strategies mentioned have already been attempted by the paper industry. The immense gains that could come from eliminating rewet have established press fabrics with one-way flow properties as a sort of Holy Grail amongst papermakers—long and arduously sought, but as yet, to little avail. This thesis embarks anew upon that quest. Prudence, however, demands that we carefully consider the skulls—formerly filled with fanciful notions—strewn along this difficult path. Victims to the rapacious, merciless maw of feasibility, their fate serves as admonition and guidance.

Creating a hydrophobic barrier within the press felt was one of the earliest strategies adopted to solve the issue [68]. Conceptually, this approach would work by leveraging capillary forces to retain water in the felt after decompression. The data available on Johnson and Shultz's previous work in this area is limited, but the idea itself is a sound one. Essentially, the hydrophobic barrier strategy parallels the work alluded to from other applications where contrasts in wetting generate the surface forces necessary to direct flow in the desired direction. Questions unaddressed by prior studies in this area include: How strong would a wetting barrier need to be to prevent flow rewet? What are the design parameters that affect the strength of a wetting barrier? And, what values would they need to have an effect? These questions are considered in great detail in the second chapter of this thesis.

Another attempt at using capillary forces to retain water in the felt was to make the felt as hydrophilic as possible. In one example, this was accomplished by Despault and Patterson via including regenerated cellulose filaments in the structure of the press felt [69,

70]. Basically, this makes the felt more closely resemble the structure and chemistry of the paper, reducing the preference water would otherwise have for the paper sheet over the felt. The limitations of this approach were that these finer filament structures were more subject to wear and that the felts themselves became more difficult to clean and dewater. To date, making the felt structure more closely resemble that of the paper has demonstrated the greatest improvement in reducing rewet, even if regenerated cellulose filaments are not used for the purpose. By creating smoother felt surfaces with finer filaments, felt manufacturers have shown modest reduction in rewet [71]. Because these developments have already run to their pragmatic limits, we aim to expand the scope of technologies available to these manufacturers. That is, we focus on evaluating less well-explored strategies that will hopefully synergize with their ongoing efforts.

A third approach to reducing rewet was to include fibers with non-circular cross-sections in the press fabric [68, 72]. Although it is difficult to find any published evidence of exactly how or to what extent this works, the idea likely hinges on improving the water's adhesion to the felt surface by pinning the liquid contact line at the filaments' sharp corners. In general, improving adhesion of water to the surface of the felt is a promising approach since most of the water refluxing from the felt to the paper comes from near the felt's surface. Questions that remain to be addressed regarding this strategy include: How effective is pinning the contact line at improving adhesion? Are the resulting adhesive forces enough to prevent rewet? How do dynamic effects alter the efficacy of this approach? Investigation into the possibility of controlling adhesion is covered in the third chapter of the thesis.

A fourth strategy to mitigate rewet was to include a low-permeability flow-control layer within the felt [73, 74]. By decreasing permeability, resistance to flow is increased. This is effective at preventing significant reflux from the fabric over the short time scales of decompression. Unfortunately, the flow control layer is also effective at reducing flow into the felt from the paper during pressing in the first place. Because the ultimate goal of pressing is to remove as much water from the paper as possible, this strategy has not proved viable.

A fifth approach stands out because, unlike the previous four strategies mentioned, it relies on a mechanical—rather than chemical—effect to achieve one way flow. Hansen aimed to design a press fabric with mini check valve-like structures in it that open during compression, allowing dewatering from paper to felt [75]. Upon expansion exiting the nip, these channels would restrict again, preventing flow. Although it was a highly creative solution to the problem, this approach was hampered by the (relatively) slow time response of channel closure, along with the tendency of these converging structures to clog.

This thesis aims not only to resolve many of the questions posed by prior works, but also to develop a new—and highly promising—mechanism for unidirectional flow fabrics: one that relies on interfacial instabilities. To set the stage for these investigations, a review of the physics of wetting and flow in porous media is necessary.

1.6 Physics of wetting and flow in fibrous media

1.6.1 Surface wettability

The interaction between a liquid and a solid can be characterized in terms of the liquid-solid contact angle (CA). The boundary where this liquid, solid, and surrounding air meet is referred to as the three-phase contact line. Along this contact line, all three phases coexist in a state of thermodynamic equilibrium. The molecular interactions of the species in each phase acting in equilibrium give rise to a macroscopically observed angle at which the liquid contacts the solid [76, 77]. This concept, first described by Young, has found numerous applications in characterizing the chemistry of surfaces ever since its discovery almost a century and a half ago.

The simplest way that the contact angle characterizes a liquid's chemical interaction with a solid is through identifying its philicity/phobicity. In the case of water, a surface is said to be hydrophilic if water spreading on it exhibits a contact angle of less than 90° . This will happen if water has a chemical affinity for the solid surface. If water does not have a chemical affinity for the solid surface, then it will not wet it, and the observed contact angle will be greater than 90° . In that case, the surface is hydrophobic (i.e. water-repellant). Extreme examples of wettability, where the contact angle approaches 0° or climbs over 150° may be referred to as superhydrophilic and superhydrophobic, respectively [78, 79].

The static contact angle (SCA), just described, does not, however, give the full picture of a liquid's interaction with the solid substrate. Non-equilibrium, or dynamic, contact angles are also possible. Departures from the static contact angle described by Young represent divergences from the equilibrium of chemical forces acting in balance.

This usually happens when some activation step inhibits the contact line from moving. A chemical contrast, sharp topography, or some other surface heterogeneity provides a place for the contact line to stick. This allows the liquid contact line to adopt a greater angle than that of equilibrium as it advances along the surface [80]. The maximum contact angle a liquid can sustain on a solid surface is therefore called the advancing contact angle (ACA). As the liquid recedes along this surface, the same heterogeneities prevent the contact line from retreating. The minimum angle a liquid can sustain on a surface is referred to as the receding contact angle (RCA).

The difference between the advancing and receding contact angles is the contact angle hysteresis (CAH). A small contact angle hysteresis characterizes a surface that behaves most like the ideal model of wettability suggested by the static contact angle. A large contact angle hysteresis corresponds to a surface where the contact line experiences great difficulty moving in either direction. Such surfaces tend, therefore, to be sticky to liquids.

When the liquid wets the inside of a solid pore, the contact angle the liquid makes with the solid surface is a crucial parameter in determining the capillary force acting on the liquid. Outlining the other parameters that contribute to this force, especially upon liquids in fibrous media, occupies the next section of the introduction.

1.6.2 Capillary forces in fibrous materials

Although my ultimate interest is in wetting barriers for a press felt application, the problem of understanding wetting barriers in fibrous networks generally is an interesting

enough question to merit detailed investigation. Furthermore, there are insights from this study that can be applied to printing, packaging, and specialty papers, for example.

Fibrous networks constitute a core class of porous media and include materials such as non-woven fabrics, electrospun mats, and papers. Their highly desired mechanical strength, flexibility, permeable structure, and scalable manufacture have led to applications in batteries, apparel, functional fabrics, liquid-liquid separations, and fluid barriers [81-87]. Understanding the wetting behavior of these materials, especially their wetting barrier properties, is key to successfully applying design principles and has been a key thrust of research [88-93].

The barrier performance of phobic fiber networks that resist liquid entry (hydrophobic in the case of water, oleophobic for oils, and lyophobic for solvents) can be characterized in terms of a critical breakthrough pressure. At applied pressures below the critical breakthrough pressure, liquid cannot enter the porous medium, and the material effectively resists wetting. At fluid pressures equal to and above the critical breakthrough pressure, the phobic barrier fails and liquid penetrates (schematic illustrated in Figure 1.7). Thus, a wetting barrier of correct strength would permit dewatering from the paper to the felt under high pressure and prevent reflux from the felt to the paper under a smaller, reverse pressure.

The exact value of this critical breakthrough pressure is determined by liquid properties (surface tension), the solid structure (pore size and shape), and liquid-solid interaction (contact angle). The Young-Laplace equation relates the critical pressure, which

is a capillary pressure (ΔP), to the interfacial tension (σ) and interfacial curvature ($\nabla \cdot n$) [94-96].

$$\Delta P = -\sigma \nabla \cdot \vec{n} \quad (1.3)$$

While generally true, implementing this equation directly is inconvenient because one must determine the interfacial curvature inside a pore. Therefore, capillary forces are often estimated using models that approximate the interface as spherical (in the case of pores with circular cross-sections) or cylindrical (in the case of slotted pores) [97-99].

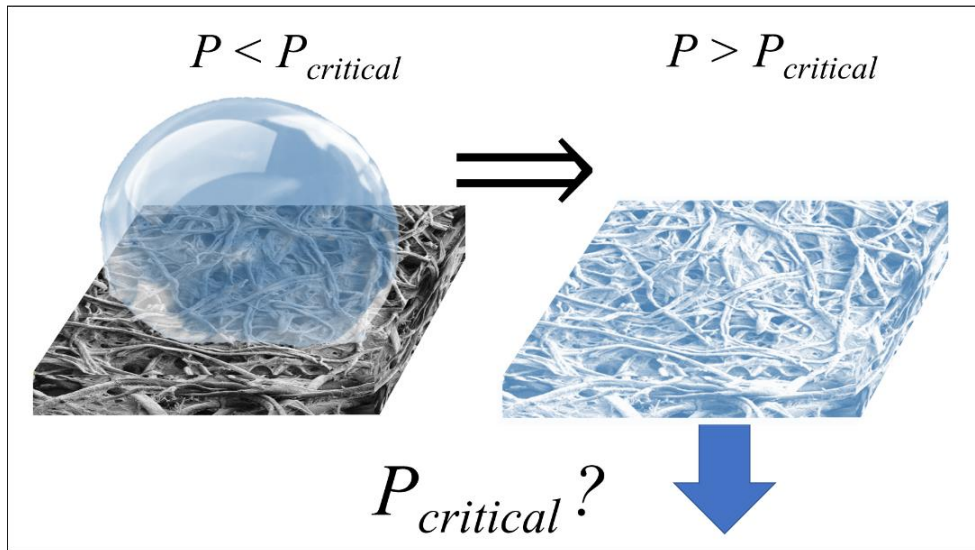


Figure 1.7 Schematic illustrating critical wetting pressure in fibrous media. At low pressures, capillary forces exclude the fluid. Higher applied pressures overcome this barrier, resulting in wetting.

The filamentous structure of fibrous networks produces fluid interfaces that resemble neither of these simple geometries. Their complex geometry poses particular difficulties to understanding, interpreting, and predicting wetting behavior [100]. For example, in non-woven materials, the interstitial space within the fiber network is an irregular, interconnected system of stochastically sized voids. The pore structure is also

reentrant, as the cylindrical cross-section of fibers causes the pores to widen when one moves further into a pore. Paper-based substrates, which constitute an important class of fibrous networks, present an especially challenging case because, in addition to stochastic voids, the fibers that comprise the network have significant variation in every dimension, including width, cross-sectional profile, and length. Amidst such complexity and randomness, there remains a need for insight into the physical parameters that influence the liquid barrier performance of these materials in various applications.

The most conventional approach to describe capillary forces within porous media is to model the void space as a bundle of cylindrical pores. Doing so drastically simplifies the description of forced wetting because the critical breakthrough pressure can be represented by a simple, analytical form, appropriately called the cylindrical pore model [101]:

$$P = \frac{-4 \sigma \cos(\theta)}{d_p} \quad (1.4)$$

The breakthrough pressure (P) depends on the surface tension of the liquid (σ), its contact angle on the solid surface (θ), and the diameter of the pore (d_p). While this model offers some basic qualitative insight—critical breakthrough pressure decreases with more wetting liquids and increases for smaller pores—it often fails to quantitatively predict the breakthrough pressure of entrant liquids through real materials. An additional challenge is to define the contact angle within the pore itself, because it can differ significantly from the apparent contact angle on the bulk material and because of a transition in the wetting regime at elevated pressures. That is, the fluid can switch from a Cassie-Baxter to a Wenzel wetting regime depending on the force applied [102].

Since the cylindrical pore model often fails quantitatively, results are sometimes discussed in terms of an effective pore size, d_{eff} , which may differ from the material's nominal pore size. By interpreting the experimentally measured breakthrough pressure with the model given by Equation 1.4, the effective pore size for wetting resistance may be found for any substrate and entrant liquid (Equation 1.5) [103]. Because this relies on back-calculation from Equation 1.4, it offers little new information about the validity of using such an approach and may not be predictive of substrate wetting behavior in other scenarios. Incidentally, this technique is the basis of mercury porosimetry, in which case the highly non-wetting fluid minimizes discrepancies due to the subtleties of pore geometry.

$$d_{eff} = \frac{-4 \sigma \cos(\theta)}{P} \quad (1.5)$$

The most advanced approach to modeling the breakthrough pressure of liquid through a fibrous network involves complex, computational simulations that can track the contact line and shape (i.e., curvature) of the liquid interface. While these analyses offer striking images and a direct visualization of what happens during liquid intrusion, they are often unwieldy in basic design applications and do not readily suggest physical interpretations for the observed phenomena [104].

An alternative model for fibrous networks was recently developed by Cimadoro et al [105]. Here, the network is modeled as a series of axially parallel cylinders separated at regular distances. The fiber cylinders have a radius (r) and a surface-to-surface separation distance of $2d$ (where d is half of the open space between fiber surfaces). The maximum pressure that a liquid interface bridging the interfiber gap can sustain in a multilayer structure is:

$$P = \frac{\sigma}{r[(D_*^2 - \sin^2 \theta)^{\frac{1}{2}} + \cos \theta]} \quad (1.6)$$

where the symbols represent breakthrough pressure (P), liquid surface tension (σ), and contact angle of liquid on the fiber wall (θ); D^* is a dimensionless spacing parameter, $D^* = 1+r/d$.

One advantage of this model is that it was developed from a more representative view of the fibrous network than simply an arrangement of cylindrical voids. While paper, for example, has neither perfectly circular cross-section fibers, nor consistent fiber size or fiber spacing, a great deal of physical insight can be garnered regarding the impact of these parameters on the real wetting behavior of hydrophobized fibrous networks. By comparison, the cylindrical pore model is unable to account for the effect of fiber radius and its corresponding reentrant geometry. In terms of design utility, the reentrant pore model has gained attention because of its convenient analytical form. Sufficiently complex to capture subtler, more intricate details of forced wetting, the equation is nevertheless simple enough for accessible analysis and intuitive understanding.

1.6.3 Adhesion

Surface forces can also dominate the transfer of water between separating surfaces, as is the case in separation rewet. The adhesive force holding a liquid droplet to a surface is the product of the length of the contact line between the liquid and solid and the receding contact angle of the liquid on the solid surface:

$$F = 2\pi a \sigma \sin(\theta_r) \quad (1.7)$$

where a is the radius of the droplet-surface contact circle, σ is the surface tension, and θ_r is the receding contact angle of a the liquid on the surface.

Thus, the wettability of a surface is not the only deciding factor in droplet transfer; the contact area of the liquid on each surface is also very important. This creates an opportunity to manipulate transport in a desired direction, even if one surface is more wettable than the other. This is especially true for surfaces with a large difference between the advancing and receding contact angle (contact angle hysteresis). A greater contact angle hysteresis results in a surface that tends to be stickier to water, even though the static contact angle would characterize the surface as hydrophobic.

Surface forces are not the only forces that affect transfer. Gravity, viscosity, and inertia all can contribute to droplet transfer, although inertia is the only other relevant force at the length and time scales present in an industrial press nip. The effect of inertial forces on droplet transfer is most evident when the two surfaces are pulled apart rapidly. The fluid mass' resistance to motion alters the balance of liquid that is transferred to each surface.

This effect can be used to create net movement of liquid from more hydrophilic surfaces to less hydrophilic ones, contrary to the incentive posed by surface wettability. However, there are limitations to this approach, as the droplet will tend to divide in half at best; at least some fluid always remains with the more hydrophilic surface.

The effect of adhesion on the fate of a droplet becomes even more complex when liquid is permitted to absorb into the boundary, rather than just wetting its surface. This is the case in papermaking because both the felt and the paper web are porous. This complicates the issue, as flow and separation phenomena begin to occur simultaneously. Due to this complexity, a general discussion of separation with flux boundaries is entertained in the body of the thesis, especially as it relates to inertially-dominated transfer.

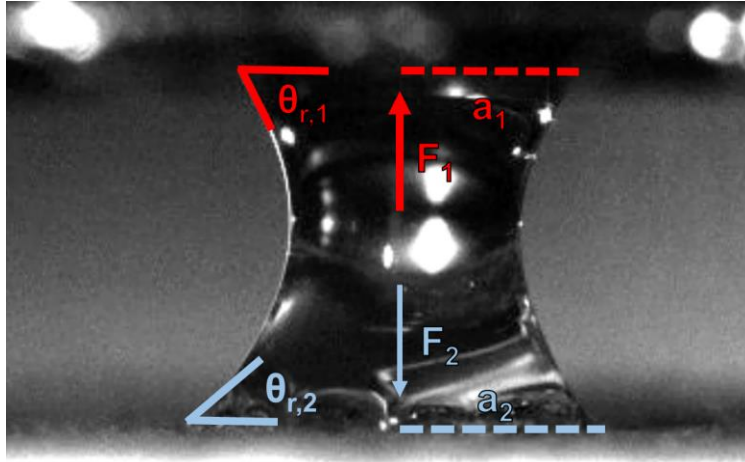


Figure 1.8 Liquid bridge adhering to two surfaces. The adhesive forces and the physical parameters contributing to them are illustrated. F is the adhesive force, r the radius of the contact line, and θ_r the receding contact angle.

1.6.4 Interfacial instability

An important consequence of Equation 1.3 is that surface tension acting on a liquid-air interface will cause the interface to assume a minimal surface area. This is because deviations from the global minimum surface area give rise to pressure gradients within the fluid that push and pull it towards the most energetically favorable state. To illustrate this point, consider Figure 1.9. A fluid with a deformed interface experiences high pressure wherever the interface is convex and lower pressure wherever the interface is less convex (or even negative pressures wherever it is concave). The difference in pressure between these two areas causes fluid to flow, reducing the deformation and creating a more uniform interface. Thus, surface tension tends to act in such a way as to damp disturbances. This is important because many small disturbances are constantly introduced to the fluid air interface from the environment or from variation in the fluid itself. The consequence of surface tension is that these disturbances decay over time, resulting in an interface that is stable (i.e. tends to restore stasis after minor perturbations).

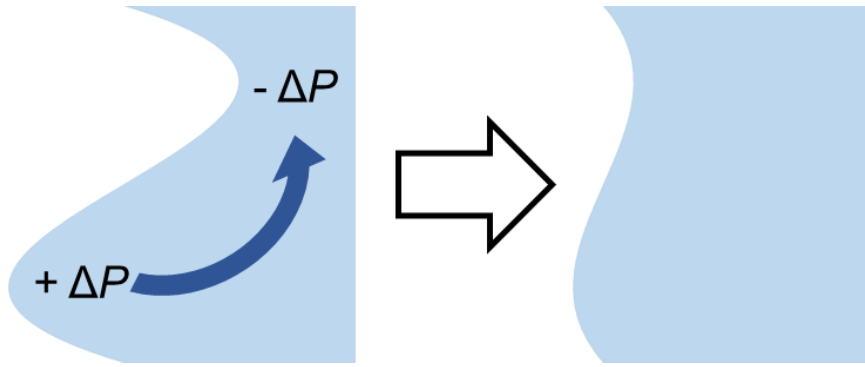


Figure 1.9 Deformations to the interface cause surface tension to create pressures that lead to self-correcting flow. Perturbations decrease with time, causing the interface to remain stable.

The effect of surface tension on interfacial stability is complicated when considering a column of liquid. Everyone has seen that water smoothly flowing from a faucet creates a clean column of liquid. At a certain distance down from the tap, however, the stream suddenly changes from a smooth, cohesive jet to breaking up into many smaller droplets. What explains this phenomenon? To understand this behavior, consider that the liquid has a two-dimensional surface that can be described as having radial and axial directions (Figure 1.10). When the radius of the column is relatively large compared to its axial length, the liquid surface is stable. Under this geometry, surface tension tends to correct for minor disturbances perturbing the interface, as was previously discussed. Things change, however, when the column becomes too narrow. Because of higher curvature in the radial direction, disturbances to the interface now result in higher pressures in axially-concave regions (Figure 1.10). This forms a positive feedback loop causing the disturbance to grow over time, rather than shrink. Thus, the miniscule variations always present at the interface grow exponentially with time, eventually breaking the stream apart [106, 107]. It is interesting to reflect that surface tension can have either a stabilizing or destabilizing effect on the interface, depending on a slight change in geometry.

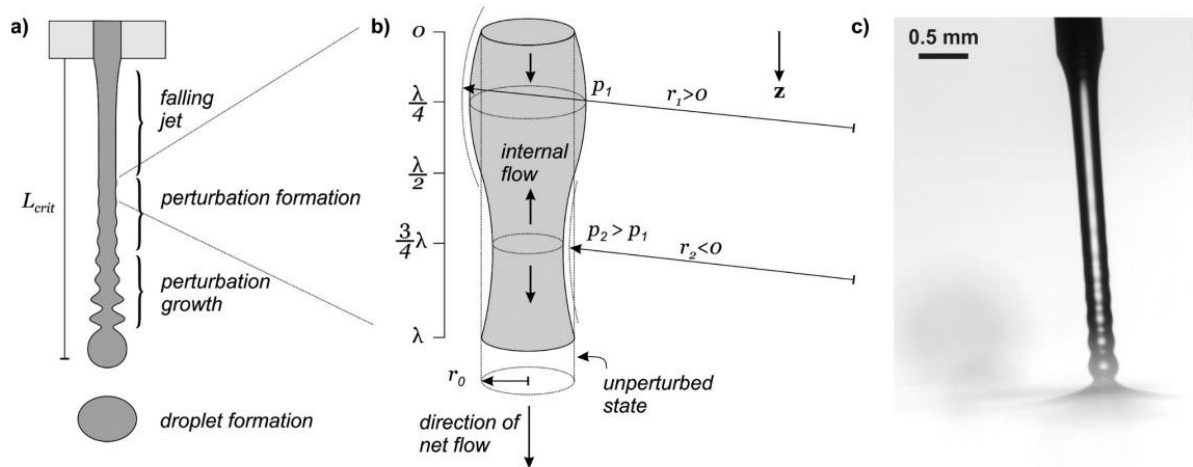


Figure 1.10 Schematic showing onset and growth of the Plateau-Rayleigh instability. Constriction of the column creates high pressure in the concavity of the disturbance, pushing fluid out and increasing the concavity. This process accelerates until droplet pinch-off. Figure reproduced from Rapp [108]

CHAPTER 2. LIQUID REPELLENCE OF PHOBIC FIBER NETWORKS¹

2.1 Background and scope

The wetting behavior of fiber networks, which are central to many research and industrial applications, can be difficult to predict accurately, owing to their complex, heterogeneous structure. The cylindrical pore model, widely used to interpret and predict the forced wetting of hydrophobic porous materials, often does not yield correct results when working with fibrous networks like paper substrates and non-woven fabrics. This is because these materials exhibit variation in pore size, fiber length, and fiber diameter, as well as a reentrant pore geometry. Quantitative prediction of the critical wetting resistance of hydrophobized papers to arbitrary entrant liquids requires a more sophisticated analytical approach that considers this unique fibrous structure and the effect of stochastic variations within the pore matrix. In this chapter, I directly measure the critical breakthrough pressure for different porous substrates across variously wetting entrant liquids. To isolate the effects of structure and stochastics on critical wetting behavior of fibrous networks, I analyze additional materials strategically chosen for their subsets of structural features. Ultimately, I formulate a method that demonstrates physical reasonableness, numerical accuracy, and ability to elucidate the effects of pore size, pore size distribution, fiber diameter, fiber diameter distribution, surface wettability, and liquid

¹ Material from this chapter was published in: Dudick, S., D.W. Hess, and V. Breedveld, *Liquid Repellence of Phobic Fiber Networks*. Langmuir, 2022. **38**(23): p. 7357-7364.

surface tension on critical breakthrough pressure of liquids through hydrophobic fibrous networks.

2.2 Experimental methods

2.2.1 Materials

Whatman Nuclepore™ track-etched polycarbonate membranes of nominal pore size 12 μm , 5 μm , and 2 μm were used. Metal meshes with nominal openings of 74 μm , 37 μm , and 11 μm were obtained from McMaster–Carr. The paper samples tested were Whatman chr17 chromatography paper, Q5 filter paper (Whatman), and Q2 filter paper (Whatman). The nylon non-woven came from a press felt used in papermaking: a tissue-grade felt manufactured by AstenJohnson. Deionized water, a solution of 35 wt.% ethylene glycol in water, and ethylene glycol (Sigma-Aldrich) were selected as probe liquids; at room temperature the surface tension of each liquid is 72.8 mN/m, 59.5 mN/m, and 46.3 mN/m, respectively. Formamide, diiodomethane, an aqueous SDS solution prepared at 1.5 times the critical micelle concentration, and Kaydol 35 mineral oil were used to test the predictive power of our method for wetting resistance of a paper sample to arbitrary liquids. Their surface tensions are 58.2 mN/m, 50.8 mN/m, 38.5 mN/m, and 31.3 mN/m, respectively.

2.2.2 Plasma treatment

A 6-inch parallel plate plasma reactor was used to hydrophobize the samples by plasma assisted vapor deposition of a fluorocarbon film from a pentafluoroethane (PFE) precursor. Further details concerning the reactor configuration can be found in previously

published papers [109-112]. Flows of 75 sccm Argon and 20 sccm PFE were used to establish a reactor pressure of 1.4 Torr; depositions were performed at 110 °C. An RF power of 100 W was applied to the upper electrode for 1 min to deposit and covalently bond a ~100 nm fluorocarbon coating (as measured on a flat, non-porous silicon wafer) on each porous substrate.

2.2.3 *Contact angle*

Contact angles were measured on a 290 model ramé-hart goniometer by introducing 4 μ L of probe liquid. The static contact angle was fitted by DROPImage, the analysis tool native to the instrument. Increasing droplet volume was used to determine advancing contact angle, while retracting droplet volume was used to determine the receding contact angle. The difference between these two, the contact angle hysteresis, characterizes the droplet adhesion to the surface.

2.2.4 *Breakthrough cell*

To measure the critical entry pressure of the hydrophobic porous materials, the apparatus depicted in Figure 2.1a was developed; this unit will subsequently be referred to as the breakthrough cell, or Bcell. Probe liquid is introduced into the column, and a spring clamps the sample to the base of the column to ensure a good seal. A syringe pump functions as a piston to generate air pressure above the probe liquid. The piston head plunges at a constant linear speed, increasing the pressure within the apparatus over time. When the fluid pressure inside the column reaches a critical value, it penetrates the porous material, and a camera aimed at the sample's bottom surface records the event. Transport time through the material can be neglected because the substrate is thin, and because the

pressure ramps slowly. To show that the measured breakthrough pressure does not depend on flow resistance or delay due to transport through the thin layer of material, the breakthrough pressure of water on two different substrates was measured for varying pressurization rates (Table 2.1).

Table 2.1 The breakthrough pressure of water on two hydrophobized papers was measured at different average pressurization rates to show that transport delays and flow resistance do not significantly affect the measurement

Average rate of pressurization (kPa/min)	Breakthrough pressure measured (kPa) [5 replicates per entry]	
	<u>Chromatography</u>	<u>Q5 filter</u>
0.55	7.2	12.3
1.7	6.6	12.2
5.5	7.2	11.9
17	7.1	11.6
55	6.8	12.6
average across all replicates	7.0	12.1
95% confidence limit	± 0.3	± 0.5
ANOVA p-value (p > 0.05 signifies no statistical difference between pressurization rates)	0.41	0.74

By synchronizing the video with the piston position, the precise value for the critical breakthrough pressure of a probe liquid through the material is determined. An example of this breakthrough determination is presented in Figure 2.1b. Liquid penetration through the material can clearly be identified from contrast changes.

2.2.5 Imaging

A Zeiss Ultra 60 scanning electron microscope (SEM) was used to image the samples. ImageJ image analysis software was used to determine the dimensions of features in track-etched membranes and paper substrates.

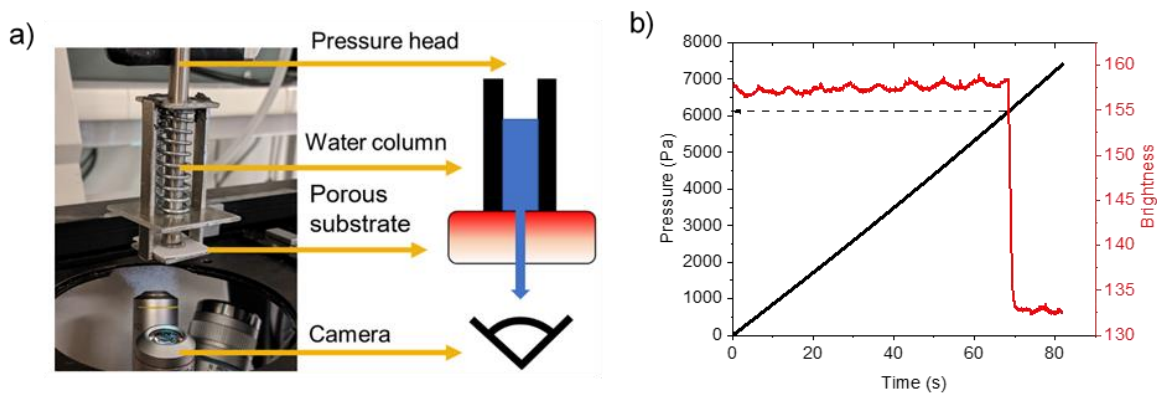


Figure 2.1 (a) Bcell: the apparatus used to directly measure the critical breakthrough pressure of hydrophobized porous media. A syringe pump increases the pressure above the probe liquid over time. When critical pressure is reached, the wetting is observed in synchronized video. (b) Brightness sharply decreases when liquid penetrated to the bottom surface.

2.3 Results and Discussion

2.3.1 Track-etched membranes: cylindrical pores with stochastic variation

To validate the experimental approach and to justify the analytical methods employed for more complex materials, the problem of critical breakthrough pressures is first simplified by considering the forced wetting behavior of track-etched membranes. As seen in Figure 2.2, pores in the track-etched membranes are mostly cylindrical, although there are some irregularities, the effect of which will be discussed later. The pores are also through-pores, created by irradiating the polycarbonate film with an ion beam [113]. That

is, transport of entrant liquid occurs in single channels through the membrane, without having to navigate a network of interconnected voids. For such a case, use of the cylindrical pore model is well-justified, as its assumptions are met.

The effective pore size d_{eff} (Equation 1.5) represents the characteristic material dimension that resists wetting and provides a basis for comparison between the material's actual and nominal pore size. The surface tensions of the entrant liquids are well known, and the breakthrough pressure is easily measured by the Bcell. Results are shown in Figure 2.3a. Measuring the contact angle of each entrant liquid on a flat, PFE (fluorocarbon) coated silicon wafer means that the liquid contact angle on the pore's PFE-coated surface is also well-defined. Regardless of the surface chemistry of the original substrate, only its structural properties (pore shape and size) are retained after coating.

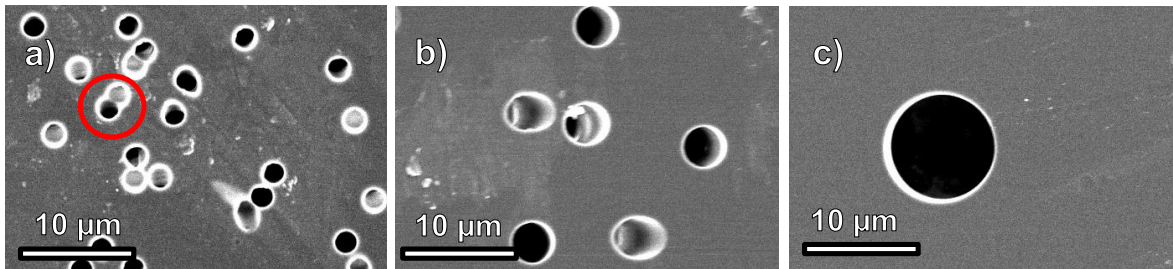


Figure 2.2 SEM of track-etched membranes of nominal sizes 2 μm (a), 5 μm (b), and 12 μm (c). Note the nearly cylindrical pores which permeate the medium. The presence of multi-core pores (see red highlight in (a)) results in an effective pore size greater than the nominal pore size.

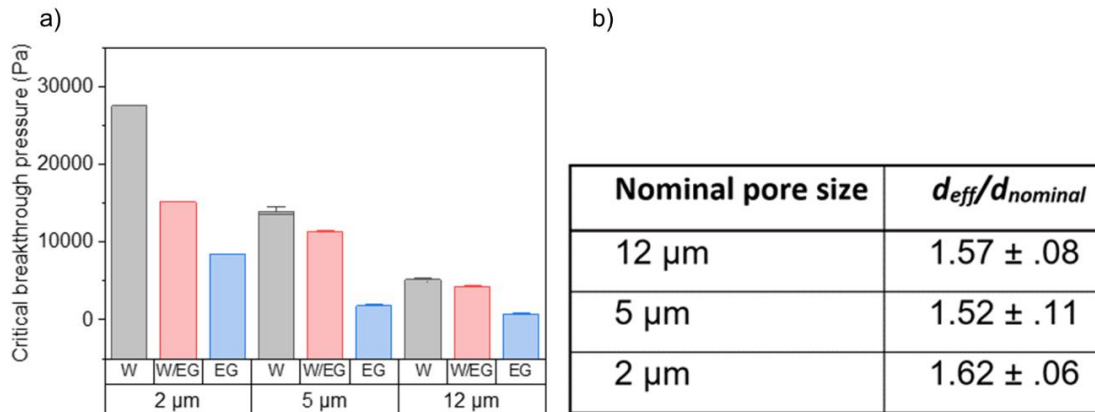


Figure 2.3 (a) Critical breakthrough pressure of liquids through track-etched membranes with different pore sizes. Water (W), 35 wt.% water in ethylene glycol (W/EG), and ethylene glycol (EG) were used. (b) Deviation of effective pore size from nominal. Error shows spread in effective pore size across the three probe liquids tested, pooled standard deviation over 15 individual replicates per membrane.

Using the cylindrical pore model, the various critical pressures can be represented as an effective pore size. Each membrane has a calculated effective pore size within 20% of a mean value common across the probe liquids used. This means that the cylindrical pore model captures the *variation* in critical breakthrough pressure with pore size and wettability. However, quantitatively, the effective pore size is consistently larger than the nominal pore size by approximately 55% across the three membranes tested (Figure 2.3b). This suggests that the characteristic pore size that determines critical entry pressure differs slightly from the nominal pore size in the membrane. A stochastic view of the microstructure of the membranes clarifies the cause. Because a larger pore diameter corresponds to a lower wetting resistance, the barrier to wetting will fail first at the upper end of the pore size distribution. The presence of multi-core pores, highlighted in Figure 2.2a, explains the observation that the effective pore size based on the wetting analysis is consistently larger than the nominal pore size of the membrane.

2.3.2 Metal meshes: regular, filamentous pores

The next layer of complexity that can be considered is a regular, well-defined structure that exhibits reentrant pore geometry. The experimental and analytical method is thus extended to consider a more complex porous system. Metal meshes constitute a single layer of intercrossed filaments. They are highly uniform: both the wire diameter and wire spacing exhibit little variation, as seen in Figure 2.4. Thus, stochastic effects can be ignored when interpreting the results of these experiments.

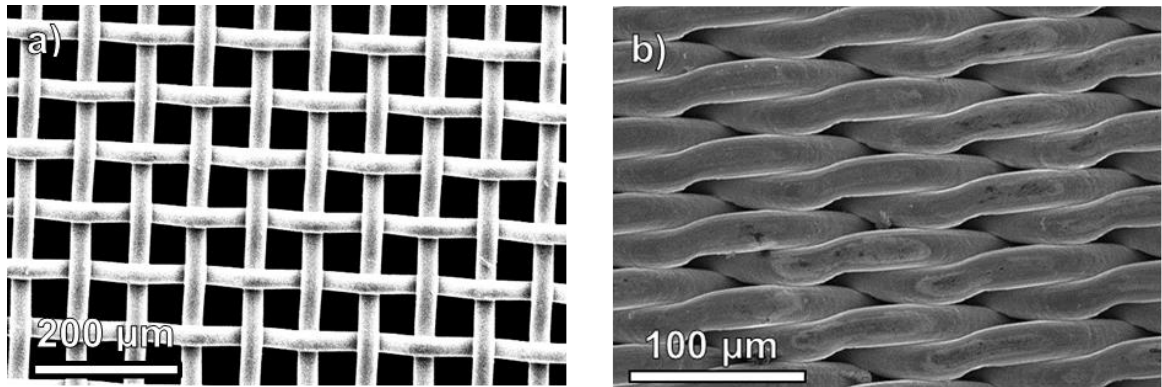


Figure 2.4 Optical microscope images of metal meshes, sized 37 μm (a) and 11 μm (b). Note the regular, well-defined structure and curved pore walls

The critical breakthrough pressures measured for hydrophobized metal meshes are summarized in Figure 2.5a. One order of magnitude range in pressures is observed. Interpreting these measurements in terms of the effective pore size again requires supplying a value for the contact angle of the entrant liquid on the treated wire surface. As before, it is reasonable to expect that for a smooth wire surface coated with PFE, the contact angle of each liquid is similar to its contact angle on a smooth PFE-coated silicon wafer. Indeed, the apparent contact angles on the hydrophobized meshes agree with the Cassie-Baxter values [114] calculated from the manufacturer-specified wire/spacing area

fractions and the contact angle measured on a flat PFE surface (Figure 2.5). The slope does not statistically deviate from 1 ($m = 0.93 \pm 0.16$) and the correlation is strong ($R^2 = 0.98$).

However, the cylindrical pore model does not reduce the wetting behavior of each mesh to a similar effective pore size, as it did for the track-etched membranes (Figure 2.6b). Each probe liquid enters with a critical pressure that diverges from the predictions of the cylindrical pore model in a non-linear way. Notably, the more non-wetting the fluid, the more closely it matches the cylindrical pore model. Water entry, for example, exhibits effective pore sizes numerically close to the nominal pore size of the mesh. Looking at the series of fluids, the failure of the model cannot be attributed to statistical variation in the mesh structure –which, as discussed, is uniform – but rather to its inability to capture the complex curvature of the fluid interface within these pores. The curvature of the wires that form the pore walls plays a key role in determining the real critical entry pressure of the liquids. Therefore, no single fix factor can be applied; as a result, Equation 1.6, which accounts for the maximum pressure sustained between parallel filaments, is used.

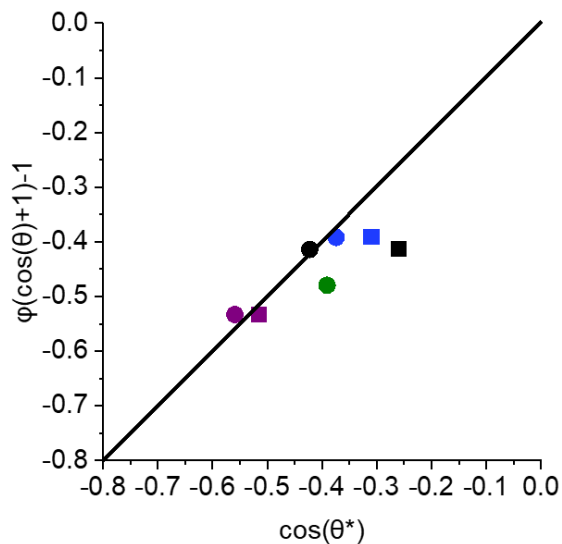


Figure 2.5 1:1 plot comparing the experimentally measured apparent contact angle on meshes (x-axis) to the apparent contact angle predicted by the Cassie-Baxter equation (y-axis). The line represents the relation $y = x$. Squares represent points for the 11 μm mesh, circles for 37 μm mesh. Colors represent droplets of different liquids: black (ethylene glycol), blue (diiodomethane), green (35 wt.% ethylene glycol in water), and purple (water). Experimental error lies within the data points.

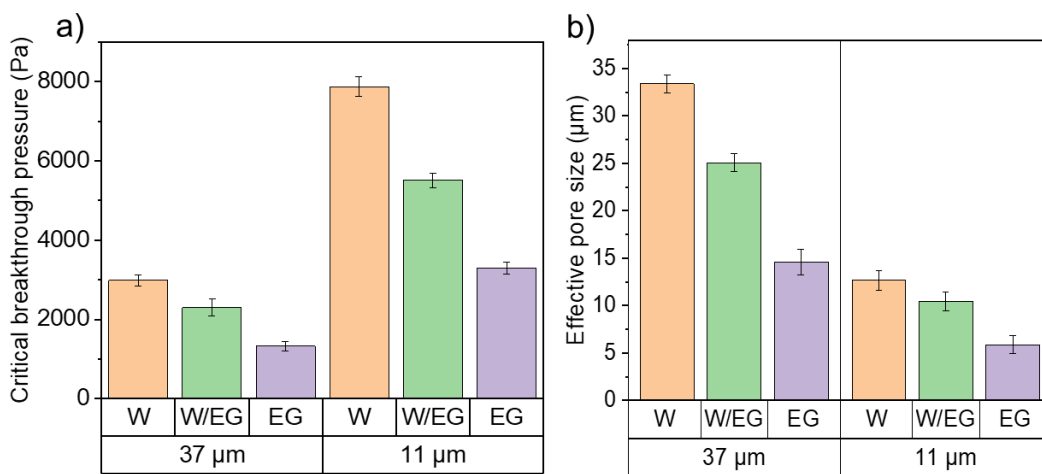


Figure 2.6 (a) Critical breakthrough pressure of various liquids through phobized metal meshes. (b) Effective cylindrical pore sizes of meshes for each liquid. Differences between liquids highlight a failure of the cylindrical pore model.

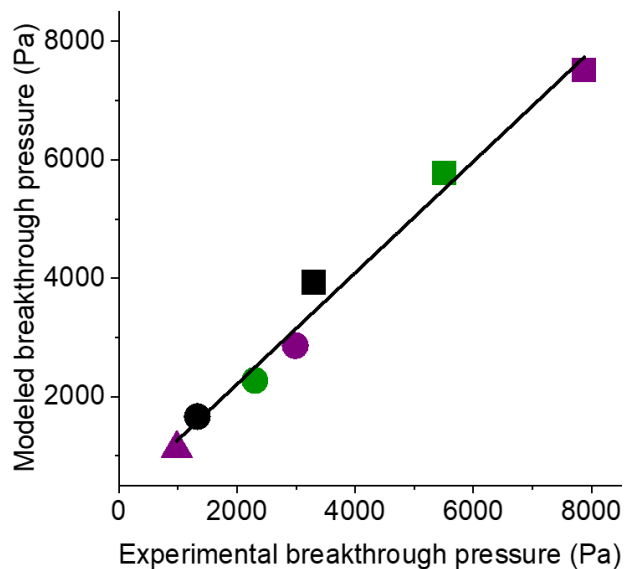


Figure 2.7 1:1 plot of critical pressure predicted by reentrant model vs. those observed by direct measurements. Purple corresponds to water, green to W/EG mixture, and black to EG. Squares, circles and triangles correspond to 11 μm, 37 μm, and 74 μm meshes, respectively. The line represents the line $y = x$. Errors fall within the data points.

Choosing this model for the treated metal meshes, quantitative agreement is obtained with the experimental data (Figure 2.7). The reentrant pore model effectively captures the variation in critical entry pressure with wire diameter, wire spacing, liquid surface tension, and liquid-surface contact angle. Such a result builds confidence in the use of this model to describe the wetting barrier of filamentous substrates. While the equation is valid for perfectly regular meshes, an intriguing possibility is application to random fiber networks, such as non-woven fabrics and papers.

2.3.3 Forced wetting of hydrophobized paper substrates

Next, we therefore apply this approach to the forced wetting behavior of an even more complex filamentous structure: paper. As seen in the scanning electron micrographs (Figure 2.8) paper has a reentrant pore structure and a distribution in both fiber spacing and

fiber diameter. The physical complexity of this material has presented a significant challenge in understanding its resistance to wetting. Fortunately, insights can be leveraged from the prior model materials: track-etched membranes and metal meshes. With a combined view of both the effect of a unique pore geometry on the liquid interface curvature and of stochastic variations in that geometry, a physical interpretation of this complex system emerges with predictive quality. From a design perspective, the fiber spacing, variation in fiber spacing, fiber diameter, surface wettability, and liquid properties all play a key role in determining the wetting resistance of a fibrous network.

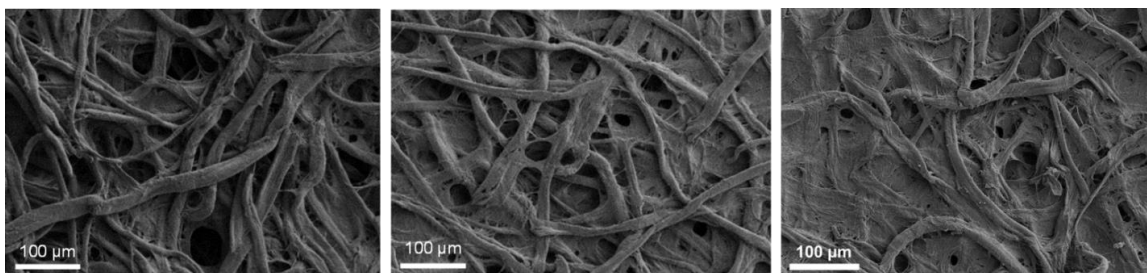


Figure 2.8 SEM images of paper samples: chromatography paper (left), Q5 filter paper (center), Q2 filter paper (right)

The first challenge associated with predicting the wetting behavior of an entrant liquid is determining the contact angle of the entrant liquid on the treated fiber surfaces within the pores. To that end, Figure 2.9 compares the contact angle on the surface of treated papers with what would be expected if the surface of a PFE coated fiber wets the same as a flat, PFE coated silicon wafer. The apparent contact angles on PFE-deposited papers are indeed consistent with the Cassie-Baxter model based on the paper porosities and the contact angles of the liquids on a flat PFE wafer. This implies that using liquid-PFE contact angles for the contact angle of entrant liquids on the surface of the fiber is justified.

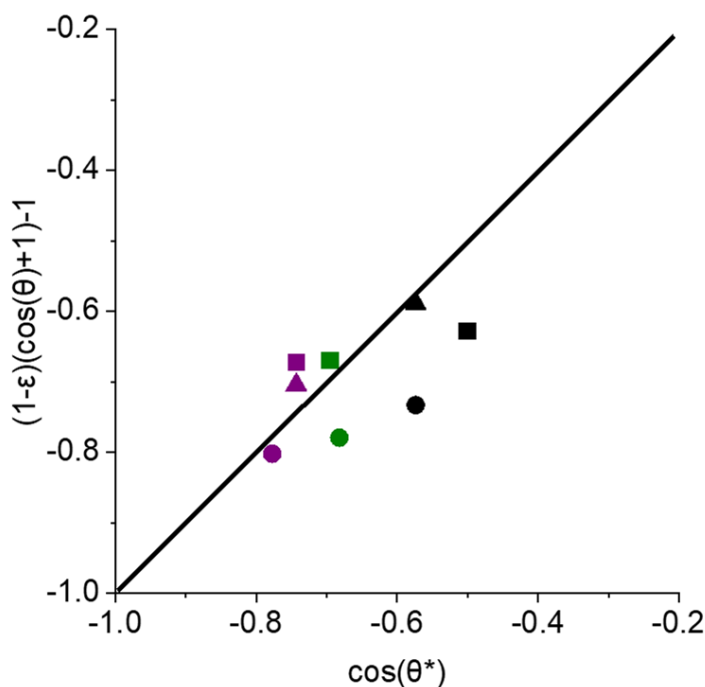


Figure 2.9 Apparent contact angle measurements on the paper surface agree with the assumption that liquid-solid interaction on a PFE coated fiber is similar to the liquid-solid interaction on a flat, PFE coated silicon wafer. Shapes correspond to chromatography paper (circle), Q5 filter paper (square), and Q2 filter (triangle). Colors correspond to water (purple), 35 wt.% ethylene glycol in water (green), and ethylene glycol (black). The slope is not statistically different from 1 ($m = 1.08 \pm 0.11$) and the correlation is strong ($R^2 = 0.98$). Errors fall within the data points.

Across the differing paper samples and entrant liquids, more than an order of magnitude in critical breakthrough pressures is observed. Understanding how the wetting resistance varies with paper structure and liquid properties, which is essential in terms of design, requires quantitatively relating the parameters via an appropriate physical model. These data cannot be interpreted in a consistent way using the cylindrical pore model, as shown in Figure 2.10a. The lack of agreement in effective pore size, both among entrant liquids and compared to porosimetry, suggests that the cylindrical pore model fails to capture the effects of key material parameters on the critical breakthrough pressure, as was

seen in the case of metal meshes. Based on the success of the reentrant pore model in interpreting the wetting of metal meshes, it is applied to the paper substrates as well.

How to choose or fit the fiber width in implementing the reentrant pore model is not obvious, however. In the case of the metal mesh, the wire diameter is well defined. However, the paper samples exhibit a considerable degree of variation in this respect. Referring once again to the scanning electron micrographs of the paper samples in Figure 2.8, the fiber width varies from fiber to fiber. Image analysis is conducted to determine both the average fiber width and standard deviation for the paper samples (Figure 2.10c). The two filter paper samples had very similar distributions and are therefore plotted as a single series. In all cases, the standard deviation in fiber width is approximately 50% of its mean—a significant variation. The median fiber diameter is used in implementing the reentrant pore model, an approach justified by the consistency of results. The effect of variability in the fiber width distribution is considered later.

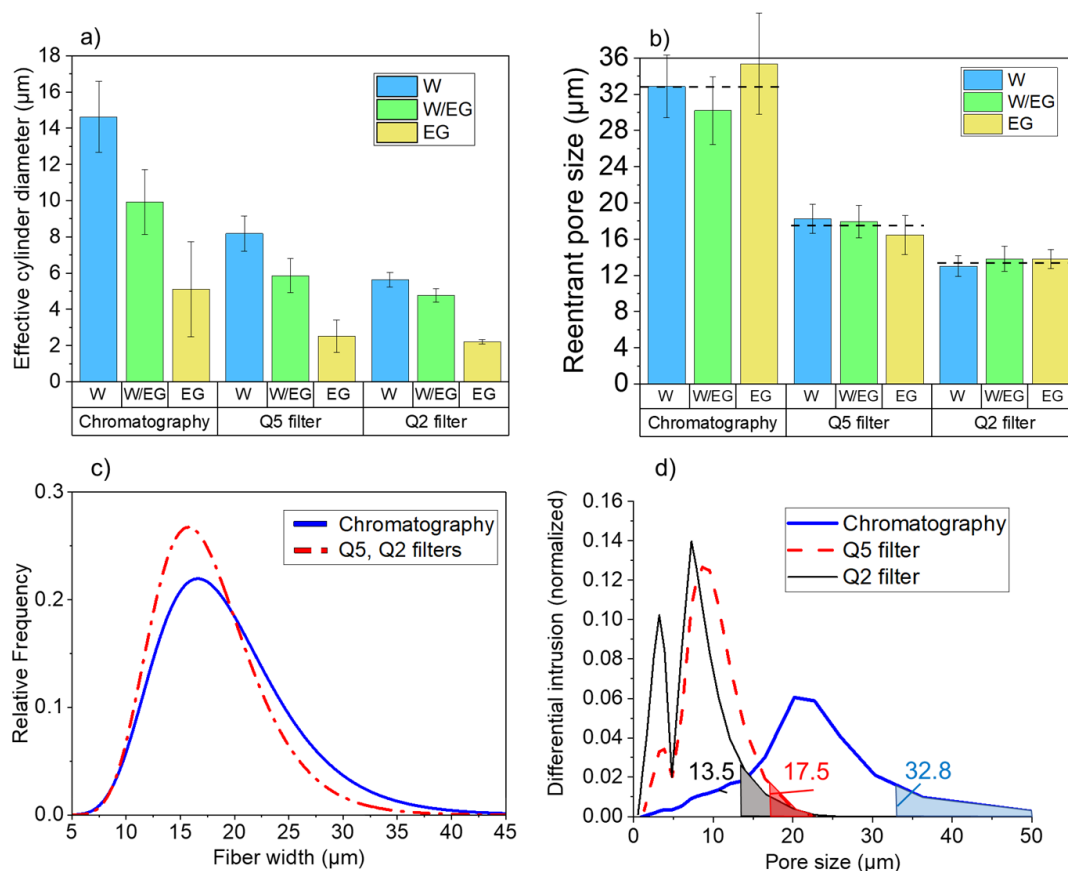


Figure 2.10 (a) Cylindrical pore analysis and (b) reentrant pore analysis for three different paper substrates and three test fluids (water, water/ethylene glycol mixture, ethylene glycol). The underlying material structure cannot depend on entrant liquid, as is suggested by (a), highlighting the insufficiency of the cylindrical pore model; reentrant pore analysis, (b), shows consistent fiber spacing values for all liquids, with the dashed lines denoting the average pore size. (c) Fiber width distribution obtained from SEM image analysis. (d) Mercury porosimetry data for paper samples. Differential intrusion measurements show a greater average pore size for chromatography paper vs. the filter papers. The singular effective pore size for wetting resistance, found from direct breakthrough pressure measurement and analysis via the reentrant pore model (see (b)), lies in the upper tail of the distribution for each sample.

Next, using the critical breakthrough pressure, contact angle, and fiber width, the reentrant pore model is used to interpret the data in terms of an effective fiber spacing ($2d$)—analogous to pore size. By this method, the effective pore size is nearly constant (Figure 2.10b). The average for each substrate is denoted with a dashed line. The error bars represent the effect of fiber width variation. Setting the fiber width one standard deviation higher or lower than its mean and solving for fiber spacing results in the limits seen. Such consistency across all entrant liquids implies that the model captures the observed wetting behavior of the system quite well. Comparing this effective pore size to the distribution obtained from mercury porosimetry (Figure 2.10d), it is found that the upper tail of the distribution determines the wetting resistance—a fact in accord with the stochastic interpretation developed in analyzing the track-etched membranes. Roughly, the 10-15% largest pores by volume fraction are responsible for the critical breakthrough behavior in the random network.

Once the effective pore size and fiber width for a given fiber network are known, the reentrant model can be used to predict the wetting resistance towards arbitrary liquids. In Table 2.1, we show the wetting resistance of phobized filter paper to a diverse range of liquids. These liquids were chosen to cover a large scope in surface tension and types of molecular interactions, to determine the generalizability of this approach. Notably, the breakthrough pressures predicted by the reentrant model are in good agreement with those that were measured directly. Since we relied only on known material properties and structural parameters, and not on any empirical factors, the agreement is a compelling result. This is a tremendous improvement over the cylindrical pore model for these materials; as shown also in the table, the cylindrical pore model yields large quantitative

errors when predicting the wetting of formamide and diiodomethane, and even qualitatively misses the wetting behavior of the SDS solution and the mineral oil. In these latter cases, spontaneous wetting is predicted by the model—as indicated by the negative sign for critical entry pressure-, while the fibrous network is in fact able to resist wetting due to the reentrant geometry of its pores.

Table 2.2 Predicted wetting resistance of various liquids for the Q5 filter paper, compared to experimental values. The critical entry pressure for water serves as the basis for calculating predicted entry pressures via the cylindrical pore model. Predictions for the reentrant model were made using Equation 1.6, utilizing the structural parameters for Q5 filter found in earlier analysis.

	liquid description	σ (mN/m)	θ_c	predicted P (cyl., kPa)	predicted P (reen., kPa)	measured P (kPa)
water	polar liquid	73	108°			12.1 ± 0.5
formamide	polar liquid	58	94°	2.2	9.3	9.5 ± 0.3
diiodomethane	nonpolar liquid	51	92°	1.0	8.2	8.6 ± 0.2
SDS solution	[surfactant] > CMC	39	72°	- 6.5	4.9	4.5 ± 0.6
mineral oil	paraffinic oligomer	31	61°	- 8.1	3.7	2.9 ± 0.4

2.3.4 Application of wetting barriers to press fabrics

To show that the stochastically-informed reentrant model is useful for a wider range of fiber networks beyond paper, we analyzed the wetting resistance of a phobized nylon non-woven that is used as a support fabric in papermaking, imaged in Figure 2.11a. The physical features of this material, fiber spacing and fiber diameter, are about an order of magnitude larger than those of the filter papers tested. Therefore, the wetting resistance of this material is quite small, about 1.5 kPa for water. Still, similar results were found as for the other fiber networks studied. Reentrant pores more effectively resist the entry of wetting liquids than would otherwise be expected with cylindrical pores. Across the probe liquids tested, the reentrant model once again relates the wetting behavior to underlying

material parameters more consistently, while the cylindrical pore model fails to yield a meaningful, consistent pore size (Figure 2.11b).

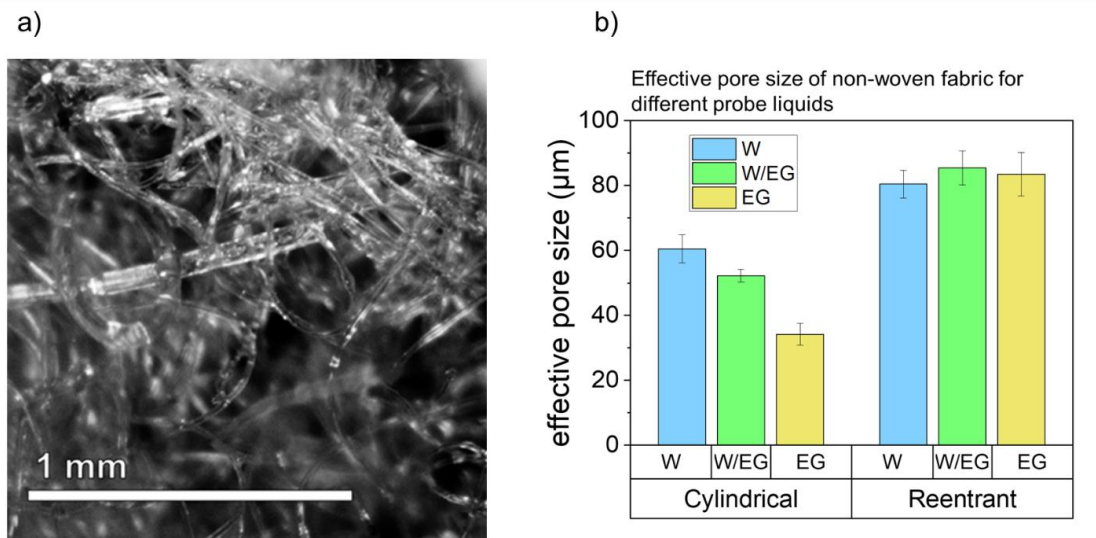


Figure 2.11 (a) Optical micrograph of nylon non-woven fabric. (b) Effective pore size for phobized nylon non-woven, comparing two analytical models, the cylindrical pore model (Equation 1.5) and the reentrant pore model (Equation 1.6), for three test fluids (water, water/ethylene glycol mixture, ethylene glycol).

Now that I know how to accurately predict the capillary barrier needed to prevent flow in a fiber network, wetting gradients as a tool for enhanced dewatering can be attempted. To test this, untreated chromatography paper will be pressed with a commercial felt, at a pressure of 10 MPa. The details of the pressing apparatus—along with the formal definition of the sheet’s water content—are described in Chapter 4. To summarize the experimental procedure, the initially dry chromatography paper is wetted with twice the mass of water as fiber (moisture ratio, MR, equal to 2). The paper is laid on a press felt, and the two are sandwiched between two steel plates. Force is applied to the plates with a screw clamp, of the type found in any woodworking shop. A force sensor, combined with fixed area of samples (half square inch), allows the targeted pressure of 10 MPa to be

applied with precision. After pressing, the mass of the dewatered sheet is measured to determine its moisture content. The amount of water remaining in the paper is then normalized to the sheet's oven dry weight (definition of moisture ratio). Thus, a sheet that has undergone better dewatering will have a lower moisture ratio.

Three press felt designs were tested via this method, with the results summarized in Figure 2.12. First, a conventional press felt served as the control. This established a reference for dewatering compromised by rewet. Second, a press felt with a suitably strong wetting barrier was used. To create this felt, a fiber network with finer features than the chromatography paper would have to be created, hydrophobized, and attached to the surface of the felt. To implement this design in a proof-of-concept, lab-scale test, I first hydrophobized a filter paper, which can exert twice as strong capillary forces as the chromatography paper, based on previous analysis. This phobic filter was then laid between the chromatography paper and press felt during pressing. The third press "felt" consists of a thick stack of paper blotters. The purpose of this configuration is to establish the theoretical limit of dewatering in the absence of rewet. Details about how the blotters work are covered in the fourth chapter, which deals with benchtop pressing at length. For now, it may be taken for granted that the blotters simulate a perfect press felt: one that permits no rewet.

Figure 2.12 shows that a sheet pressed with a standard press fabric is significantly wetter than one pressed against blotters. This indicates that rewet can result in a sheet with more than twice as high a moisture content, at least when pressed on the lab-scale. Granted, the experimental conditions chosen tend to exaggerate the phenomenon of reflux, compared to what would likely be seen in an industrial press nip. This is because the felt

remains in contact with the paper web for a long time after decompression (order of seconds). However, conditions that pronounce this phenomenon are actually helpful in the investigative phase of this project, because they allow for a clearer delineation of effects.

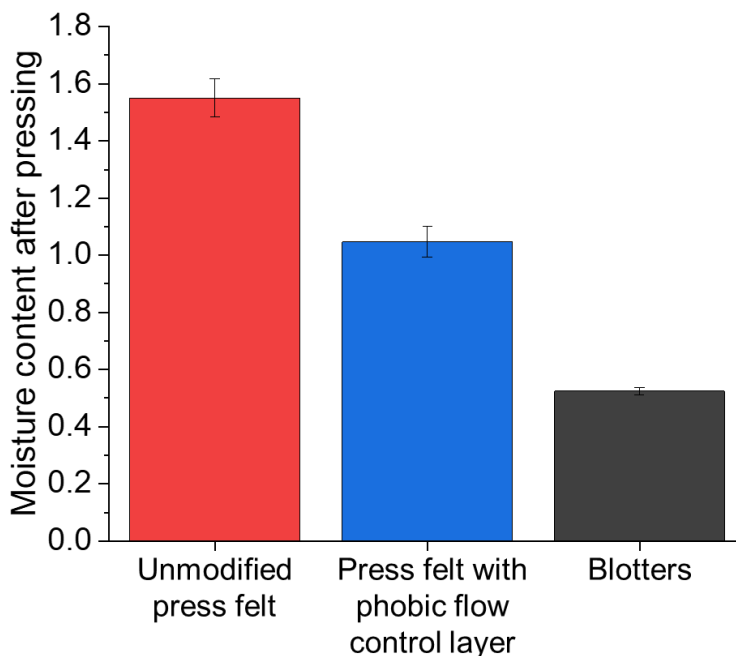


Figure 2.12 The effectiveness of using wetting gradients to prevent rewet is assessed. Chromatography paper initially at $MR = 2$ was pressed at 10 MPa for these experiments. The unmodified press felt resulted in the worst dewatering as the sheet pressed with it had the highest moisture content after pressing. Blotters were used to simulate a press felt that completely prevents rewet. The hydrophobic barrier prevented some, but not all, rewet.

Introducing a hydrophobic control layer to the felt was successful in mitigating rewet. The moisture content of the sheet pressed with this felt design was significantly lower than that of the control press fabric. The moisture ratio of the dewatered sheet was about 1, compared to its initial value of 2. First, this demonstrates that dewatering is possible through the hydrophobic barrier at the relatively high pressures applied. 10 MPa

of applied stress was sufficient to push water through the phobic filter, which had an estimated critical wetting pressure of only about 15 kPa. Second, the felt with the wetting gradient was able to decrease the amount of reflux to the sheet, compared to the control. Interestingly, the felt with an adequately large wetting barrier did not completely eliminate rewet, as can be seen by comparison to the blotters.

I speculate that the reason for this revolves around the forced wetting of the hydrophobic barrier during dewatering. By forcing water into this hydrophobic fiber network at high pressures, cavities on the rough fiber surface may be partially wetted. This would result in a small amount of liquid remaining in some pockets of the phobic region during decompression. The existence of residual water in the network provides a path for reflux through the otherwise repellent wetting barrier. Essentially, the barrier might be short-circuited by the presence of these wetted channels.

Another reason to reconsider the effectiveness of using wetting gradients to improve dewatering is that a layer with rather small pores had to be introduced to the surface of the felt to get strong enough capillary forces. According to Equation 1.1, this results in a higher resistance to flow. In the benchtop press used in these experiments, a higher flow resistance does not impact dewatering because of the relatively long time the sheet is pressed. However, higher resistance (and thus slower flow) drastically compromises dewatering in an industrial press nip because of the short dwell time. Additionally, the smaller fibers needed for a strong enough wetting barrier are more subject to wear under the abrasive process conditions of the application. For these reasons, additional strategies need to be explored to control the transfer of fluids between fibrous materials.

2.4 Conclusions

This portion of the thesis has focused on the wetting of various phobic materials, particularly paper substrates as they represent the most challenging of complex fibrous materials for which to interpret and predict wetting behavior. By using more uniform and homogeneous substrates (track etched membranes, metal meshes), a semi-quantitative understanding of the factors that influence wetting resistance was established. Results from these studies were used to identify an analytical approach for heterogeneous systems such as paper and non-woven fabrics. The fiber diameter and variation in pore diameter are as impactful as other material parameters, even though more conventional models may only consider average pore diameter and surface wettability. The wetting resistance of a fiber network to arbitrary liquids can be accurately predicted a priori, by a calculation based only on liquid properties and the network's structural parameters. This was true for a broad range of liquids with widely ranging surface tensions and intermolecular forces. I proved the applicability of this approach to fiber networks with features on the scale of 2 μm , all the way to fiber networks with features on the scale of 100 μm . In systems with well-defined filaments (such as electrospun mats, non-wovens, etc.), these insights could provide highly useful information regarding design parameters and performance of engineered materials.

While a wetting barrier with sufficient capillary forces could prevent some rewet, at least some water still refluxed to the sheet during decompression. Furthermore, practical issues stemming from the decreased permeability and increasing sensitivity to wear preclude this approach from being implemented in the press section of a paper machine. Clearly, additional techniques need to be investigated to eliminate rewet.

CHAPTER 3. ADHESIVE TRANSFER OF FLUIDS BETWEEN FIBER NETWORKS

3.1 Background and scope

As described in the introductory Chapter 1, two transport phenomena are primarily responsible for rewet: flow and separation rewet. In Chapter 2, the possibility of using wetting barriers to prevent reflux from the press felt was investigated. Conceptually sound, the physics of this approach were elucidated in such detail that a successful demonstration was performed on the lab-scale. However, practical limitations to implementing this strategy at scale in a manufacturing process were identified. Control over capillary forces within the felt alone does not suggest an immediate path to eliminating rewet.

Fortunately, a review of literature on the subject suggests that separation rewet is likely to be as significant as flow rewet, at least in state-of-the-art machines [115]. Evidence suggests that the majority of water refluxing to the sheet comes from the surface layer of the felt or from space between the felt and paper web. However, the distinction between water at or near the felt surface is difficult to make because of the fibrous nature and deformability of the felt and sheet. Nevertheless, the observation suggests that there may be an opportunity to use surface forces to control the fate of fluid transport in these scenarios. Controlling the adhesion of liquid to fiber substrates is the starting premise for this chapter. Of primary interest is the transfer behavior of liquids from paper surfaces to surfaces of contrasting wettability. The effects of droplet shape (contact line pinning), inertial forces, and flux into a porous boundary will all be explored.

I show that a wide variety of techniques are available to control transfer of liquids between separating surfaces. In one notable example, a water droplet can be encouraged to preferentially transfer from one surface to another simply by altering the distance to which the surfaces are brought together before being pulled apart. No special patterning, topography, or switchable chemistry is needed to achieve this control. I show also how changing the speed of separation can enhance transport of liquid from hydrophilic surfaces to hydrophobic ones, going against the wetting gradient. Extension of the strategies developed in this study to the extreme operating conditions in a paper machine press nip is unfortunately neither obvious nor practical, as will be shown in the discussion. The findings, however, could be useful to control fluid transport in other applications involving porous substrates. For example, water-repellant fabrics, electrospun membranes, personal protective equipment, flow battery electrodes, and environmentally-friendly packaging.

A general introduction to the influence of wetting and contact line conformation on adhesion of liquids to surfaces was given in the introduction. This chapter aims to focus that broader background into more specific insights that can be used to control transfer of liquids in a press section. Based on previous work done in this area, it is well known that tools like patterning and modification of surface topology can be leveraged to control transport. However, I was curious what can be done with the intrinsic features of fibrous materials alone as these insights would be most informative for guiding press fabric design. Furthermore, the lack of data in the existing literature on liquid transfer specifically between fibrous media justifies honing in on that class of materials. Therefore, the experimental approach in this chapter was tailored to show the immense degree of control available over liquid droplets partitioning between separating surfaces, using tools intrinsic

to fiber networks. Whether by leveraging the geometry of the fibers themselves, the fibrillar nanostructure of cellulose, inertial and viscous forces inherent to the liquid, or any combination of these, a surprising degree of control over the transfer of liquids between separating fiber networks can be reached.

3.2 Experimental Methods

3.2.1 Surface treatment

The same chemical-assisted plasma vapor deposition reactor detailed in Chapter 2 was used to create surface modifications for exploring the effect of adhesion on droplet transfer. Here, an additional tool available in the reactor, not previously mentioned in this thesis, was employed to change the contact angle hysteresis of the fluorocarbon-deposited paper substrates. By first subjecting the paper samples to an oxygen plasma etching pretreatment, the microscopic morphology of the fiber surface can be manipulated [116-118]. Because the cellulose fibers are composed of both crystalline and amorphous domains, there is a variation in reactivity across the fiber surface. When an oxygen plasma is introduced, it reacts selectively on the more vulnerable amorphous domains. This process etches away amorphous domains on the fiber surface, increasing its microroughness [119, 120]. A fluorocarbon film deposited on a surface with such hierarchical roughness will exhibit a smaller degree of contact angle hysteresis. This is because the wetted area of the surface is reduced and because the three-phase contact line is pinned at finer intervals [121]. The relatively smaller jumps the contact line must make to advance or recede along the surface reduces the amount of hysteresis [122-125].

Figure 3.1 illustrates the reactor's ability to precisely control the contact angle hysteresis by adjusting the extent of oxygen etching pretreatment. Without pretreatment, the fluorocarbon-deposited paper exhibits a contact angle hysteresis of about 130°. Although the paper is hydrophobic, a water droplet will remain fixed firmly on its surface, even if the paper is turned upside-down or shaken, due to the relatively low receding contact angle. After an hour of 15 sccm oxygen flow at 110 °C, with the reactor powered at 100 W, the advancing and receding angles of the subsequently-hydrophobized paper have converged to a narrow window around the static contact angle. At this near-zero level of hysteresis, it is difficult to get a water droplet off the pipette tip onto the paper, and the water droplet will glide off the sheet if it is tilted even slightly.

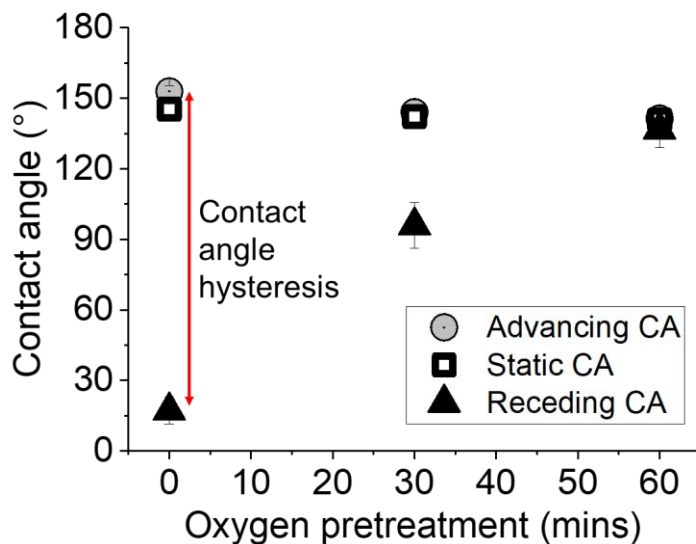


Figure 3.1 The contact angle hysteresis (difference between advancing and receding contact angles) on a paper substrate can be controlled by oxygen etching prior to fluorocarbon deposition. High-adhesion paper (HAP) and Low-adhesion paper (LAP) have the same level of hydrophobicity (static contact angle) but very different interactions with liquids.

3.2.2 *Transfer experiments*

To conduct transfer experiments, an apparatus called the Transfer Cell, or TCell, was developed (Figure 3.2). The tool consists of two parallel plates, the upper of which is moved by a position feedback controlled electric linear actuator (Actuonix P16-P 100mm stroke 64:1 gearing). Thus, the displacement (separation distance) between two surfaces can be precisely controlled. The controller parameters also enable some adjustment of the separation velocity, which is important for assessing the effects of inertia on transfer. Unless specified, the transfer experiments were conducted slowly enough to ensure that only the effect of surface forces was being considered. This was accomplished by separating the surfaces gradually, in small discrete steps, advancing to further distances only after any motion in the droplet had ceased. The average velocity of the upper plate throughout the experiments was about 10^{-4} m/s.

Observations of this motion were enabled by a camera viewing the droplet side-on. Incorporation of a camera facilitated measurements of transfer, which were estimated visually. This was accomplished by calculating the volume of a droplet from its profile, according to the equation for a spherical cap: illustrated in Figure 3.3. Provided that the droplets are sufficiently small ($< 5 \mu\text{L}$), and the surface has spatially homogeneous wettability, the droplet will adopt the geometry of a spherical cap. With a convenient method of calculating droplet volumes, their transfer behavior between surfaces can be represented by the transfer ratio (TR) [126, 127], with terms defined in Figure 3.3:

$$TR = \frac{V_t}{V_i} \quad (3.1)$$

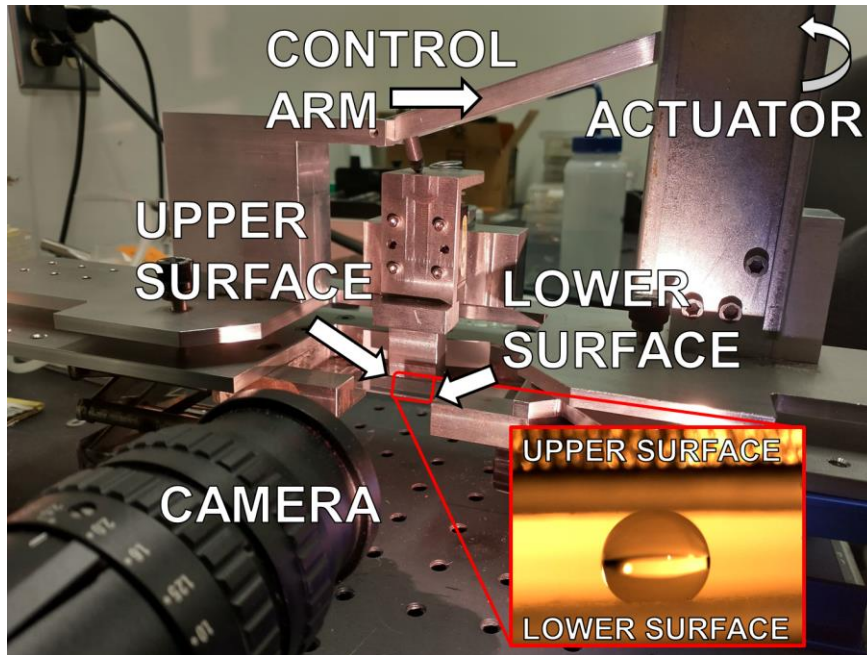


Figure 3.2 Transfer cell (TCell) used to conduct transfer experiments. The linear actuator pushes on a control arm that moves the upper surface down or up. The advantage of the control arm is that it trades down the length of the actuator's stroke for accuracy in the upper surface's displacement. The lower surface is fixed in place. A camera enables estimations of volume transferred. The figure inset highlights how the upper and lower surfaces are used to transfer droplets.

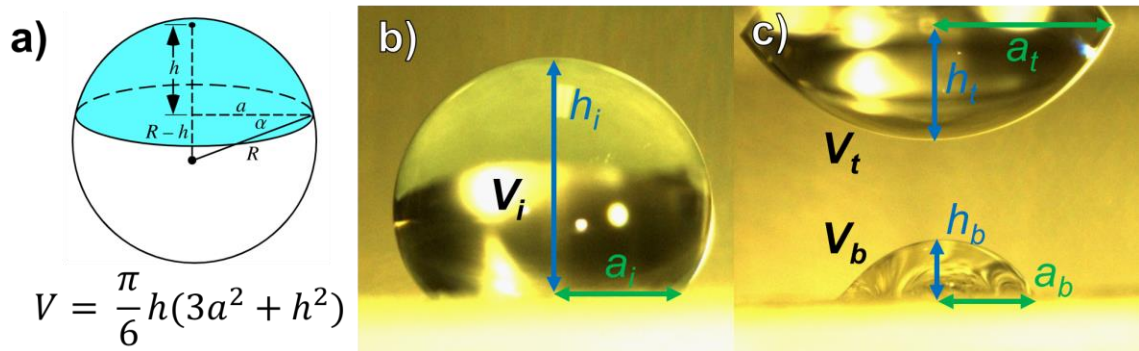


Figure 3.3 (a) Geometry of a spherical cap and the equation of its volume. Note, this equation is valid even when $h > a$. (b) Droplet in its initial state resting on the surface of the paper. The two measurements needed to estimate its volume are shown. (c) The quantity of the droplet which has been transferred to the opposite surface is estimated using the same equation. Equation and geometric model referenced from Wolfram MathWorld [128]

When the transfer ratio is zero, all of the droplet remains on the initial surface. When the transfer ratio is one, all the liquid transfers from the surface it was initially placed on to the opposing surface. For the sake of consistency, the droplet is always initially placed on the bottom surface in our experiments. The top surface, which has no liquid, is placed far away from the droplet. With the camera trained on the droplet, an initial measurement is taken of the droplet's volume. Then, the top surface is lowered and brought into contact with the drop. Once contact is made, the droplet forms a liquid bridge by adhering to the two surfaces. This bridge is then stretched by gradually pulling the top surface away from the bottom one. Eventually, the bridge breaks, resulting in a fraction of the liquid adhering to each surface. At this point, another measurement is made of the droplet volumes, to characterize the transfer behavior. Image stills illustrate this experimental procedure in Figure 3.4.

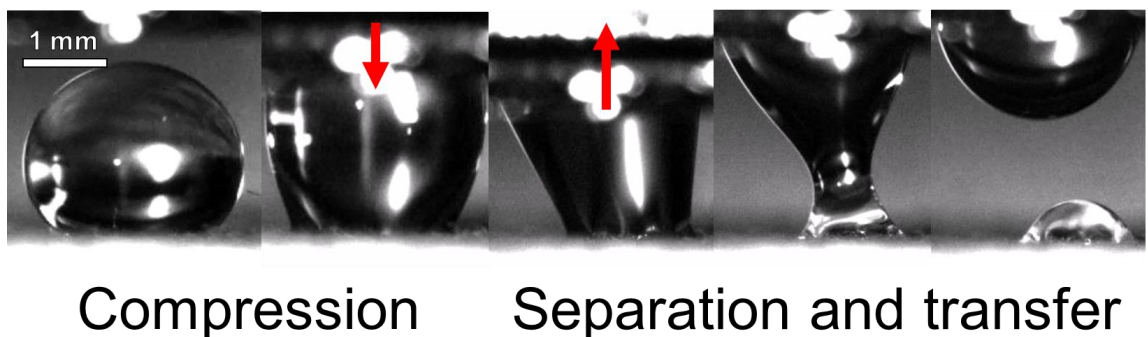


Figure 3.4 Frames taken from a transfer experiment. The droplet is squeezed between two surfaces that are subsequently pulled apart. This allows liquid to be transferred from its initial surface to another surface.

To justify the visual approach to volume estimation, the data in Figure 3.5 are reported. This graph illustrates the errors in volume conservation, across the trials conducted to formulate Figure 3.6. Notably, the vast majority of data points fall within $\pm 5\%$. Reassuringly, there is no pattern in these residuals; high levels of transfer have about as much error as low levels of transfer, and there are about as many positive errors as negative ones, in either direction. There is, however, a shortage of data points in the center, associated with $TR = 0.5$. This is because events where the droplet splits in half, under surface forces alone, are extremely rare. For that to happen, the wettability of the two surfaces must be nearly identical [129-131].

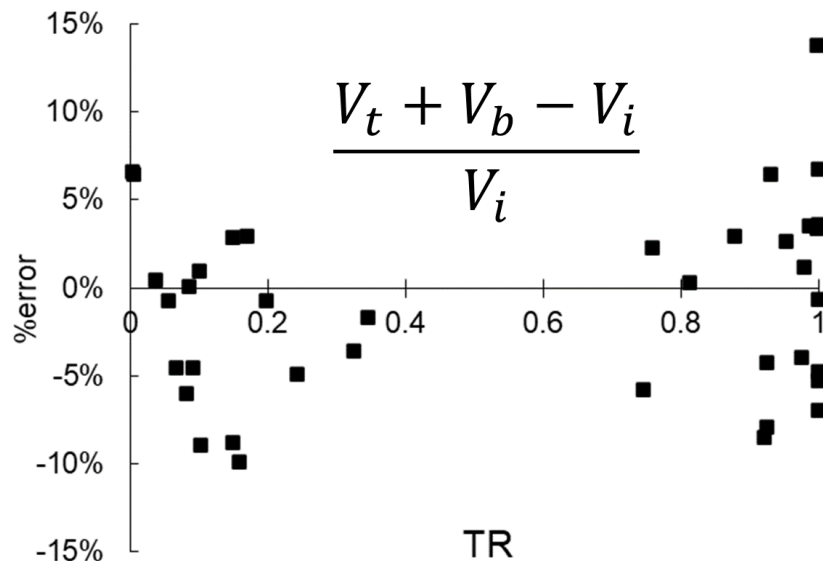


Figure 3.5 Errors in conservation of volume across trials conducted for the experiments in Figure 3.6. Volume subscripts refer to the drops depicted in Figure 3.3. The majority of errors fall within $\pm 5\%$, and there is no trend in the errors. Thus, the optical method used to estimate volumes in the experiments is justified.

3.3 Results and discussion

3.3.1 *Effect of contact angle hysteresis on adhesion of droplets to paper substrates*

To show how control over contact angle hysteresis affects the transport behavior of liquids between fibrous substrates, a water drop was placed on the surface of a sheet of paper with known contact angle hysteresis. Another surface was brought into contact with the droplet and pulled away. The two surfaces chosen for this exercise were a silicon wafer that had accreted a native oxide layer (SiO_x) and a fluorocarbon-deposited silicon wafer. Observing transfer to the two surfaces revealed the ability of a fiber network to transfer liquid to differently wettable surfaces.

As shown in Figure 3.6, contact angle hysteresis (adhesion) has a strong effect on transfer of droplets. Clear clustering is seen for trials with low hysteresis vs. high hysteresis. At low levels of adhesion on the paper substrate (circles), water droplets will leave almost no liquid on the phobic paper substrate when they are presented with another surface to wet. Whether the opposing surface is composed of native silicon oxide (hydrophilic: CA 60° ; open circles) or fluorocarbon-deposited wafer (hydrophobic: CA 110° ; solid circles) the droplet will still fully transfer. This is because of the large receding contact angle of the liquid on the low-hysteresis paper surface. Because the three-phase contact line can move freely along the surface, nothing prevents the droplet from leaving entirely [130, 132]. If however, contact angle hysteresis on the paper is high (triangles), the droplet does not so easily transfer from the surface. When presented with the fluorocarbon deposited wafer to wet (solid triangles), the majority of liquid stays on the adhesive paper, even though the paper substrate has a higher static contact angle ($140^\circ >$

110°) and is thus more hydrophobic. The total free energy of the system would be minimized if more of the droplet transferred away from the paper, but the high activation associated with a less-mobile contact line prevents this configuration from being realized. A smaller receding contact angle on the paper surface (oxidized silicon wafer; open triangles) results in a greater wetted area on the paper surface, according to Equation 1.7. Thus, a greater volume of liquid is retained on the paper when the liquid connection between the two surfaces is broken once the upper plate is raised.

Looking at the transfer of a water drop from a hydrophobic paper with high contact angle hysteresis to a silicon oxide surface reveals an exciting subtlety about surface forces at work in this system. I will explore in greater detail why drastically different transfer of liquid can occur between two surfaces, depending on the configuration of the liquid interface. The open triangle series in Figure 3.6 shows that drastic differences in transfer behavior are possible when liquid adhering to a high-hysteresis surface wets an opposing, hydrophilic surface. The outcome of transfer is highly sensitive to the configuration of the droplet [133]. With the hydrophobic, highly-adhesive paper, it is possible to observe a transfer of all, little, or some liquid to the silicon oxide surface, even though the surface and liquid chemistry remain constant. This range of outcomes is, on its surface, surprising, considering how much more wettable silicon oxide is than fluorocarbon-deposited paper.

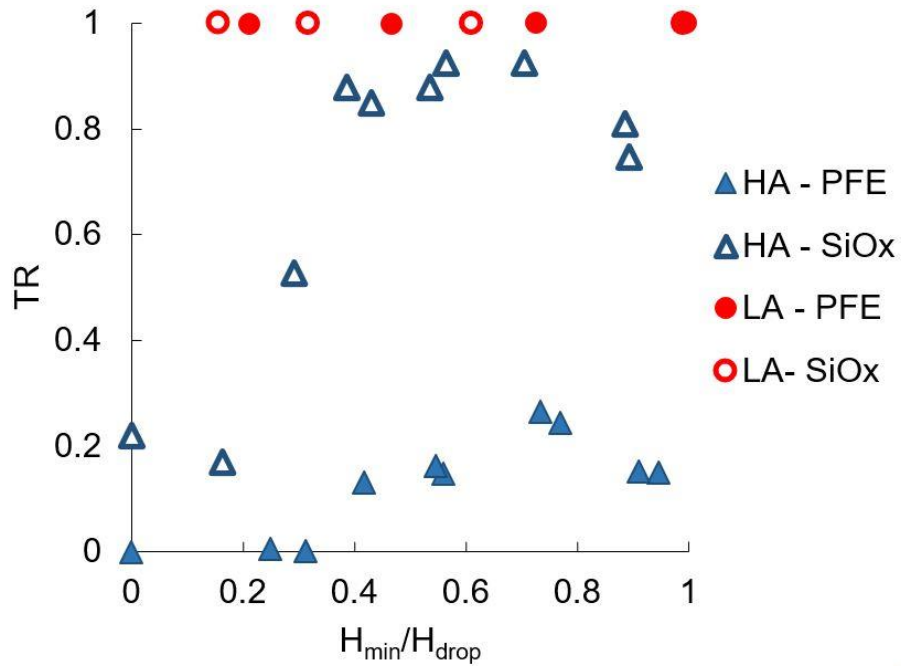


Figure 3.6 The transfer behavior of water droplets from papers of high (HAP) vs. low (LAP) adhesion to surfaces that are hydrophilic (SiO_x) or hydrophobic (PFE – fluorocarbon film). TR = 1 shows that papers with low contact angle hysteresis transfer all their liquid to another surface. The outcomes for transfer from high-hysteresis papers are much more varied. Depending on how much the droplet is compressed prior to separation, different transfer behavior is observed.

When the droplet is initially placed on the surface of the paper, its footprint is relatively small. Due to its high advancing contact angle, the water droplet will not spontaneously wet the surface beyond an angle of about 140°. When the hydrophilic silicon oxide surface is just barely brought into contact with the droplet, water easily wets it, resulting in a large footprint on the upper surface. If the upper plate is retracted at this point, the hydrophilic surface—with a larger contact area and smaller receding contact angle—will pull the majority of the water with it. The influence of both contact area and contact angle, identified in Equation 1.7, can be probed by compressing the droplet with the upper surface prior to separation.

Different transfer behavior is observed if, instead of barely touching the droplet with the upper surface, the upper surface is depressed to well within the original height of the droplet. Doing so squeezes the droplet between the two surfaces, expanding its contact line on both the upper and lower surface. When the surfaces are subsequently pulled apart, the contact line on the hydrophilic surface is once again more mobile than the contact line on the high-hysteresis paper. This time, however, the effect results in a greater contact line on the paper side. Because the contact line was expanded outwards on the paper surface during compression (and pinned in place with high hysteresis), the hydrophobic paper now holds the majority of liquid when the bridge breaks and the transfer ratio is low, even though a simple comparison of equilibrium contact angles would suggest a different outcome [134-137].

Altogether, these effects suggest that a great deal of control over the transfer of liquids between separating surfaces is possible. By adjusting the contact angle hysteresis, in tandem with manipulating the position of the contact line, a droplet can be encouraged to favor one surface over another.

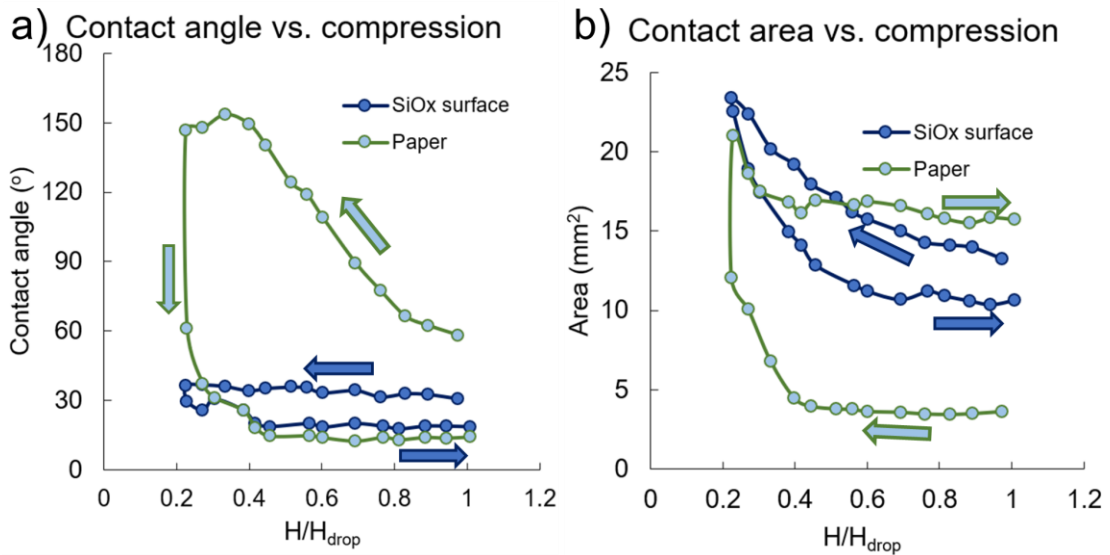


Figure 3.7 Profiles of contact angle and contact area of water droplets during compression and separation between high-hysteresis paper and a silicon oxide wafer. Arrows indicate the direction of compression or separation. Inflections around $H/H_{\text{drop}} = 0.4$ explain the transition in the open triangle series of Figure 3.6.

This picture can be explored in further depth by quantitatively analyzing videos of the transfer process. Figure 3.7 shows the contact angle and total contact area of the water droplet on each of the two surfaces for these transfer experiments during the compression and decompression phases; for this particular experiment the droplet was compressed to 20% of its original height. In Figure 3.7a, the large vertical gap in contact angles between compression and separation cycles for the droplet on the paper surface is indicative of high hysteresis, by definition. The initial contact angle of the droplet on the paper surface is about 140° . However, contact with the SiO_x surface deforms the droplet into a liquid bridge, changing its geometry and reducing the initial angle of the bridge on the paper surface to $\sim 60^\circ$. As the droplet is compressed, the contact angle with the paper surface gradually increases, while the contact line remains frozen (Figure 3.7b). The maximum angle (advancing contact angle) of 150° is reached at a relative compression of ~ 0.4 . Upon

further compression, the contact angle does not rise past 150° ; as expected, this advancing contact angle of water on the paper surface is in good agreement with the value measured on a goniometer (see Figure 3.1). Past a relative compression of 0.4, the footprint of the droplet on the paper surface begins to expand (Figure 3.7b). When the direction of compression is reversed, i.e. separation, the contact angle of the liquid on the paper surface adopts a minimum value as the contact line is retracting (definition of receding contact angle). Due to the high hysteresis of the fluorocarbon deposited paper, this receding angle is actually lower than the receding contact angle on native silicon oxide. The relatively close paths in Figure 3.7 for the silicon oxide surface are indicative of low hysteresis. The fact that the compression-decompression curves for the paper surface entirely encompass the oxide surface's is what makes such a wide range of transfer outcomes possible.

Another way to understand how transport behavior changes—although the fluid and the surfaces it contacts remain completely unchanged—is to realize that the boundary conditions defining the system are subtly changing [138, 139]. In Figure 3.7, relative compression of 0.4 corresponds to the moment when the contact angle transitions from increasing to being fixed. At the same time, the contact area transitions from being fixed to increasing. Another way to state this transition would be to say that the boundary condition of the liquid bridge contacting the paper shifted from an r -boundary to a θ -boundary [140-142]. That is, the defining aspect of the bridge's geometry changed from its contact radius to its contact angle. Notably, the degree of compression at which this change in boundary condition occurs ($H_{\min}/H_{\text{drop}} = 0.4$) is the same place that the transition in transfer regimes was witnessed in Figure 3.6. Thus, a change in the boundary condition defining the liquid bridge causes a change in droplet transfer efficiency.

3.3.2 Estimation of forces

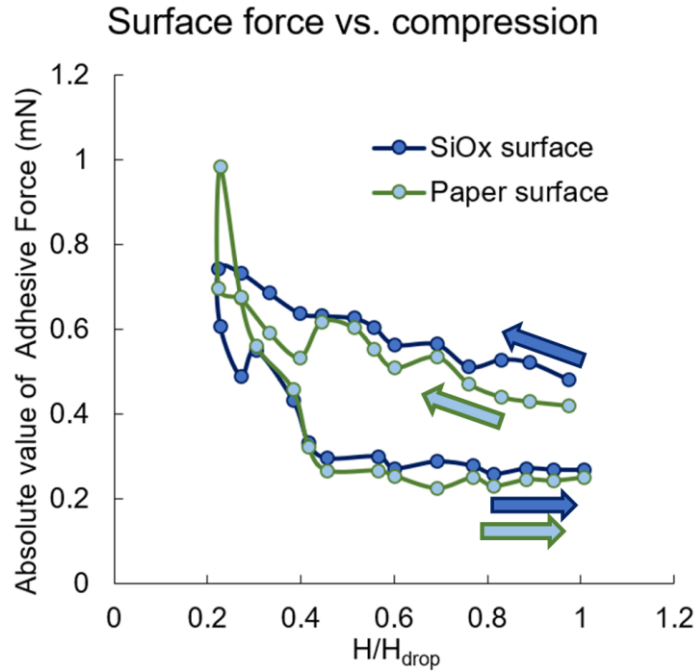


Figure 3.8 Surface forces estimated from measurements made in Figure 3.4 and Equation 1.7. The good agreement in the force balance suggests that my methods are accurate and that Equation 1.7 is a good description of adhesive forces on fibrous substrates.

With the data from Figure 3.7, the adhesive forces acting on the droplet can be calculated according to Equation 1.7. Estimates of the adhesive forces that the paper and silicon oxide surfaces exert on the droplet over the compression and separation cycle are depicted in Figure 3.8. The curves mostly overlap, indicating that the calculated forces are balanced. This is reassuring because the actual forces acting on the droplet must be balanced, as there is no motion of the droplet at each point of measurement in these pseudo-static experiments [143].

One interesting question is why Equation 1.7, which was derived for perfectly flat, chemically uniform surfaces, does such a good job at modelling adhesive forces of droplets

on a sheet of paper. After all, the previous chapter discussed paper's complexity and heterogeneity—and the ultimate importance of these factors on wetting. Why does adhesion not seem to be similarly affected by the unique structure of paper?

The reason likely hinges on the difference in length scales between the two studies [144]. In Chapter 2, the fluid was flowing into and through the pores of the fiber network, so the paper's microscale geometry had a significant impact on the curvature of the fluid interface—and thus, critical wetting behavior. In the case of adhesion, the paper's microstructure still affects the observed, overall wetting behavior—albeit in a subtly and importantly different way. The structural and chemical heterogeneity of the hydrophobized paper gives rise to the receding contact angle of a droplet on the surface, as discussed before. This receding contact angle can then be treated as a macroscopic property of the surface. Thus, at the length scale of the droplet's contact line with the paper, the effect of all those heterogeneities and complex pore geometries can be captured by a single number. Because the radius of the droplet is about 2 orders of magnitude larger than the intricate features of the paper surface, the paper “appears” to the droplet as a macroscopically uniform surface with a characteristic wettability [103, 145, 146].

Having demonstrated that Equation 1.7 has some validity for modeling the adhesive forces of liquids to paper substrates, we can use it to assess the effectiveness of leveraging adhesion to prevent rewet. The main conclusion is that the adhesion of water to the wet web cannot be overcome with surface forces. The near-zero receding contact angle of water on wet cellulose results in a correspondingly large contact line [147, 148]. The only way to combat this would be to oppose the highly hydrophilic paper web with a felt of equally high hydrophilicity, or otherwise engineer the felt material to have a zero degree receding

contact angle. Even in this limiting case, half of the water would still adhere to the paper surface, implying that separation rewet cannot entirely be avoided with this strategy [149-152].

3.3.3 *Dynamic effects*

If surface forces alone cannot overcome the adhesion of liquid to the paper web, perhaps another force can be leveraged to overcome its high hydrophilicity. In the case of droplet transfer, two such forces are available. Inertial forces will tend to oppose any acceleration of the fluid [153-155]. If the fluid begins at rest, such as in the case of these transfer experiments, inertial forces act to prevent flow. Another possibility are viscous forces, will act to retard flow in any direction [156, 157]. In both cases, the impact of these forces is most relevant at high velocities (dynamic regime). After all, the transfer experiments described above were conducted extremely slowly to avoid the influence of these forces. By conducting transfer experiments at higher speeds, it should be possible to use these forces to obtain transfer outcomes that differ from expectations informed by surface wettability alone [158].

Figure 3.9 summarizes a demonstration of transfer under dynamic conditions, compared to the static (surface force-controlled) case. Amazingly, it is possible to transfer water from a highly hydrophilic glass surface to an opposing surface coated in a hydrophobic fluorocarbon film. This is done by bringing the droplet in contact with both surfaces, then rapidly pulling them apart. Some of the liquid leaves the glass surface and adheres to the fluorocarbon surface. If the two surfaces are separated slowly, however, all the water remains on the glass surface. Under rapid separation, the separation velocity is

about 0.3 m/s, so the Weber and Capillary numbers are about 1 and 0.004, respectively. This implies that inertial forces are about as strong as the surface forces on the droplet, while viscous forces on the droplet are not dominant at this length and time scale in spite of the higher fluid velocities.

Clearly, the inertial forces present at short time scales can play some role in counteracting the surface forces that favor rewet. While this is potentially encouraging for applications in a press nip—where high velocities are present—there are limitations to using this strategy to prevent rewet. Because inertia opposes motion, flow in the droplet is arrested. The limiting case of this behavior divides the droplet in half when two surfaces with similar wettabilities are separated. Although the tendency to wet the more hydrophilic surface can be overcome to an extent, half of the droplet would still adhere to the paper web under a purely inertial regime [159]. Once again, the conclusion is that separation rewet cannot be entirely avoided.



Figure 3.9 Dynamic transfer can be used to transfer liquids against the wetting gradient. By separating the surfaces quickly, 30% of a droplet initially on a silicon oxide surface can be transferred to a fluorocarbon deposited surface.

3.3.4 *Flux boundaries*

As a final consideration, the porous nature of the paper web and the press fabric means that fluid can also flow into each of these separating substrates while they are being pulled apart; this complicates the transfer behavior immensely. To fully understand the mechanics of separation rewet in a press section, it is necessary to simultaneously consider adhesive surface forces, inertial forces, and flux into each of the substrates. Although this is far too complex a study to be given the full attention it merits here, I hope to illustrate a few concepts that emerged during this research and ultimately inspired a new approach to solving rewet that is described in Chapters 4 and 5.

The possibility of fluid flowing into a substrate, rather than only wetting its surface corresponds to an entirely new boundary condition available to define the liquid bridge system. As was seen earlier in this chapter, changing the boundary condition that defines a liquid's interaction with a solid can result in radically different transfer outcomes. In the final set of experiments for this chapter, a water droplet resting on high-hysteresis hydrophobic paper was brought into contact with an absorbent piece of paper. The rate of flux into this absorbent paper was controlled by partially hydrophobizing it with a light deposition of fluorocarbon film (Figure 3.10a). The extent of this deposition is represented by the approximate thickness of fluorocarbon film that builds on a flat silicon wafer placed next to the samples during coating.

The effect of dynamics can be seen in Figure 3.10b. The slowest absorbing paper was able to transfer the most liquid off the highly adhesive surface. When the rate of flux into the boundary was large, however, less liquid was transferred—even though this

absorbent paper was more hydrophilic. Once again, higher velocities resulted in increased inertial forces and a tendency of the droplet to resist the influence of surface wettability.

Figure 3.10b shows that, regardless of absorbency, fluid tends to transfer away from a no-flux boundary towards a flux boundary (all TR > 0.8). Although that may seem incredibly obvious, it was this realization that initiated the course of investigation that will be covered in the next chapter. For now, it suffices to suggest that creating conditions under which the paper web serves as a no-flux boundary, while the felt serves as a flux boundary, could be the first step towards achieving a fabric with unidirectional flow properties.

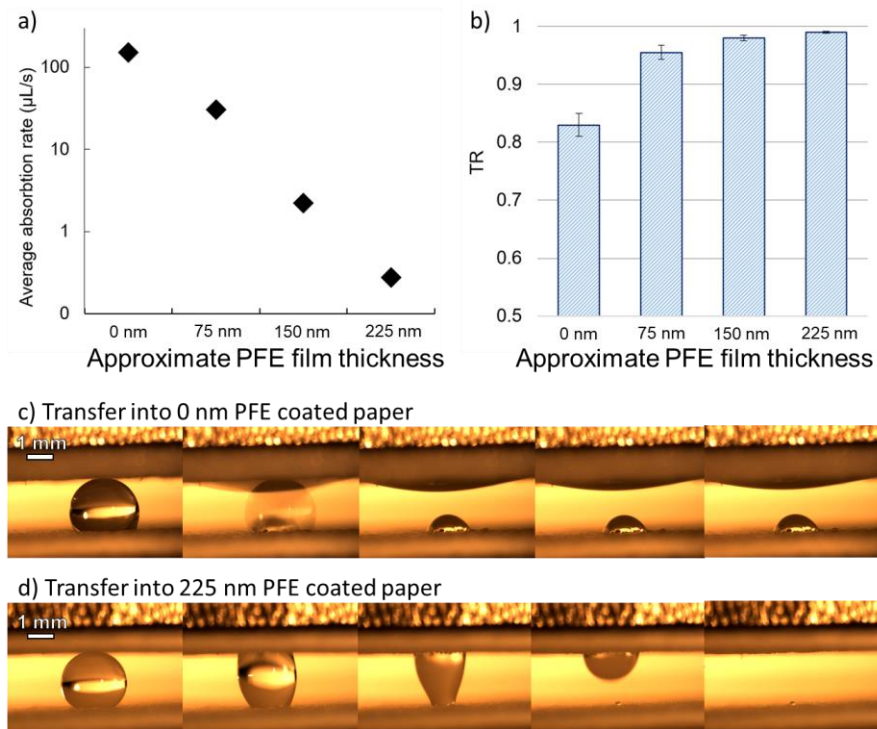


Figure 3.10 Flux into the boundary must be considered when the substrates are porous. (a) The rate of flux can be controlled by partially hydrophobizing the absorbent material. (b) Transport will tend to move liquid from the no-flux boundary to the flux boundary. (c, d) The effect of dynamics is visible for experiments involving flux into the boundary.

3.4 Conclusions

In this chapter, we saw that contact angle hysteresis (adhesion) can be controlled by manipulating the microstructure of a surface. Changing the level of adhesion resulted in control over transfer of a droplet from this surface. At the same level of hydrophobicity (static contact angle), drastically different droplet transfer behavior was observed, depending on the level of adhesion. For low-adhesion samples, droplets tended not to stick, no matter what alternate surface wettability was available. For high-adhesion samples, the picture was more complex. When a water droplet resting on a hydrophobic, but sticky, surface was contacted by a hydrophilic surface, how much liquid transfer occurred varied wildly. As was discussed, this could be accounted for by the changing boundary conditions that define the liquid's interaction with the solid surfaces. Even in cases where the liquid and two solid surfaces are exactly the same, the gamut of possible transfer outcomes testifies to the subtleties of the physics of wetting. Properly understood, knowledge of these effects can be used to precisely control the fate of liquid between separating surfaces.

When it comes to paper, however, its near-perfect hydrophilicity ties our hands. Only so much can be done to combat wetting on a perfectly wettable surface, even if inertial forces are leveraged. Such limitations meant that controlling adhesion was not a viable path to completely eliminating rewet. Furthermore, these mitigation strategies are already largely discussed in industry studies. For example, previous authors have mentioned that separation velocity should be increased as much as possible and that the felt should be made as hydrophilic as possible. Because of the complexity of the real process, fundamental problems with developing an effective solution that relies on adhesion, and

fairly comprehensive discussion in the existing literature, the project needed to innovate a radically new conceptual approach to eliminate rewet.

Fortunately, the work on flux boundaries provided an inkling on where to begin this next stage. Three simple, but key, observations from that study motivated the course of investigation that ultimately led to this thesis's most novel and impactful contributions. One, surfaces do not have to be in direct contact to transfer liquid. Two, liquid will transfer from a no-flux boundary into a flux boundary. Three, when the liquid bridge becomes too thin at the end of this transfer, it breaks.

CHAPTER 4. INSTABILITY ENHANCED DEWATERING

4.1 Background and scope

Given the limitations of eliminating rewet identified in the previous two chapters, a new approach to solving the problem is clearly necessary. The capillary forces exerted by the sheet are too strong to overcome while also maintaining high permeability in the press fabric. Likewise, the adhesion of liquid to the highly hydrophilic web means that at least some water will always transfer back to the sheet under separation. The work in this chapter of the thesis began with the revolutionary concept of inverting the order of operations during pressing to overcome these limitations. I reasoned that if the felt were separated from the paper web before decompression, instead of simultaneously, perhaps the driving forces that cause rewet could be sidestepped entirely. Essentially, this idea flowed from the key conclusions of work on transfer of liquids between surfaces in the previous chapter. I just needed to find a way to translate the concepts of no-flux boundaries and liquid bridge breakup to a press section.

Fortunately, the mechanical properties of the felt and paper sheet suggest a way of accomplishing this vision. Because paper is more compressible than the press fabric, its void volume becomes completely collapsed under the pressures applied in the nip. After all, this is how removal of the sheet's free water is accomplished in the first place. That means that under pressure, the paper substrate can be treated as a surface with an impermeable boundary. Since I want to encourage transport away from this surface, the opposing material, a press felt, should retain an open pore structure to absorb water. The only remaining challenge is to suspend the felt at a distance from the paper—all under nip

pressure—so that a gap is created for the liquid channels to break at the end of transfer. Fortunately, these goals can be accomplished mechanically. Insertion of a stiff spacer between the felt and web preserves void space under pressure, allowing air to enter the interface after the liquid bridges break. Now, when the system undergoes decompression, the sheet has already been completely dewatered and there is no path for reflux to the sheet.

This starting idea evolved over the course of experimentation from demonstrating a simple proof of the concept, to exploring the intricate fundamentals of liquid bridge breakup. As I quickly discovered, basic ideas about inverting the order of events during pressing and simply creating void space at the paper-web interface are not the full picture. For the spacer to work most effectively, its geometry and surface chemistry must be carefully coordinated. This can only be done with an appreciation of the fundamental fluid mechanics that drive enhanced dewatering.

Ultimately, the technology developed in this chapter constitutes an entirely new approach to achieving one-way flow. While other methods have previously been developed to promote unidirectional flow, this approach provides a solution where those existing techniques fail to be practical, such as in a paper machine press section. This thesis is the first to develop, discuss, and optimize the Plateau-Rayleigh interfacial instability to enhance dewatering of porous media. Key advantages of leveraging the Plateau-Rayleigh instability to prevent reflux include: a passive design with no moving parts, a highly permeable structure that does not restrict flow, and a short timescale of operation amenable to rapid industrial processes.

In this chapter, I investigate the effect of the spacer's structural parameters on enhanced dewatering, as well as the impact of surface wettability. One major insight is that this technology results in enhanced dewatering for liquids with a wide range of surface tensions and viscosities. In addition to numerous data exploring the effects of surface wettability and liquid properties on enhanced dewatering, analysis of videos of the dewatering process supplement and inform discussion of the fundamental aspects of fluid physics at play.

4.2 Experimental methods

Whatman cr17 chromatography paper was used as the paper substrate in this study. Its chemical purity (98% cellulose of softwood origin) eliminates any complexities that would arise from chemical heterogeneity. Furthermore, its thickness (0.9 mm), elasticity (1 GPa, wet), and pore size (75 μm) exacerbated the reflux phenomenon. An elastic, highly hydrophilic paper sample with larger pore volume—compared to other papers—tends to increase the quantity of water that can return to the web. This was helpful in exploring the effect of spacer and fluid properties on mitigating reflux, as their effects were more pronounced. Overall, the fiber mat that constitutes the paper sample exhibits anisotropy, due to the aspect ratio and orientation of the fibers that results from prior processing. By the time that the paper sheet arrives at the press, its internal structure is largely already fixed. This means that the structure of the sheet is not a controlled variable in dewatering. The details of this pore structure are important in determining the extent of dewatering achieved in the compression phase. However, we are primarily interested in the extent of reverse flow in the decompression phase, which arises in the film outside the surface of the paper and is thus less sensitive to the intricacies of porosity.

Prior to pressing, the initially dry half square inch sheet was wetted to a moisture ratio of 2 (67 wt.% water and 33 wt.% solids). The sheet was then pressed with varying felt configurations at a given pressure for 30 seconds. A screw press (Figure 4.1) was used to apply a one-dimensional pressure gradient, and a TE Connectivity FC23 500 lb. piezo load cell enabled accurate control of applied stress. After pressing, the mass of the pressed sheet was compared to that of the dry sheet to determine its moisture content. Moisture content is reported in terms of the moisture ratio, which is defined as:

$$MR = \frac{m_{water}}{m_{fiber}} \quad (4.1)$$

The press felt used in the study was obtained from a commercial supplier, AstenJohnson. The felt consists of a non-woven nylon batt—thin randomly oriented fibers used as the surface layer—spun from 3 dtex cap fibers stitched onto a woven base. The stainless steel meshes used as spacers were obtained from McMaster—Carr. Metal meshes of standard mesh numbers were used: 20, 30, 70, 200, and 400. Additionally, a 150W mesh (nonstandard version of 150 mesh with wider holes) with higher than standard open area was tested as a counter-example to liquid bridge instability. The mesh parameters are summarized in Table 4.1.

Table 4.1 Static contact angle of water on each mesh and physical dimensions. 70+ and 70- refer to #70 meshes that were hydrophobized and hydrophilized, respectively.

Mesh #	Static water contact angle (°)	Wire diameter (μm)	Hole width (μm)	Radial / axial curvature	Open area
20	wets	427	849	1.0	44%
30	63.8	325	516	1.3	38%
70	68.3	136	180	1.5	32%
70 +	118.3	136	180	1.5	32%
70 -	wets	136	180	1.5	32%
200	78.3	53	75	1.4	34%
400	83.1	25	36	1.4	35%
150W	63.7	45	118	0.76	52%

In trials exploring the effect of spacer wettability, the surface of the metal mesh was modified in two ways. First, plasma-assisted chemical vapor deposition of a fluorocarbon film resulted in a surface with a water static contact angle of 110°. Second, electrochemical etching of the mesh in nitric acid resulted in a hydroxylated surface that had a water static contact angle of 40°. For details about the plasma and electrochemical reactors, please refer to the references [58, 61, 160].

In trials exploring the effect of surface tension, sodium dodecyl sulfate (SDS), sourced from Sigma-Aldrich, was used to alter the interfacial tension of the fluid phase. Because surfactants tend to aggregate at the surface, it was assumed that addition of SDS did not affect the thermodynamic concentration of water absorbed in the cellulose fibers at any given pressure. By using concentrations of 0, 2.0, and 6.0 mM SDS, fluids with surface tensions of 72, 61, and 40 mN/m were achieved, respectively [161].

Videos of pressing were captured on a Leica DM IRB inverted fluorescence microscope and subsequently analyzed with image processing functions in Matlab

software. To make the liquid phase more visible, dilute fluorescein-labeled dextran was dissolved in the water. Analysis, therefore, could take advantage of changes in brightness to estimate the spatial distribution of moisture in the system over time. With synchronized pressure data from the load cell, the dependence of this moisture distribution on the applied stress was determined. Due to optical constraints, the distribution of water is observed at the edge, not the center, of the media. Because of this limitation, I am reluctant to claim that this analysis provides quantitative data about water distribution throughout the bulk of the pressed paper. Nevertheless, the video data serves as a strong semi-quantitative visualization of how the enhanced dewatering mechanism operates.



Figure 4.1 Screw press (foreground) used to exert a one-dimensional pressure gradient in dewatering experiments. A force sensor (readout in background) allows precise control of the applied stress.

4.3 Results and discussion

4.3.1 Effect of spacer parameters on enhanced dewatering

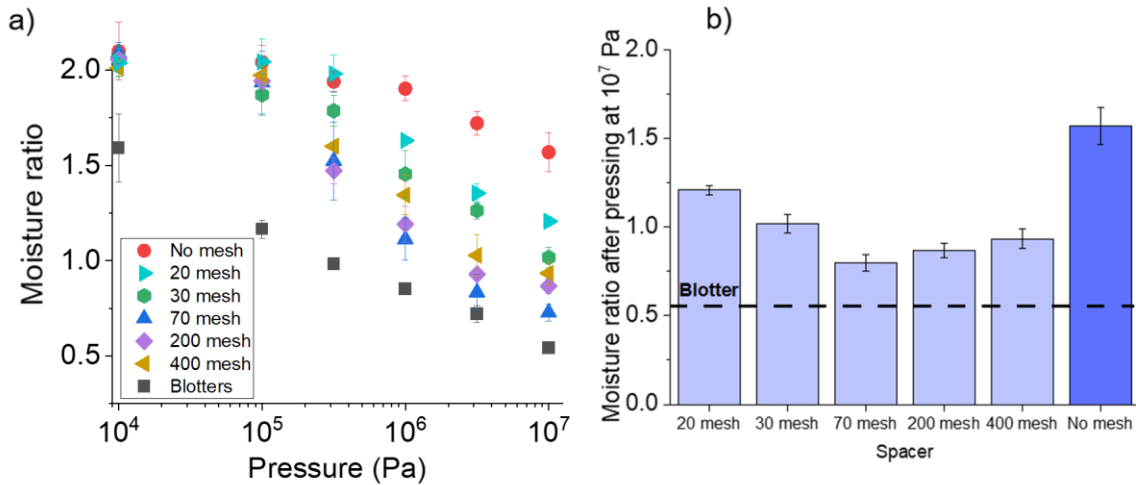


Figure 4.2 (a) Effect of mesh number on final moisture ratio of chromatography papers pressed against a commercially available press felt. Various spacers were layered between the paper and the felt, as specified in the legend. No mesh series refers to a scenario where the paper is pressed directly against the press felt. To capture the limits of dewatering, with no reflux, a stack of blotters (Blotters series) was used. (b) The data points at the highest pressure tested in (a) are compared. Structural parameters of the meshes have a strong impact on enhanced dewatering, and the 70 mesh was the optimum of materials tested.

Figure 4.2a shows what happens to paper pressed with different felt configurations as the applied stress is increased. As pressure is increased, more dewatering is accomplished. For low applied pressures, the extent of dewatering is minimal, because there is not enough force to push the water out of the paper into the fabric, which is slightly less hydrophilic. Once the pressure reaches a threshold of about 300,000 Pa, significantly more water is removed. This aligns with the moment that observable deformation of the web, which has a modulus on the order of 10^6 Pa, occurs. As applied stress is further

increased, additional dewatering is obtained, although an asymptotic limit is approached. The diminishing return can be attributed to the components of free and bound water. At lower pressures, mechanical work primarily collapses the void volume of the paper web, driving out the relatively easy to remove free water that fills the large pores between fibers. At higher pressures, additional mechanical energy is devoted to removing bound water, water that is chemically interacting with the cellulose fibers. These intermolecular interactions determine the thermodynamic equilibrium of water content for the sheet at any given pressure. This can be expressed as a balance between the applied stress and the osmotic pressure of water absorbed in the fibers.

The equilibrium moisture value at any given pressure is captured by the bottom series in Figure 4.2a (black squares). These data were created by pressing the sheet against a stack of paper blotters that is sufficiently thick ($n = 3$) to irreversibly absorb water, instead of against a press felt. Blotters are highly absorbent sheets of paper that are used to remove water during manual manufacturing of paper sheets. Although it would be utterly impractical to dry paper commercially using three times the amount of paper produced, blotters provide a convenient way to eliminate reflux on the lab scale. Three blotters were used because preliminary experiments showed that addition of a fourth blotter showed no marginal improvement in dewatering, compared to using three blotters. This was done to ensure that dewatering was not limited by the capacity of the sink. Because the blotters are as hydrophilic as the paper being dewatered, reflux from a blotter stack to the sheet is presumed to be minimal. The cyan series in Figure 4.2a illustrates what happens when a conventional press fabric is used to dewater the sheet. The higher moisture ratio for the sheet pressed against the commercial fabric compared to the sheet pressed against the

blotters is attributed to rewet. At the highest stress applied, rewet results in more than double the moisture content after pressing—a significant problem, because all moisture after pressing must be removed through energy-intensive thermal drying.

Figure 4.2a also compares the moisture ratio of pressed sheets with various commercial meshes sandwiched between the sheet and paper web. At low applied pressures these spacers have a negligible impact on dewatering; when the pressure is too low to deform the paper sheet, the mesh—if anything—diminishes contact between the sheet and paper web. In contrast, at higher pressures, when the sheet becomes significantly deformed and void volume in the paper is decreased, the enhanced dewatering capability in the presence of mesh spacers becomes apparent. Addition of a stiff, porous spacer layer to the surface of a commercial press fabric results in less moisture in the pressed paper. For all the mesh structures tested, there was significant improvement in dewatering, but the details of the mesh design and dimensions clearly matter. For the best performing mesh spacer in Fig 4.2 (70 mesh), the dewatering efficiency approaches the theoretical limit defined by the blotter stack.

It is perhaps non-intuitive that adding a spacer between the web and felt could result in improved dewatering. After all, the spacer decreases contact between the two media, and good contact is presumably necessary for transfer of water. This surprising result led me to wonder what fluid physics phenomena are causing enhanced dewatering.

4.3.2 Mechanism of enhanced dewatering

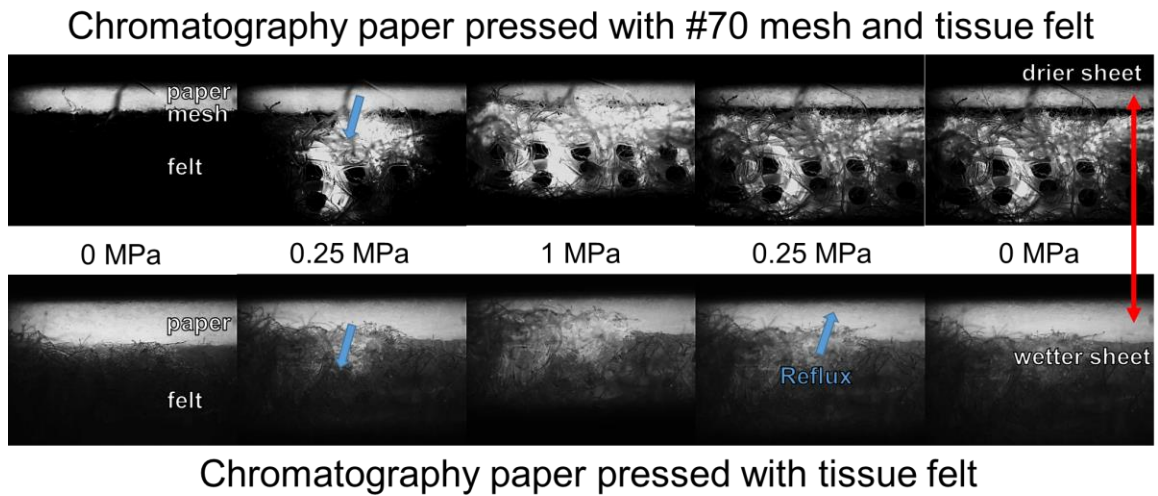


Figure 4.3 Frames from videos of paper being compressed. Fluorescent dye was added to the water to make the liquid phase more apparent. Higher brightness corresponds to more moisture. The breakup of liquid bridges is responsible for preventing reflux to the sheet.

To elucidate the mechanism of enhanced dewatering, I performed video microscopy of the pressing process. Water was labeled by dissolving a low concentration of dextran with fluorescein tag, so that the water presence can easily be detected in epifluorescence mode of the microscope; the light areas in the videos thus represent the liquid phase. Selected frames from two of these videos are shown in Figure 4.3, one with and one without mesh. The full videos are included in a supplementary media.

The bottom row of images (Figure 4.3b) shows the water distribution when pressing the sheet with a commercial fabric. From left to right, the system first undergoes compression then decompression. As pressure is increased, water is driven from the sheet into the fabric. Under the maximum applied pressure (middle image), much of the water is removed from the web, but a continuous liquid bridge spans the interface between the web

and the felt. As the system is decompressed, this bridge provides a path for reflux of water from the felt back into the sheet.

When a mesh is added between the paper sheet and felt (top row of images-Figure 4.3a), water is once again driven out of the sheet as pressure is applied. However, as it flows into the fabric, the liquid bridge breaks, leaving no continuous path for fluid to reflux. Therefore, once the system is decompressed, minimal amounts of water return to the web. There is still a driving force for transport from the felt towards to the sheet, which exhibits stronger capillary forces, upon decompression. However, the mesh creates a void space filled with air that provides a barrier to rewet. A more detailed consideration of the physics of this breakup process—which is at the very heart of enhanced dewatering—will be given in the discussion section. For now, these basic, qualitative observations will be augmented with a more quantitative analysis of the pressing videos.

In addition to the illustration provided by Fig. 4.3, frame-by-frame analysis of the distribution of water was carried out to illustrate in more detail, at least semi-quantitatively, how the improvement in dewatering was obtained. For every frame, the brightness values are averaged over each horizontal row of pixels in the image; this yields a vector that characterizes the spatial distribution of water in this one-dimensional flow scenario. With this tool, mathematical methods can be applied to more exactly describe the behavior of this system. First, some technique is needed to identify what features of this brightness profile correspond to water in the paper sheet. Looking at Figure 4.4a, the peak in brightness associated with the wet paper is symmetric and looks roughly normal. Inspired by signal deconvolution used in spectroscopic applications, I decided to regress the brightness peak to a Gaussian curve. The exact choice of what model was used to regress

this peak is not essential; likely, a simple Riemann sum would have sufficed to calculate the peak area. Ultimately, the approach adopted is justified by the excellent fits obtained by regression of the brightness vector to a Gaussian throughout the analysis.

The area under this peak (normalized area of brightness) was used as a proxy for the water content of the sheet. Strictly speaking, this is not a perfect quantitative representation of water content due to optical effects. The videos record the sheet from the side, so that only the edge of the sheet is imaged, which may not be fully representative of the bulk sheet. Furthermore, the fluorescent imaging is not fully quantitative due to scattering from the sheet itself. For example, the apparent peak area changes slightly with applied pressure, even in the absence of dewatering, likely due to changes in scattering as a result of changes in void volume fraction. Nonetheless, remarkable agreement was obtained between optically-estimated moisture content and that directly measured in prior experiments under the same conditions. Since pressure data acquisition was synchronized with the microscopy, the evolution in normalized brightness (as proxy for sheet moisture content) can be tracked as a function of applied pressure during the course of a pressing experiment; thus a dynamic equivalent to Figure 4.2 can be produced directly from the video data (Figure 4.4b). The similar behavior between the two separate experiments suggests that there is no time delay in dewatering, at least under the conditions in these experiments. For each frame (time point) the dynamic video data agrees with the static experiment. Thus, we can conclude that pressing is conducted under pseudo-equilibrium conditions. Another conclusion that can be drawn is that concerns about optical limitations, while valid, do not override the value of the data sets generated from analysis of the videos.

Comparing the analyzed videos of dewatering with and without a spacer, one notices a couple key features. First, the behavior under compression is nearly identical. As stress is applied, the sheet relinquishes its water to the same extent, in either case. It is only upon decompression that a difference arises. With the spacer, rebound in the water content of the sheet is minimal. Without the spacer, however, significantly more water returns to the sheet as pressure is relieved. This observation shows that the spacer really is preventing the *reflux* of water, not increasing water removal in the first place.

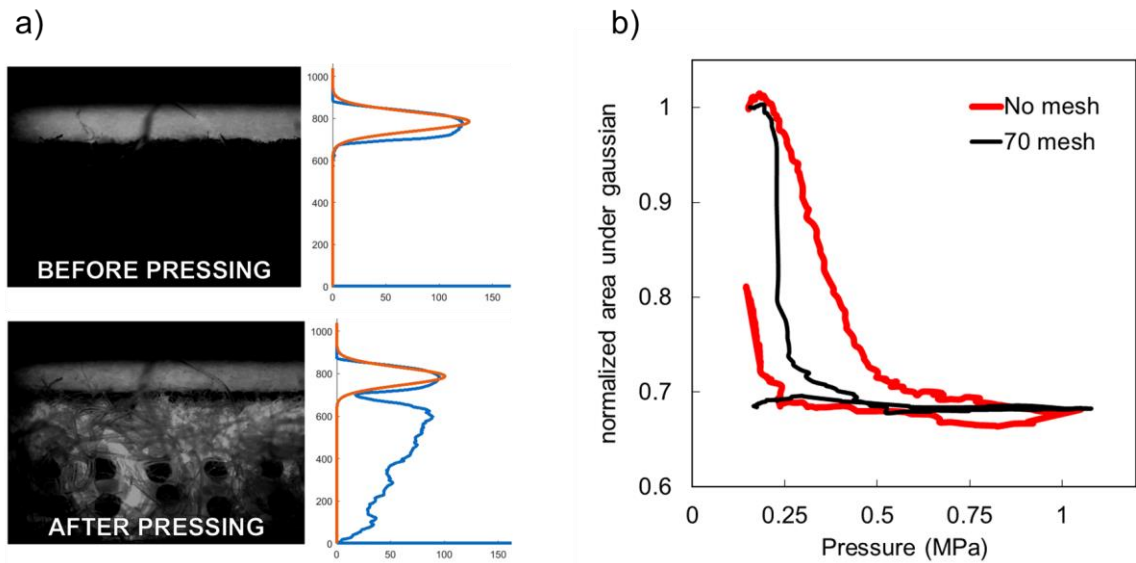


Figure 4.4 Frames from the videos are analyzed. (a) The brightness distribution in the felt-web system is averaged row-wise to create a vector of the moisture content in the direction of flow (blue curve). The peak is fit to a Gaussian distribution, whose area corresponds roughly to the water content of the sheet (orange curve). (b) The area under the orange curve is normalized against the total brightness in the image and plotted against synchronized pressure data. With or without the mesh, the sheets are pressed to the same minimum moisture content. The no mesh series, however, regains brightness after decompression.

4.3.3 Effect of spacer wettability

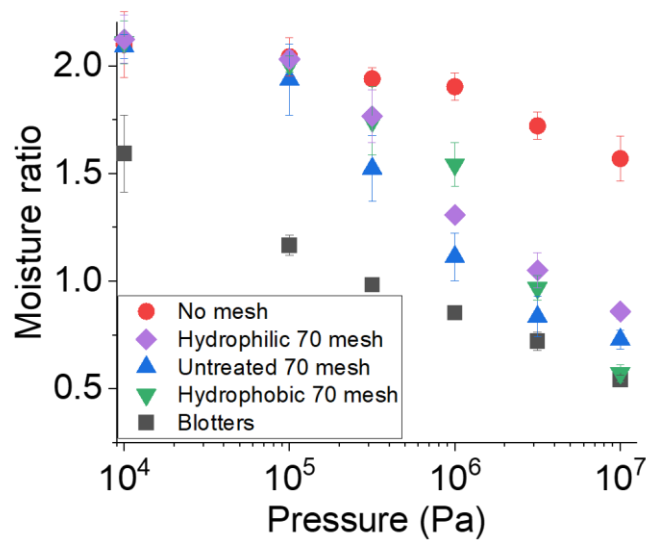


Figure 4.5 Effect of mesh wetting properties on enhanced dewatering. Altering the wetting properties of the spacer changes pressed moisture of the sheet by about 10%, on average. Compare this to the effect of the spacer’s presence. Removing the spacer increases the sheet’s water moisture by 120%. At the highest applied pressure, the hydrophobized mesh falls almost on top of the blotters, nearly eliminating reflux

Clearly, the extent to which water is able to remain at the felt-web interface during pressing has a strong impact on the final moisture content of the dewatered paper. In the discussion section, we will reason more generally about the factors that contribute to this outcome. To facilitate that discussion, and to provide more evidence for the conclusions that will ultimately be advanced, the effects of the spacer’s surface wettability and of the liquid properties on dewatering are explored. Because the liquid bridge’s behavior is the crux of the issue, it stands to reason that varying the liquid’s physical parameters—including its interaction with the solid substrate—will elucidate the fundamental causes of enhanced dewatering.

First, I investigate the effect of changing the spacer's wetting properties on dewatering. The chemistry of the stainless-steel mesh was altered with electrochemical etching in nitric acid to make it more wetting [162, 163]. The contact angle on the oxidized stainless-steel surface was about 40°, compared to native stainless steel which had a static contact angle of about 70°. Another mesh was coated with a fluorocarbon film, using the plasma reactor referenced in the previous two chapters [59, 62]. This brought the contact angle of water on the surface up to 110°. All three of these meshes, when used as spacers between the felt and the paper web resulted in better dewatering of the paper. Compared to pressing with the press fabric alone, insertion of a spacer with any wettability results in less water remaining in the sheet. The obvious clustering of these data, especially compared to the no-spacer control, suggests, at a quick qualitative glance, that surface wettability is not the predominant driver of enhanced dewatering. In the interest of being more quantitative, the relative sizes of these effects can be calculated from the data in Figure 4.5.

The cosine of the contact angle is representative of the surface wettability, so $\frac{dMR}{d \cos \theta}$ characterizes the effect of surface wettability on enhanced dewatering. From the data in Figure 5, $\frac{dMR}{d \cos \theta} = -0.1$ at an applied pressure of 10 MPa. That means, changing the surface from neutrally wettable (contact angle = 90°) to perfectly non-wetting would result in a 10% drier sheet. On the other hand, changing the surface from neutrally wettable to perfectly hydrophilic would result in a 10% wetter sheet. The magnitude of this effect can be compared to the difference in sheet moisture observed with having a spacer at all. Removal of the untreated 70 mesh spacer results in a 120% wetter sheet: more than twice as much water remains in the paper after pressing. Considering this fact, the data in Figure 4.5 suggest that the mechanical, rather than chemical, properties of the spacer are the most

relevant. The effect size differs by about an order of magnitude. Combined with the data from Figure 4.2b—where large differences in dewatering enhancement were seen with spacers of varying geometries—a picture is emerging that mechanics are fundamentally driving this process. Thus, stiffness and geometric parameters (e.g. pore shape and size) of the spacers are key.

Although the effect of spacer surface wettability is relatively minor, it is still statistically significant. Therefore, the effect of wettability, while certainly not the main cause, cannot be entirely ignored. As was quantified in the previous paragraph, making the spacer more hydrophobic reduces the residual water of the sheet—at greater pressures. At intermediate pressures, a more hydrophobic spacer results in worse dewatering, compared to more wettable spacers. Reasoning about why this happens can best be conducted after the fundamental physics of the enhanced dewatering mechanism are properly considered. For now, it is worth appreciating that pressing with the hydrophobized spacer at the highest pressure results in near theoretically perfect dewatering. That data point falls on top of the blotter series, showing that this approach has the potential to entirely eliminate undesired reflux of water from the press fabric.

4.3.4 Effect of liquid properties

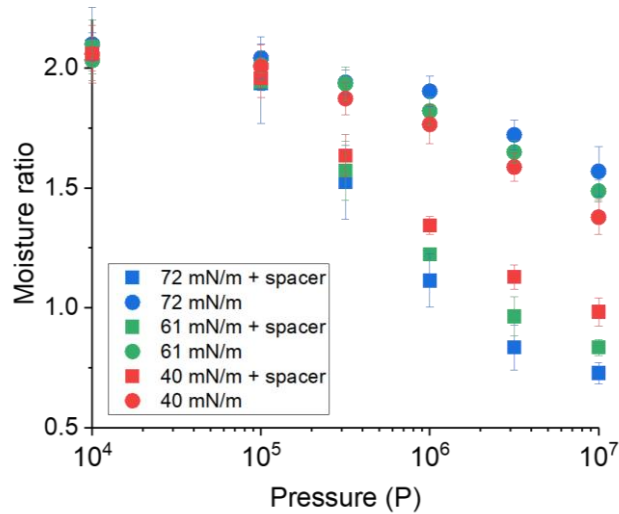


Figure 4.6 Effect of liquid surface tension on dewatering. Decreasing the surface tension of the liquid tends to improve dewatering with commercial fabrics and worsen the performance of the spacer. Even at extreme cases of surface tension for aqueous solutions (40 mN/m), the spacer-modified fabric still shows better dewatering than the conventional press fabric.

In addition to the surface chemistry, fluid properties like surface tension and viscosity could play a significant role in fluid transport, and the effect of those properties on dewatering was investigated next. To determine how liquid properties affect dewatering, the impact of surface tension was investigated in Figure 4.6. Simply changing the surface tension of the liquid phase, however, is not so straightforward. Altering the chemistry of the liquid could change its molecular interactions with the cellulose fibers in the paper. This changes the equilibrium moisture content of the sheet, which establishes the theoretical limit of water removal. Additionally, independently varying the fluid's surface tension while holding all other properties constant is nearly impossible. For these reasons, addition of surfactant was chosen as the method to vary surface tension. Because of their

tendency to aggregate at the liquid-air interface, surfactant molecules are less likely to interfere with the cellulose-water equilibrium. Furthermore, the dilute quantities of SDS needed to achieve changes in surface tension have a minimal impact on the liquid's density or viscosity. Surfactants are, however, not without their limitations. Their tendency to contaminate surfaces meant that extreme care had to be taken to conduct experiments with fresh fabrics, spacers, and paper for every trial.

Overall, changing the surface tension of the fluid has a relatively minor effect on dewatering, when the confounding effect of surface wettability (previously discussed) is accounted for. The effect of surface tension explored in Figure 4.6 cannot be entirely disentangled from the effect of surface wettability seen in Figure 4.5. There, it was shown that a more wettable surface resulted in marginally worse dewatering. Adding surfactant not only decreases the surface tension of the fluid, it also increases wetting of the fluid on the spacer surface. At least some of the increase in moisture content after pressing should be attributed to this effect. Explaining the opposite trend in the absence of the spacer, i.e. lower surface tension results in improved dewatering, is somewhat subtler. Consideration of this problem is saved for the discussion section. Overall, decreasing the surface tension of the liquid closes the gap between dewatering with and without the spacer. The lowest surface tension tested, however, was quite extreme for aqueous solutions. In a typical papermaking application, the surface tension of the process water, which is contaminated with some surfactants, falls in the range of 50-60 mN/m.

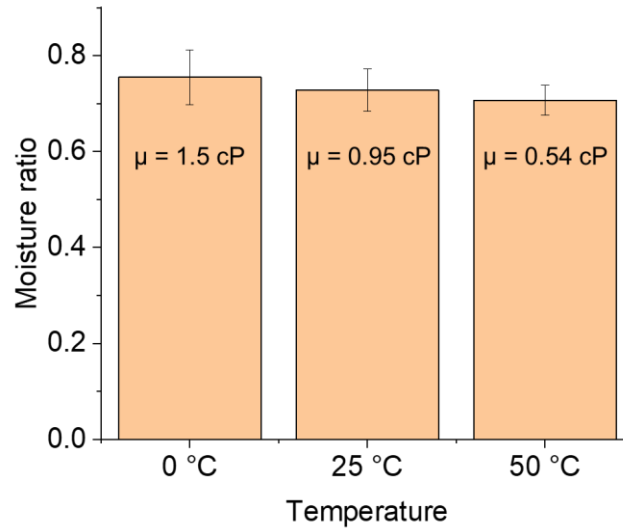


Figure 4.7 Effect of temperature (viscosity) on paper pressed at 10^7 Pa with a number 70 mesh in between the web and felt. The trend in temperature suggests that better dewatering is attained at higher temperatures, although the effect is so minor as to be statistically insignificant.

Moving on to other fluid properties that could be relevant, the effect of changing viscosity was explored. To investigate the effect of liquid viscosity on bridge breakup, I chose to vary the temperature of the fluid. Because it is difficult to change only one property of a liquid at a time, this approach was accepted as the most reasonable way to probe the contribution viscosity makes without introducing too many extraneous variables. For example, the viscosity could have been increased by addition of polymer solution. However, this would raise questions about significant changes to the surface tension of the fluid. Another possibility would be to use different liquids/liquid mixtures like glycerol or ethylene glycol. However, doing so would drastically change the equilibrium moisture content of the sheet, making comparisons impossible. From 25 °C to 0 °C, the viscosity increases from 0.95 cP to 1.5 cP. At 50 °C, the viscosity decreases to 0.54 cP. There is approximately a 50% change in either direction [164, 165]. Over the same intervals, the surface tension changes by only 5% in either direction [166].

Figure 4.7 shows that the effect of viscosity is minimal. In fact, the change in moisture ratio of the sheet after pressing with the spacer is smaller than the uncertainty due to experimental error. This result suggests that viscous forces are not relevant to the breakup of liquid channels in our system, under the conditions tested. This result, along with all the other observations collected in experimental results, can be properly interpreted by considering the physics of liquid bridge breakup.

4.4 Discussion

4.4.1 Interfacial instability

The process of liquid bridge breakup was first considered by Plateau in 1873 and expounded upon by Lord Rayleigh five years later [167, 168]. In the more than hundred years since, scientists and engineers have added to these insights, as they explored a wide range of subproblems, technologies, and applications. The fundamental principle of enhanced dewatering is that the spacer somehow severs liquid bridges spanning the felt-web interface. Thus, this vast body of existing physical knowledge can be employed to interpret the results of enhanced dewatering experiments. A surface-level understanding of the general mechanism was illustrated in the videos recorded of pressing: cutting the channels between the paper and felt, paths for reflux are eliminated. Even if there is still a driving force for reflux to the web, the spacer, which fills with air during the breakup process, provides an effective barrier for preventing return flow. It is the subtleties of this mechanism, however, that make for such a rich discussion of results obtained in this work.

For liquid bridges in the void space between the felt and paper to become unstable, their curvature in the radial direction must be greater than the curvature introduced by

disturbances along the axial direction [169-171]. It is this instability criterion that creates the conditions for liquid bridge breakup. When the liquid bridge experiences axial disturbances with wavelengths smaller than radial circumference of the bridge, surface tension acts to counter these disturbances because minimizing deformations to the interface is energetically favored. But if the axial disturbance's wavelength grows to the same order as the bridge's circumference, then this self-correcting tendency of surface tension is inverted. Within the neck of the axial disturbance, the Laplace pressure increases. This results in a positive feedback scenario where liquid gets pushed out of the high Laplace pressure neck, further increasing the radial curvature, and thus pressure, of the bridge's neck. This process accelerates until the bridge pinches off, and the liquid filament or channel is ruptured [172].

In the case of the spacer, the profile of the wires constituting the mesh provide the axial disturbance necessary for transition to the Plateau-Rayleigh instability to arise. Once initiated, this breakup process is driven by surface forces and retarded by some combination of inertial and viscous forces. The characteristic times for the regimes where either the inertial or viscous force predominantly slows breakup are [173-175]:

$$t_I = \sqrt{\frac{\rho L^3}{\sigma}} \approx 3 \text{ ms} \quad (4.2)$$

$$t_V = \frac{\mu L}{\sigma} \approx 0.01 \text{ ms} \quad (4.3)$$

From these estimates, it is clear that inertial forces dominate over viscous forces in this system. Notably, the inertial breakup timescale is still smaller than the dwell time within a paper machine press nip, which is on the order of 10 ms. Thus, the technology can likely overcome challenges which have previously prevented other reflux mitigation strategies [176-179] from being implemented.

These timescales, and the relative importance of forces they imply, explain why almost no effect on dewatering was seen when changing the temperature (viscosity) in Figure 4.7. Compared to inertial and surface forces, viscosity does not play a role in liquid bridge breakup. Therefore, it makes sense that even doubling the viscosity—or cutting it in half—had no impact on enhanced dewatering. Another way to think about this is to nondimensionalize the Navier-Stokes equation, and normalize every term to surface forces

$$\frac{PL}{\sigma} = -We \hat{v}\nabla\hat{v} + Ca \nabla^2\hat{v} + Bo + 1 \hat{\kappa} \quad (4.4)$$

where P is the pressure, L the length scale, σ the surface tension, We the Weber number, Ca the capillary number, Bo the Bond number, \hat{v} the nondimensional velocity, and $\hat{\kappa}$ the nondimensional curvature. Thus, the relative importance of inertial, viscous, and gravitational forces are represented by We , Ca , and Bo , respectively. For the experiments in this work, these nondimensional groups have values on the order: $We = 1$, $Ca = 0.01$, $Bo = 10^{-4}$. By expressing all forces relative to surface forces, it is apparent that inertial and surface forces dominate in this system, with viscous forces having a much smaller effect and gravity completely irrelevant. This helps further explain why changes in surface wettability and surface tension have some effect on dewatering, but temperature—which mostly changes the viscosity—does not.

Regarding surface tension and surface wettability, I can now make a more informed speculation about the trends observed in Figure 4.5. By raising the contact angle of the liquid on the surface of the solid spacer, its contact line is more mobile. Thus the liquid-air interface can move more freely. When breakup of the bridge is initiated, the rupture process proceeds more uniformly and smoothly. However, this effect occurs in tandem with

another consequence of the spacer's geometry. Because the wires in the mesh are cylindrical, there is a potential for some water to get trapped between the underside of these wires and the paper web. A hydrophilic mesh will always exhibit this tendency, as there is an energetic incentive for fluid to wet these capillary nooks. Thus, the spacer with a more wettable surface generally results in more water retained by the sheet. The differing performance of the hydrophobic spacer at differing applied pressures can be explained through similar considerations. In Figure 4.5, the hydrophobic spacer had worse dewatering at low applied pressures, although it showed the best dewatering at high pressures. The mesh structure and compliance of the sheet account for this. At lower pressures, the paper web is less deformed, so there is greater liquid between the sheet and the underside of the mesh wires. The hydrophobic mesh is more effective at breaking the liquid channel; however, this results in higher reflux to the sheet if the channel breaks far above the paper surface. At higher pressures, the paper deforms around the wires of the mesh, bringing the narrowest part of the neck of the spacer pores closer to the surface of the paper. Also, this deformation reduces the volume of liquid that can potentially get trapped on the underside of the mesh wires. When the liquid bridge breaks under these circumstances, reflux to the sheet is almost completely eliminated.

These considerations also explain the variation in dewatering with the spacer for liquids of varying surface tension. When the surface tension of water is reduced by addition of surfactant, it also becomes more surface-wetting. Therefore, the spacer became less effective at dewatering as the surface tension was reduced; it is the same effect that accounts for why the more hydrophilic spacer results in marginally worse dewatering. The fact that both experiments exhibited similar sized effects testifies to this interpretation.

Explaining why reducing surface tension improves dewatering in the absence of the spacer is more challenging. I speculate that, in the base case of pure water, the fluid is strongly cohesive and maintains stable bridges at the felt-web interface. Decreasing the surface tension possibly results in a very modest amount of bridge breakup as the fluid is inherently less cohesive. Therefore, a slight decrease in pressed moisture is observed for sheets pressed only with commercial fabrics, when wetted by lower surface tension fluids.

Thinking about the mechanism of interfacial instability, and the fundamentally geometric conditions which drive it, the results from Figure 4.2 become more intelligible. Specifically, the moisture content of the sheets after pressing goes through a minimum as the structural parameters of the mesh are changed. This is caused by a tradeoff between a couple of effects ensuing from the geometry of the spacer. If the spacer is thicker, more water is present in the bridge spanning the gap between the sheet and the felt. When this bridge is ruptured, water that was in the lower half of the bridge may then reflux to the sheet. Rewet has been mitigated but not eliminated. In extreme cases of spacer thickness, there may not even be enough water in the sheet to bridge the gap created by the spacer. As the spacer becomes thinner, it begins to approximate the structure of the felt as it was originally. Finer features may be less effective in destabilizing the liquid bridges, resulting in reflux upon decompression. Thus, the greatest improvement in dewatering was observed in between with the number 70 mesh. Compared to the commercial fabric alone, adding this spacer between the fabric and the sheet eliminated over 80% of rewet. Unidirectional water transport was largely achieved simply by selecting the correct structure of the spacer.

4.4.2 Instability hypothesis falsification

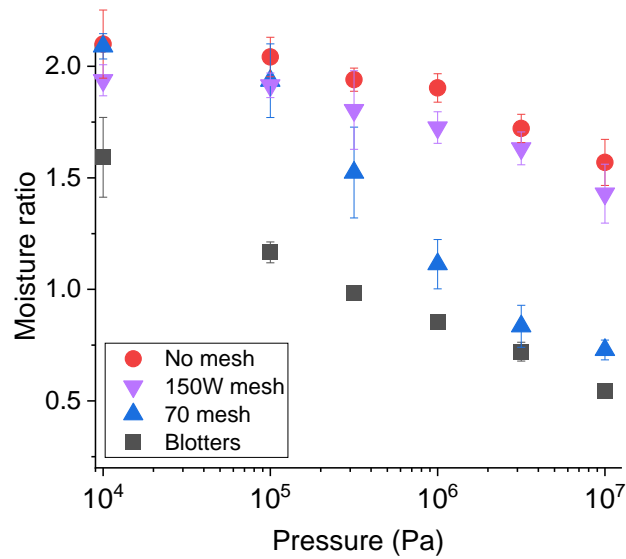


Figure 4.8 Dewatering with an included spacer that intentionally fails to meet the requirements dictated by the Plateau-Rayleigh criterion. In this case, dewatering is similar to the control, in which no spacer is used.

To test whether it is, in fact, the conditions for bridge instability which are primarily responsible for the observed improvement in dewatering, I revisit the approach summarized in Figure 4.2. However, instead of choosing a mesh with pores of roughly equal radial and axial curvature, I repeat the experiment with a mesh that has pores that are twice as wide as they are deep (150W). This intentionally violates the geometric criterion needed for interfacial instability. If the Plateau-Rayleigh instability is really the fundamental driver of enhanced dewatering, it should be evident. The model I am basing this claim on dictates that axial perturbations with a wavelength of the same order as the radius of the bridge increase exponentially with time. While the exact geometry of the liquid-air interface inside the stiff spacer is difficult to model or simulate from first principles due to its complexity, λ/R (the ratio of radial to axial curvature) characterizes

the outcome of the dewatering experiments (values for each mesh summarized in Table 4.1).

Indeed, Figure 4.8 shows that enhanced dewatering is not observed if the spacer's structure does not correspond to the criterion first identified by Plateau. If $\lambda/R > 1$, then reflux is not observed upon decompression. When $\lambda/R < 1$, reflux is observed, similar to the control experiment with no spacer. The vertical gap created by the 150W mesh spacer falls within range of other meshes tested in Figure 4.2 (refer to Table 4.1). However, the final moisture ratio of the sheet pressed with this spacer shows almost no improvement compared to pressing with the fabric alone. Therefore, it is clear why, of all the factors tested, the structural parameters of the spacer itself have the greatest impact on enhanced dewatering. It is primarily the shape of voids which the spacer creates that drives the breakup of liquid bridges. Decreasing the surface wettability can have a positive supplemental effect, but the basic conditions of liquid instability evidently must be met first.

4.5 Conclusions

Adding a stiff spacer layer between two porous media can allow unobstructed, rapid transport during compression while preventing reflux upon decompression. The structure of the spacer layer has a strong impact on the extent of enhanced dewatering. There was a tradeoff between having a large volume of fluid in the ruptured bridge and not having a spacer sufficiently thick to destabilize the liquid bridge effectively. Therefore, there is clearly a need to optimize the structure of the spacer. In the future, this optimization can consider design space beyond what is simply available with commercial meshes. In the

discussion, it was revealed how having wire curvature at the paper-spacer interface is generally detrimental, even though that same curvature is necessary to destabilize the liquid bridge within the spacer pore itself. Future designs might involve creating a spacer with a smooth surface that interfaces with the paper web, while retaining the internal pore curvature needed to break liquid bridges.

The effects of surface tension and surface wettability, while statistically significant, were relatively minor. This implies that instability-enhanced dewatering can likely be applied to many different materials and liquids. Even in applications where harsh process conditions prevent surface wettability from being a viable tool to control flow, this approach may be helpful. In the experiments conducted in this work, a combination of chemical and mechanical effects led to reflux being completely eliminated in one instance: hydrophobic 70 mesh spacer. That is not to say, however, that further optimization is not needed. Moving forward, it is worth considering how the structural parameters of the spacer can be further optimized. The timescale of bench-top pressing conducted in this study may not fully reveal what further challenges of enhanced dewatering need to be designed around. Further geometric optimization is likely required for rapid dewatering processes, thinner paper webs, heavy cycling, and other practical considerations.

Analyzing liquid bridge breakup in these complex structures is inherently difficult. In this study, video analysis gave some additional insight into the mechanism that prevents reflux. Seeing the liquid channels rupture as they flowed through the spacer layer provided strong evidence that the Plateau-Rayleigh instability is indeed the phenomenon responsible for enhanced dewatering. Based on this insight, I determined that inertial forces, rather than viscous forces, dictate the characteristic time of breakup in the spacer layer. However, a

more detailed analysis of the interfacial instability acting inside the spacer is certainly warranted. Modeling the motion of the interface within the spacer void, even in a simplified representation of the geometry, could reveal whether and to what extent key assumptions and conclusions from our experiments are valid.

Finally, the characteristic breakup time is less than the dwell time of the web and felt in an industrial press section of a paper machine. This implies that the technology has a strong potential to realize unidirectional flow in an application that has long found the implementation of one-way flow fabrics elusive. With focus on the fundamental physics of interfacial instability, there is strong potential to translate this enhanced dewatering mechanism into a successful application. Implemented successfully, a conservative estimate of this technology's impact would result in a 0.1% reduction in the world's total energy usage: an impressive illustration of the importance of fluid mechanics.

CHAPTER 5. REWET SUPPRESSION THROUGH PRESS FELT ENGINEERING²

5.1 Background and scope

Having proved in the previous chapter that instability enhanced dewatering has strong potential to eliminate rewet, questions remain about practical aspects of applying this technology to a paper machine press section. In this chapter of the thesis, I aim to address questions related to the feasibility of this approach to press fabric design, insofar as it is possible to do on the lab scale.

In the previous chapter, premade sheets were wetted to a moisture ratio of 2 prior to pressing. While this experimental design elucidated the effects of liquid bridge stability on enhanced dewatering, it is not the most reflective of how paper is made. In the work for this chapter, the paper sheets are made according to the TAPPI method, first dispersing the fibers in a dilute suspension, then draining through a wire screen to obtain the wet web. Thus, this web starts at a higher moisture content than the experiments of the previous chapters. One advantage of this protocol is that the dewatering of both free and bound water are seen in the data series of this chapter. To compensate for the higher initial water content of the sheet, the paper is pressed three times, much like it would be on a paper machine, which often has multiple nips in the press section.

² Material from this chapter was published in:
Dudick, S., D.W. Hess, and V. Breedveld, *Rewet suppression through press felt engineering*. TAPPI Journal, 2022. **21**(6): p. 327-332

The applicability of this technology to various grades of paper was tested by pressing sheets of varying basis weight. The basis weight is the area density of the sheet. Board grades, for example, have heavy basis weights, while tissue grades have lighter basis weights. This series of experiments also yielded data that helped me answer another question about enhanced dewatering.

Experiments measuring the moisture content of the sheet after pressing have one limitation. Straightforward and highly replicable, they leave no doubt that dewatering is improved by adding a spacer. However, how do we know that this is due to eliminating reflux, rather than simply pressing more water out during compression? For example, maybe the geometry of the spacer concentrates forces applied to the sheet in such a way as to press more water from the matrix at a given applied load. An unlikely explanation, to be sure, but the question remains. Is there a way to look inside the sheet during pressing to determine that I am, in fact, measuring what I think I am? The videos and their analysis in the previous chapter offered one way of evaluating this question. By pressing sheets of varying basis weights, we gain another piece of evidence that the sheets are pressed to the same minimum moisture content regardless of press fabric design and that the spacer prevents rewetting thereafter.

Another question relating to the practicality of instability-enhanced dewatering is the choice of material used for the spacer. Due to safety concerns—as well as wear on the equipment—metal should not be fed into a tight gap subject to tons of force, moving at hundreds of feet per second. However, I hypothesize that the required stiffness of the spacer is well below that of steel. In fact, many polymeric materials already used in paper machine applications meet this needed stiffness. This hypothesis is tested with nylon mesh spacers.

5.2 Experimental methods

Wet handsheets were prepared at different basis weights from SBSK pulp, which was obtained as dry lap and resuspended in water. The handsheet protocol followed the standard TAPPI method up until pressing. Instead of pressing, the wet webs were adjusted to a moisture ratio of 3 (25% solids) to simulate the couch solids on a paper machine. Solids content (also called consistency) is defined by the mass composition of water and fiber in the sheet:

$$solids = \frac{m_{fiber}}{m_{fiber} + m_{water}} \quad (5.1)$$

The wet web was then pressed against various felt configurations in a benchtop screw press (Figure 5.1). A force sensor allows the applied stress to be measured and controlled. One primary advantage of using a platen press is that the imposed pressure gradient is essentially unidirectional. This simplifies the problem of analyzing flow in three-dimensions—which is already complicated by the heterogeneity of the materials involved. The paper is pressed three times at a given pressure to simulate the sequence of nips on the machine, to reduce variation introduced from control of the initial moisture ratio, and to show the limits of enhanced dewatering. Following pressing, the moisture content of the paper was determined by comparing the weight to that after oven-drying at 105 °C for 8 hrs.



Figure 5.1 Screw press used for dewatering trials. From bottom to top are seen: the bottom platen, paper, press felt, top platen, force sensor, and screw press.

5.3 Results and discussion

5.3.1 Effect of spacer on dewatering of prepared handsheets

The impact of sandwiching a mechanically stiff layer between the press felt and web is illustrated in Figure 5.2. In this case, a commercially available #70 stainless steel mesh was used as the stiff spacer layer (red data series). The blue series, which represents pressing with a commercial tissue felt, serves as the base case. The black series, in which the paper is pressed with a thick stack of blotters, shows the upper limit of solids that can be realized at a given pressure in the absence of rewet. At low pressures, no mechanical dewatering is done; the blotters result in increased solids content because of the strong capillary forces exerted. As pressure is increased, more water is expelled from the web, resulting in higher press solids. At pressures relevant to industrial conditions (7 MPa) the web is significantly deformed, resulting in dewatering. The presence of a stiff spacer layer enhances the dewatering potential of the press felt, as seen in the transition of the red series from the blue series to the black series. Pressing has shifted to a scenario where limited

rewet occurs. An improvement of 13% solids from 48% to 61% corresponds to a 40% reduction in the residual moisture content of the sheet. That translates to a 42% reduction in the dryer load, assuming the sheet is dried to 95% solids.

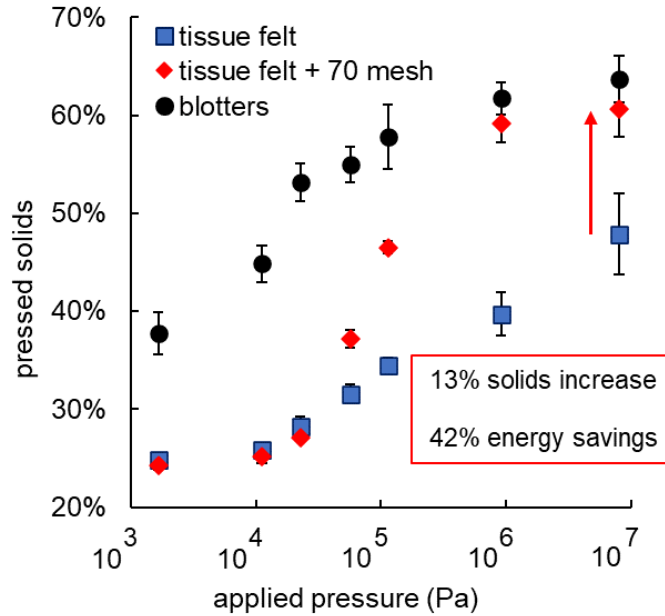


Figure 5.2 Pressed solids of 120 gsm SBSK handsheet vs. applied pressure for various pressing conditions: (blue squares) commercial tissue felt, (black circles) stack of dry blotters that represents limit of maximum drying and (red diamonds) tissue felt with metal #70 mesh.

To illustrate how sandwiching a spacer between the felt and web improves dewatering, the paper and felt were videographed as they were pressed.

Figure 5.3 depicts frames from these videos. Fluorescent dye was added to the water so that it would be easily detectable under the microscope. The brighter a region, the more water it contains. As time progresses from left to right, the pressure is increased, then reduced. A stark difference can be observed between pressing only with the felt (top row of images) and with the mesh-added felt (bottom row). Initially, both start the same: the

(wet) paper is very bright, and there is no water in the felt. Upon compression, water is driven from the sheet into the felt. Here, the mechanism of the technology can be seen; the mesh layer destabilizes liquid bridges between the paper and felt. In the top images, a continuous bright channel spans the paper and felt. Upon decompression, water flows back through this channel, rewetting the paper. In the bottom row, the liquid bridges snap once water is transported into the felt. Upon decompression, there is no path for water to rewet the paper. After pressing, water has moved from the paper into the felt, regardless of the felt configuration. With the mesh-added felt, however, the paper is noticeably drier.

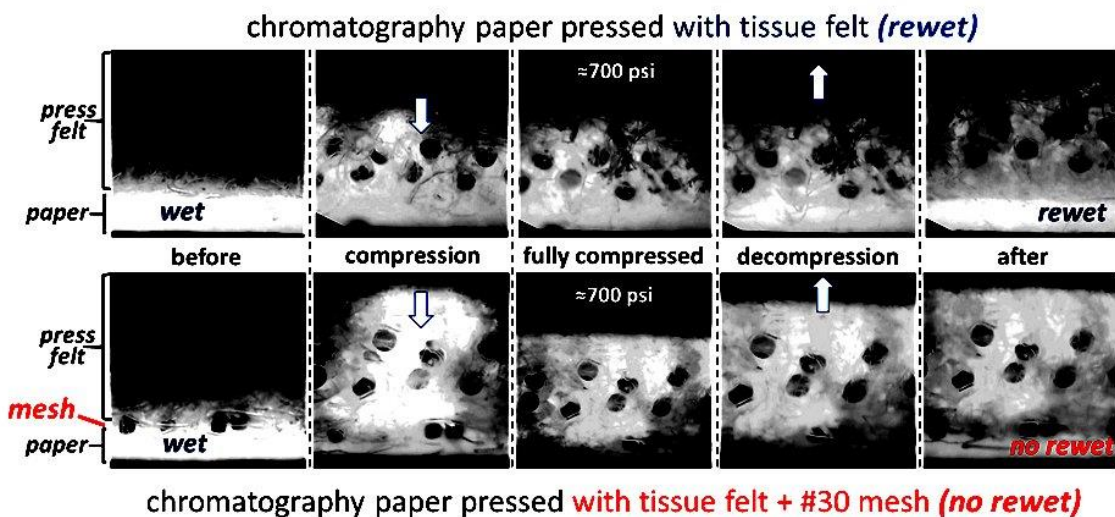


Figure 5.3 Still images from videos taken during the pressing of wet chromatography paper (initial solids 25%) up to maximum pressure of ~5 MPa with: (top) commercial felt, and (bottom) commercial felt + #30 mesh (wire thickness 165 μm ; openings 681 μm). Sideview image with fluorescently labeled water; greater brightness indicates larger amounts of water present.

5.3.2 Effect of mesh size

The dimensions of the spacer layer have a significant effect on the stability of liquid channels between the felt and paper. The pressed solids obtained with different

commercially available meshes between the felt and paper are shown in Figure 5.4. The solids appear to go through a maximum as the mesh size is changed; this suggests a certain tradeoff between various contributions. If the mesh number is too low (thick wires and large openings), the pressure applied to the sheet will not be uniform. Also, there is a greater volume of fluid within the liquid bridges (i.e., mesh openings). When these bridges are disrupted, more fluid can return to the sheet. On the other hand, high mesh numbers have small mesh openings that are similar in size to the filament and pore sizes already present in the felt. If the gap is too small, the liquid bridges are less likely to break, and the mesh-added felt system begins to resemble the felt alone. The optimum mesh size depends on the basis weight of the sheet, since deformation of the paper web into the spacer pores affects the gap height and, thus, liquid breakup.

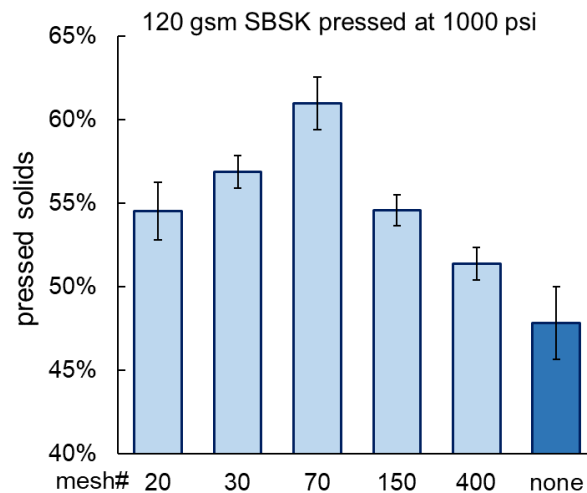


Figure 5.4 Effect of mesh size on press solids. The dimensions of the spacer layer have a significant impact on dewatering. A mid-size mesh balances tradeoffs between gap thickness, pressure distribution, and sheet contact.

5.3.3 *Effect of basis weight*

Figure 5.5 shows a Sweet plot of the moisture ratio obtained at different basis weights. Reassuringly, the technology is effective over a wide range of basis weights. At high basis weight, the effect of reducing rewet on solids is lower because rewet constitutes a lower fraction of the sheet's mass. At lower basis weights, the spacer layers that were used did not perform as well as hoped. Two factors likely contribute. First, issues with pressure uniformity introduced by a stiff layer are exacerbated by a thinner sheet. Second, there is likely not enough water initially in the sheet to fill the open spaces in the mesh and span the gap introduced by the spacer. For low basis weight sheets, the design of the spacer will have to be optimized beyond these standard meshes to effectively mitigate rewet.

Sweet plots enable regression to estimate the rewet and equilibrium moisture in the press. Plotting moisture ratio vs. inverse basis weight produces a line whose slope is equal to the rewet and whose intercept is equal to the equilibrium moisture ratio of the paper. For reasons mentioned above, the data point of mesh-added felt at lowest basis weight was excluded from the regression, because its dewatering is not fully representative of liquid channel breakup. As expected, the series share the same intercept, because equilibrium moisture of the sheet should only depend on the furnish properties and pressure applied—not the felt characteristics. The series have different slopes, however, suggesting that rewet has been reduced from 61 gsm to 10 gsm by adding the mesh. These values display excellent agreement with those of the rewet values suggested by Figure 5.2, 62 gsm and 9.6 gsm.

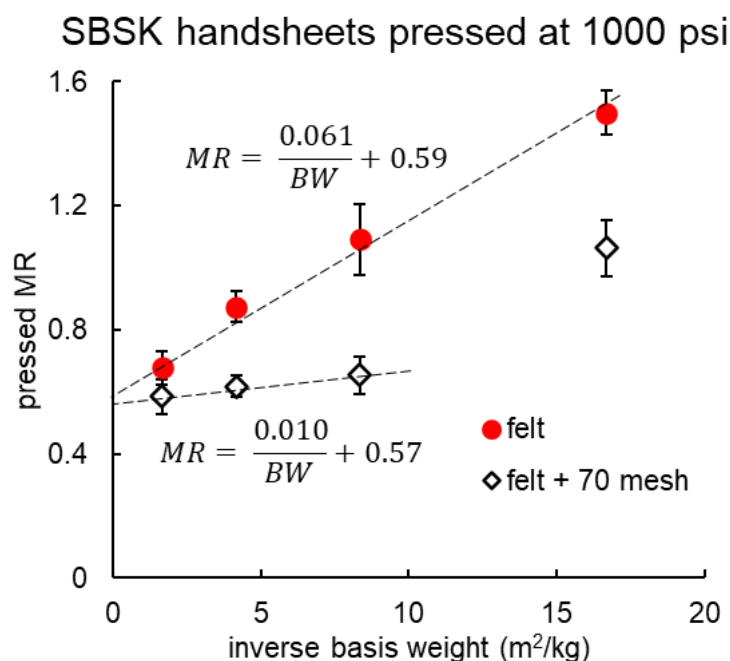


Figure 5.5 Sweet plot shows the effect of basis weight on dewatering. The intercept on each line indicated the minimum moisture content of the sheet during pressing. The slope of the line measures rewet. The lines have the same intercept but different slopes, indicating that the spacer reduces rewet. Even a simple, non-optimized, implementation of the instability-enhanced dewatering concept eliminates over 80% of rewet, effective across a range of basis weights.

5.3.4 Nylon meshes

For reasons of safety and wear, metal structures would be difficult to implement in a paper machine press nip. Metal materials, however, should not be necessary to achieve the desired liquid bridge breakup. Provided that the spacer layer is sufficiently stiff to resist significant deformation under nip loads, the approach should work well. Given that stress applied in the nip is around 10 MPa, any material that has a stiffness (i.e., elastic modulus) of at least 1 GPa will likely work. Fortunately, there are many candidate materials that satisfy this criterion. Among them, nylon meshes are a natural choice as nylon is already used in press fabrics.

Figure 5.6 shows the enhanced dewatering performance that nylon meshes add to a commercially available felt. Similar to the effect demonstrated with metal meshes, less water remained in the sheet after pressing when the spacer layer is included. Once more, the dimensional parameters of the spacer layer have a significant impact on the mitigation of rewet. Compared to pressing with the felt alone, each of the mesh-added felts showed at least some improvement in press solids. The greatest improvement was seen with the medium-sized mesh, implying that there is an opportunity to optimize the design of the spacer layer beyond the commercially available meshes. As in Figure 5.2, the gap between the blue and red series highlights the progress already made in developing this technology. The gap between the red and black series corresponds to the opportunity to further optimize this process. Although less improvement was seen with the nylon meshes compared to metal meshes, this is more indicative of only testing three structures, which is less likely to capture the optimum value.

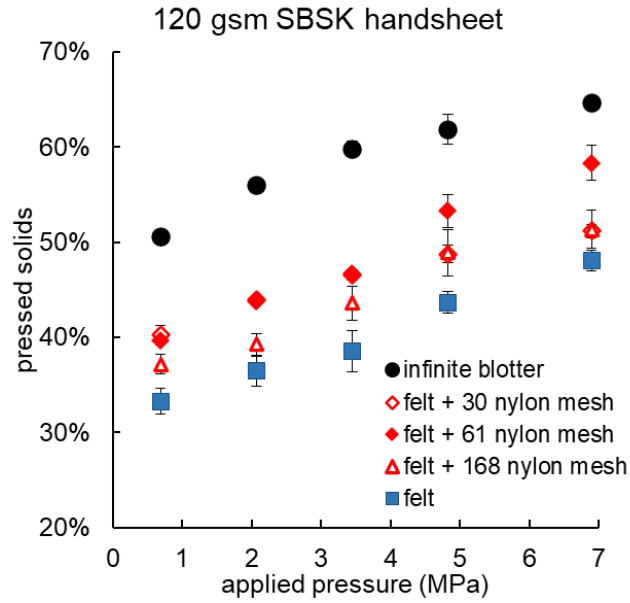


Figure 5.6 Enhanced dewatering observed with nylon meshes. The medium size mesh (#61) performs best of the ones tested, for reasons previously discussed. Two of the mesh series, #30 and #168 fall on top of one another.

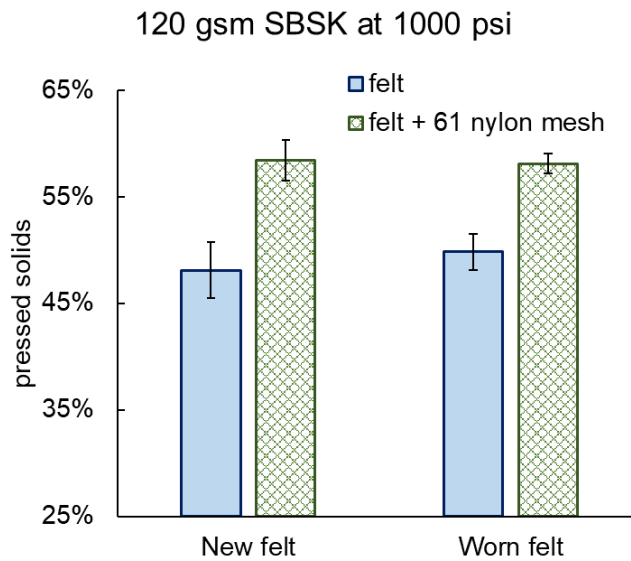


Figure 5.7 Enhanced dewatering observed with new and used tissue felts

5.3.5 *Compatibility of technology with different felts*

Because the technology works by disrupting the fluid phase, improved dewatering should be observed regardless of what felt is used, or in what condition the felt may be. Figure 5.7 shows results obtained from pressing a 120 gsm SBSK handsheet at 1000 psi with new and used felts. Addition of a mesh improved dewatering in both cases. The used felt appears to have marginally better dewatering ability, compared to the new felt. However, this is only because the new felt has not been sufficiently well conditioned. Overall, it is encouraging to see that the technology has high potential to work over the lifetime of the felt.

5.4 Economic Impact

The financial value of reducing rewet comes in two main ways: energy savings and increased production. By removing more water in the press section, less has to be dried later—a notoriously intensive and costly process. Reducing the drying load by 40% would result in an enormous reduction in energy. Assuming that, in the base case, energy devoted to drying the sheet costs about \$20/finished ton, the impact on energy savings would be \$8/finished ton. In application, the control/base case—pressing with conventional press fabric—could perform better than suggested by experiments on the platen press, simply due to dynamics. Even if the drying load were only reduced by 10%, energy savings would still be about \$2/finished ton, an attractive value for technology that is essentially drop-in.

The value that could be created from increased production in debottlenecking the dryers is more difficult to estimate. For those mills currently struggling with dryer limitations, marginal profitability attained with higher production volume could be at least as valuable as energy savings. The analysis is complicated by other process streams that

would then become production-limiting. In theory, reducing the dryer load by 40% could result in up to 40% increase in production for this case. However, in practice, upstream processes engineered around the initial dryer limitation would quickly become new bottlenecks. Understanding how reducing energy use in the dryers results in higher production requires a detailed analysis that would have to be performed on a mill-by-mill basis. Additionally, the economic considerations complicate quickly. Significant increases in production, especially those that can be realized sector-wide, are likely to affect the pricing—and thus, profitability—of marginal tons. Taking conservative values for the two contributions to financial impact, I estimate that this technology would be worth about \$1.6 billion per year.

Conclusions

Enhanced dewatering can be realized by severing the liquid channels that would otherwise span the felt-web interface. One mechanical way of accomplishing this is to introduce a stiff, porous spacer between the felt and web. Doing so effectively changes the boundary conditions of the interface while it is in the nip. Because the mechanism works by disrupting the fluid phase, it should only be indirectly influenced by other parameters in the system like nip load, pulp furnish, or press fabric. This means that application is likely to be wide-ranging, although I do expect some of the design optimization to depend on paper grade. While there is additional work to be done, initial results of this approach are promising. Improved dewatering observed on the lab-scale, coupled with a preliminary economic analysis, shows that structures that destabilize liquid channels at the felt-web interface have enormous potential in paper manufacture.

CHAPTER 6. CONCLUSIONS AND FUTURE WORK

6.1 Contributions to the field

The study of flow in porous media can be complex, surprising, and even beautiful at turns. The same forces acting on these physically complex liquid-solid systems can manifest drastically different outcomes, by making subtle alterations in initial or boundary conditions. For example, surface tension of the fluid at a paper-felt interface can either hold the liquid neatly at the interface, or tear it apart. This outcome, as was seen, depends on slight differences in the interfacial geometry. Surface forces were also used to create capillary barriers within a material, as well as to control the adhesive transfer of fluids between materials. The contributions this thesis made to understand the subtleties of wetting in fibrous materials—and, ultimately, improved dewatering—are briefly summarized.

6.1.1 *Capillary barriers in fibrous materials*

In the second chapter of the thesis, I aimed to show how wetting gradients could be used to control the flow of fluid within a fibrous network. By hydrophobizing metal meshes, papers, and press-felts, wetting barriers were created that successfully resisted liquid penetration—up to a certain pressure. How to predict the exact value of this critical pressure for fibrous substrates was a question that had not yet been adequately answered by the existing literature on the subject. By taking direct measurements of this critical pressure, along with precise knowledge of the chemical and physical characteristics of the

substrates, I was able to adapt a mathematical model of the Laplace pressure for axially aligned cylindrical fibrils. This adaptation required considering the effect of stochastics on wetting. Although the paper and fabric samples were highly heterogeneous and physically complex, taking a statistical view of the effective pore size gave reproducible results. The utility of the approach developed in this phase of study was most evident in predicting the wetting behavior of nearly-wetting fluids. On the whole, two competing effects make the wetting of fiber networks unique. On the one hand, their reentrant pore structure increases resistance to wetting, when compared to straight-walled pores of the same diameter. This means that a sheet of paper, owing to its unique structure, can repel liquids that would wet other media with identical contact angles. On the other hand, statistical variability in the pore structure decreases resistance to wetting, mostly because large pores yield the weakest barriers.

By accounting for both of these effects, I was able to accurately predict the critical wetting behavior of several arbitrary liquids into hydrophobized paper. Based on these calculations, I showed the design parameters that would be necessary to create a wetting barrier strong enough to resist rewet. A simple implementation of this design was executed on the lab scale and shown to be effective at mitigating rewet. However, the small pore sizes needed to bolster capillary forces made such a design impractical for application on a paper machine. This was because small pores also reduce the felt's permeability, restricting initial dewatering of the sheet. Regardless, the insights developed from this investigation should be useful far beyond the constraints of the press section of a paper machine. Design of wetting-resistant papers, non-woven fabrics, and analogous materials could all benefit from this work.

6.1.2 *Adhesion of fluids to fibrous materials*

In the third chapter, the influence of adhesion over droplet transfer between two fiber networks was investigated. In experiments conducted on equilibrium time scales, it was seen that the forces exerted on the droplet by the fiber surfaces were in good agreement with those predicted by the classical model developed for flat surfaces. The agreement is likely due to the much larger length-scale of the droplets tested, compared to the length scale of the fibers in the paper. That is, from the zoomed-out perspective of the macroscopic droplet, each surface can roughly be treated as a uniform interface with given wetting properties. Under the right conditions, complete control over the transfer of a droplet is possible. When the droplet is placed on a sheet of paper with high contact angle hysteresis, the amount of liquid transferred can be controlled solely by choosing how much to compress the drop prior to picking it up. This drastic change in transfer behavior corresponded to a transition in the boundary conditions that define the liquid bridge. When the droplet is perturbed little, the contact line remains in its original (small) position. The adhesive force holding the droplet is correspondingly small, and it is easily carried away. By simply expanding the contact line (via compression), the contact between liquid and solid becomes pinned outward, at a given receding contact angle, thereby increasing the adhesive force.

The challenge of separating a droplet from wet paper became apparent. On the highly hydrophilic surface, the liquid quickly spreads to a large contact area (with a near-zero contact angle). The best-case scenario for transfer in such a case is 50-50, when the alternate surface is also made to be fully hydrophilic. Still, it was seen that liquid could be moved against the direction imposed by surface forces, so long as a stronger force is

leveraged. I illustrated how inertia could be used to transfer water from a hydrophilic surface to a hydrophobic one under dynamic transport. However, the extreme limit of this method would also result in 50-50 transfer, implying that adhesion of water to a highly hydrophilic substrate can never be fully overcome.

6.1.3 Instability-enhanced dewatering

With these limits on the feasibility of using wetting gradients to eliminate rewet in mind, a new way of controlling flow was obviously needed. In the course of conducting transfer experiments, observing the rupture of a liquid bridge gave me the revolutionary insight of how to approach rewet from an entirely new perspective. If the film between the felt and paper were somehow broken, there would be no way for reflux to occur, even if the driving force for rewet remained. Rather than eliminating or counteracting the capillary forces of the sheet, the order of operations during pressing was inverted. Inserting a stiff spacer between the press felt and the paper web was, ultimately, a simple engineering solution that accomplished this goal. As was explored, however, the physics underlying this technology were far from simple.

First, I showed that enhanced dewatering obtained with a stiff spacer between the felt and web was highly sensitive to the structure of the spacer. Choosing the right dimensions for the spacer is critical to reducing rewet. Considering the dynamics of interfacial instability, the reason became clear. The stability of liquid bridges depends strongly on the geometry of their interfaces. By intentionally experimenting with a spacer that violated the necessary geometric criterion for instability, I showed that it is indeed this mechanism that is primarily responsible for enhanced dewatering. Additionally, surface

wettability contributed a modest effect to enhanced dewatering, though this was for subtly different reasons than the effects of wettability covered in the two prior chapters. Because the technology primarily works on a mechanically-imposed alteration to pressing, better dewatering was seen across liquids of varying surface tension and viscosity. This is greatly encouraging for a potential application because, while marginally beneficial, maintaining the proper surface chemistry is not essential to the spacer's success.

6.1.4 Process applicability / feasibility

In the subsequent chapter, practical questions related to the implementation of fabrics with improved dewatering capabilities were investigated—insofar as it was possible to do so on the lab scale. Measuring the pressing performance over a range of basis weights of the paper substrates showed that the technology has potential to work for a wide variety of paper grades. Additionally, this enabled the construction of a Sweet plot, allowing me to quantify the magnitude of rewet with and without the spacer. Thus, I showed that—in my lab-scale set-up—rewet was reduced by over 85% with just a commercially available mesh and no surface treatments. I also examined how a spacer would work with worn vs. new felts. In either case, the technology for improved dewatering was a success.

6.2 Future work

As many questions as were answered in the course of these investigations, far more were raised. I'd like to reflect on some opportunities to increase the impact of these studies through future work.

6.2.1 Geometry of spacer, custom pore profile

As was discussed in Chapter 4, the performance of the spacer is highly dependent on its geometry. The investigation conducted so far was limited in this respect by utilizing commercially-available metal (and nylon) meshes. Although their convenience made them indispensable for the first phase of developing this technology, an attempt to design the spacer from the ground up should be made in the future. Doing so would overcome the limitations of using ready-made meshes. For example, one cannot independently vary the pore size, wire diameter, and mesh thickness to a great extent in commercially available meshes. This unnecessarily reduces design choices. Another drawback is that the curvature of the wires in the mesh—while essential to inducing interfacial instability—also likely trap some water between the spacer and paper surface. Designing a custom spacer could overcome this problem by having a smooth spacer surface meet the paper and pore walls with the appropriate interior curvature.

Fluid simulations might help discover what curvature for the pore walls is ideal. There are immense caveats, of course, to simulating multiphase breakup of fluid on the microscale. However, such a tool may be useful in quickly scanning potential spacer designs, to facilitate fabrication and testing. Because materials with known parameters have already been tested, it should be straightforward to assess the validity of such simulations. For breaking water channels, I hypothesize that more slender openings relative to gap thickness would be preferable; such simulations might be a convenient method for testing that hypothesis.

6.2.2 Dynamic process conditions

One important question remaining about the applicability of the spacer layer concept to industrial manufacturing is to what extent it will function under process conditions. My analysis of the physics that govern liquid bridge breakup suggest that the technology will be effective at process time scales. However, the only way to make certain is to actually test it. Doing so would require access to a pilot paper machine. Notably, the path to such tests is bottlenecked by the concerns above, as well as the possibility of multidimensional flow.

6.2.3 *Multidimensional flow*

In the studies conducted for this thesis, care was taken to establish unidimensional pressure gradients in the transverse direction only. This was done to simplify the problems of flow and elucidate some of the fundamental aspects of enhanced dewatering, at least for initial investigations. In the press section of a paper machine, the curvature of the press roll can create pressure gradients in the machine direction as well. However, the extent to which this poses a real problem is somewhat unclear. Compared to lab-scale nips—with high roll curvature and, thus strong machine-direction pressure gradients—industrial presses have less curvature and are more likely to exhibit more one-dimensional pressure profiles.

The possible influence of machine-direction pressure gradients cannot be overlooked in spacer design, however. In such cases, spacers that create channels along the machine direction could result in compromised dewatering as the press pushes water forward into already-dewatered paper. Since the spacer technology works by maintaining voids at the paper-felt interface, this is a concern that must be recognized. Given appropriate attention to design, these potential problems can be confidently avoided.

6.2.4 *Effect on sheet properties*

The effect of the spacer on sheet properties is an essential question that must be thoroughly considered in future work on this project. First, the spacer can impart roughness to the sheet, which may or may not be desired, depending on the application. Understanding how the spacer's structure contributes to final sheet surface roughness, after additional processing steps like coating and calendering is a question best investigated at the pilot scale. Second, the enhanced dewatering possible with a spacer means that similar sheet dryness can be achieved by applying less pressure. Doing so could result in a bulkier sheet, as it has undergone less consolidation in the press. Bulk is a highly sought after sheet property for grades that benefit from bending stiffness, absorbency, softness (in the case of tissue), and all grades sold by area rather than weight. This adds another dimension to fabrics for improved dewatering and is a benefit that should serve as a major focus in future work with this technology.

6.2.5 *Definition of stiffness*

The stiffness of the spacer layer plays an essential role in achieving enhanced dewatering. However, the exact definition of what is meant by stiffness has been left somewhat ill-defined in the thesis. Clearly, thinking of the stiffness simply in terms of a material parameter of the substance used to create the spacer is inadequate. The stiffness that is relevant to instability-enhanced dewatering is the resistance of the spacer to deformation, such that void volume is preserved at the felt-web interface even under the high stresses applied in the press nip. This apparent, overall, or bulk stiffness is a combination of the material composition, as well as the porous spacer's structure. A simple

analogy is to consider a steel rod. Steel itself is very stiff and difficult to deform with human strength. However, a rod made of steel that is thin and long may easily be bent. This is because the rod's bending stiffness—the structured material's resistance to deformation—depends on the material's dimensions, as well as the intrinsic properties of steel. Likewise, a spacer made of “stiff” material may not perform well if the structure deforms under load. What threshold fraction of void volume that must be preserved during compression to prevent rewet is a question that future work in this area should consider.

6.2.6 Introduction of air to the interface

For breakup of the liquid channels to occur, air must be supplied to the interface to displace the liquid. It is unknown whether this requirement places limitations on the practical implementation of this technology in a paper machine. At the small scales and long time frame of laboratory experiments, bringing air to displace the ruptured liquid channels is not an issue. At larger length scales and shorter time scales, this could, however, be an important consideration. Preliminary experiments showed that a stiff spacer was still able to achieve enhanced dewatering when pressing paper samples of area 100 times those reported in Chapter 4. Additional work will have to consider length scales equivalent to those on a commercial machine. In designing the spacer, consideration should be paid to how air enters the interface, and whether it is possible to store this air within the spacer itself prior to and during compression—for example, by including hydrophobic pockets in the spacer pore walls.

APPENDIX A. VIDEO ANALYSIS CODE

```
ds = imageDatastore("C:\vids\chrom");
framenum = length(ds.Files);
F(framenum) = struct('cdata', [], 'colormap', []);

for i=1:framenum
    img = readimage(ds,i);
    g = img(:,:,2);
    bv = mean(g,2); lenbv=length(bv); bv = flip(bv);
    bv(1)=256;

    fitbound=810;

    b = bv(fitbound:1040); d = length(b); q = (1:length(b));
    f = fit(q.',b, 'gauss1');

    coeffs=coeffvalues(f); lower=round(fitbound+coeffs(2)-
coeffs(3));
upper=min(1040,round(fitbound+coeffs(2)+coeffs(3)));
    b=bv(lower:upper); d = length(b); q = (1:length(b));
    f = fit(q.',b, 'gauss1');

    coeffs=coeffvalues(f);

    factor(i)=coeffs(1); average(i)=coeffs(2)+lower;
    stdev(i)=coeffs(3);
```

```

    for j=1:lenbv
        fitt(j)=coeffs(1)*exp(-(j-
(coeffs(2)+lower))/coeffs(3))^2);
    end

    y = [1:length(bv)];
    p = plot(bv,y);
    p.LineWidth=3;

    hold on

    fittplot = plot(fitt,y);
    fittplot.LineWidth=3;

    hold off

    F(i)=getframe(gcf);

    barea(i)=coeffs(1)*coeffs(3)*sqrt(2*3.14159);

    peak(i)=max(fitt);

end

stdev=stdev';          average=average';          factor=factor';
barea=barea'; peak=peak';

fig=figure;    movie(fig,F,1,5);    v=VideoWriter('chrom1');
v.FrameRate=15; open(v); writeVideo(v,F); close(v);

```

REFERENCES

1. Ahn, C.H., et al., *Disposable smart lab on a chip for point-of-care clinical diagnostics*. Proceedings of the IEEE, 2004. **92**(1): p. 154-173.
2. Foudeh, A.M., et al., *Microfluidic designs and techniques using lab-on-a-chip devices for pathogen detection for point-of-care diagnostics*. Lab on a Chip, 2012. **12**(18): p. 3249-3266.
3. Stone, H.A., A.D. Stroock, and A. Ajdari, *Engineering flows in small devices: Microfluidics toward a lab-on-a-chip*. Annual Review of Fluid Mechanics, 2004. **36**: p. 381-411.
4. Brass, L.F. and S.L. Diamond, *Transport physics and biorheology in the setting of hemostasis and thrombosis*. Journal of Thrombosis and Haemostasis, 2016. **14**(5): p. 906-917.
5. Du, E., et al., *Kinetics of sickle cell biorheology and implications for painful vasoocclusive crisis*. Proceedings of the National Academy of Sciences of the United States of America, 2015. **112**(5): p. 1422-1427.
6. Mangione, F., et al., *Renal blood flow redistribution during acute kidney injury*. American Journal of Kidney Diseases, 2010. **56**(4): p. 785-787.
7. Cherepovitsin, A.E. and O.A. Marinina, *Methodical approaches to the economical estimation of CO₂-enhanced oil recovery projects*. Journal of Mining Institute, 2011. **194**: p. 344-348.

8. Safonov, E.N. and E.V. Lozin, *Enhanced oil recovery methods: reality, perspectives, scientific problems*. Neftyanoe Khozyaistvo, 2003(4): p. 46-48.
9. Zhou, Y.Z., et al., *A comprehensive review of emulsion and its field application for enhanced oil recovery*. Energy Science & Engineering, 2019. **7**(4): p. 1046-1058.
10. Berkowitz, B. and I. Balberg, *Percolation theory and its application to groundwater hydrology*. Water Resources Research, 1993. **29**(4): p. 775-794.
11. Furuberg, L., et al., *Dynamics of invasion percolation*. Physical Review Letters, 1988. **61**(18): p. 2117-2120.
12. Wangemann, S.G., R.A. Kohl, and P.A. Molumeli, *Infiltration and percolation influenced by antecedent soil water content and air entrapment*. Transactions of the ASAE, 2000. **43**(6): p. 1517-1523.
13. Jue, M.L., V. Breedveld, and R.P. Lively, *Defect-free PIM-1 hollow fiber membranes*. Journal of Membrane Science, 2017. **530**: p. 33-41.
14. Nazarov, V.G. and A.V. Dedov, *Permeability of composition fiber materials*. Inorganic Materials-Applied Research, 2022. **13**(1): p. 111-115.
15. Epps, H.H. and K.K. Leonas, *The relationship between porosity and air permeability of woven textile fabrics*. Journal of Testing and Evaluation, 1997. **25**(1): p. 108-113.
16. Berkowitz, B. and R.P. Ewing, *Percolation theory and network modeling applications in soil physics*. Surveys in Geophysics, 1998. **19**(1): p. 23-72.

17. Bethune, M.G., B. Selle, and Q.J. Wang, *Understanding and predicting deep percolation under surface irrigation*. Water Resources Research, 2008. **44**(12).
18. Deng, D., et al., *Hydrophobic meshes for oil spill recovery devices*. ACS Applied Materials & Interfaces, 2013. **5**(3): p. 774-781.
19. Bai, M.Z. and G. Amu, *Study on physical properties of camel cashmere*. Journal of Camel Practice and Research, 2019. **26**(2): p. 191-193.
20. Rizo, A., et al., *A novel process for obtaining smoke-flavoured salmon using water vapour permeable bags*. Journal of Food Engineering, 2015. **149**: p. 44-50.
21. He, F., et al., *Developing a unidirectionally permeable edible film based on kappa-carrageenan and gelatin for visually detecting the freshness of grass carp fillets*. Carbohydrate Polymers, 2020. **241**.
22. Tiseo, I. *Production volume of paper and paperboard worldwide from 1961 to 2020*. 2022.
23. Afshar, P., et al., *Sequential modelling of thermal energy: New potential for energy optimisation in papermaking*. Applied Energy, 2012. **89**(1): p. 97-105.
24. Hubbe, M.A., *Energy efficiency challenges in pulp and paper manufacturing: A tutorial review*. Bioresources, 2021. **16**(4): p. 8567-8639.
25. Laurijssen, J., et al., *Optimizing the energy efficiency of conventional multi-cylinder dryers in the paper industry*. Energy, 2010. **35**(9): p. 3738-3750.
26. Smook, G.A., *Handbook for pulp & paper technologists*. 2nd ed. ed. 1992, Vancouver: Angus Wilde Publications.

27. Wiseman, N., *Effect of felt properties on pressing of paper*. Pulp & Paper-Canada, 1976. **77**(9): p. 29-33.
28. Schiel, C., *Presses, felts, paper quality*. Papier, 1975. **29**(4): p. 137-&.
29. Carlsson, G., T. Lindstrom, and B. Norman, *Some basic aspects on wet pressing of paper*. Pulp & Paper-Canada, 1983. **84**(9): p. R101-R106.
30. Maloney, T. and H. Paulapuro, *The centrifugal compression value*. TAPPI Journal, 1999. **82**: p. 150-154.
31. Wahlstrom, B., *Wet pressing in the 20th century: Evolution, understanding and future*. Pulp & Paper-Canada, 2001. **102**(12): p. 81-88.
32. Laurijssen, J., A. Faaij, and E. Worrell, *Benchmarking energy use in the paper industry: a benchmarking study on process unit level*. Energy Efficiency, 2013. **6**(1): p. 49-63.
33. Kershaw, T.N., *3 Dimensions of water flow in press felts*. TAPPI, 1972. **55**(6): p. 880-&.
34. Pettersson, P., T.S. Lundstrom, and E. Wassvik, *Modeling pressure distribution in a belt press during manufacture of fiberboards*. Wood and Fiber Science, 2007. **39**(3): p. 493-501.
35. Darcy, H., *Les fontaines publiques de la ville de Dijon: Exposition et application des principes à suivre et des formules à employer dans les questions de distribution d'eau*. 1856: V. Dalmont.

36. Thibault, X., et al., *Measurements of the permeability of press felts*. Paperi Ja Puu-Paper and Timber, 2004. **86**(2): p. 95-101.
37. Lindsay, J.D. and P.H. Brady, *Studies of anisotropic permeability with applications to water removal in fibrous webs: Experimental methods, sheet anisotropy, and relationships to freeness*. TAPPI Journal, 1993. **76**(9): p. 119-127.
38. Thibault, X. and J.F. Bloch, *Permeability measurements of strained fibrous networks*. Textile Research Journal, 2008. **78**(6): p. 473-485.
39. Kerekes, R.J. and J.D. McDonald, *A Decreasing permeability model of wet pressing - theory*. TAPPI Journal, 1991. **74**(12): p. 150-156.
40. Plaisted, W.E., *Equilibrium moisture ratio of press felts under simulated paper-machine conditions*. TAPPI, 1976. **59**(3): p. 93-95.
41. Busker, L.H. and D.C. Cronin, *The relative importance of wet press variables in water removal*. Pulp & Paper-Canada, 1984. **85**(6): p. 87-&.
42. Fitt, A.D., et al., *Multiphase flow in a roll press nip*. European Journal of Applied Mathematics, 2002. **13**: p. 225-259.
43. McDonald, J.D. and R.J. Kerekes, *Pragmatic mathematical models of wet pressing in papermaking*. Bioresources, 2017. **12**(4): p. 9520-9537.
44. Wahlstrom, P.B., *Our present understanding of the fundamentals of pressing*. 1969.

45. Washburn, E.W., *The Dynamics of capillary flow*. Physical Review, 1921. **17**(3): p. 273-283.
46. Owens, T.L., et al., *Control of microfluidic flow in amphiphilic fabrics*. ACS Applied Materials & Interfaces, 2011. **3**(10): p. 3796-3803.
47. Yang, X.L., et al., *Underwater curvature-driven transport between oil droplets on patterned substrates*. ACS Applied Materials & Interfaces, 2018. **10**(17): p. 15258-15269.
48. Li, J.Q., et al., *Topological liquid diode*. Science Advances, 2017. **3**(10).
49. Comanns, P., et al., *Directional, passive liquid transport: the Texas horned lizard as a model for a biomimetic 'liquid diode'*. Journal of the Royal Society Interface, 2015. **12**(109).
50. Breedveld, V. and D.W. Hess, *Modification of paper/cellulose surfaces to control liquid wetting and adhesion*. Advances in Contact Angle, Wettability and Adhesion, Vol 2, ed. K.L. Mittal. 2015. 365-377.
51. Choi, W.T., et al., *Creation of wettability contrast patterns on metallic surfaces via pen drawn masks*. Applied Surface Science, 2017. **426**: p. 1241-1248.
52. Hess, D. and V. Breedveld, *Controlled wetting, adhesion, and absorption of water and oils on paper*. Abstracts of Papers of the American Chemical Society, 2017. **254**.
53. Li, H., et al., *"Plug-and-Go"-type liquid diode: Integrated mesh with janus superwetting properties*. Advanced Materials Interfaces, 2016. **3**(19).

54. Zheng, L.Z., et al., *Superwetable Janus nylon membrane for multifunctional emulsion separation*. Journal of Membrane Science, 2022. **642**.
55. Afsari, M., H.K. Shon, and L.D. Tijing, *Janus membranes for membrane distillation: Recent advances and challenges*. Advances in Colloid and Interface Science, 2021. **289**.
56. Nau, M., et al., *Janus-Type Hybrid Paper Membranes*. Advanced Materials Interfaces, 2019. **6**(18).
57. Yang, H.C., et al., *Janus membranes: Creating asymmetry for energy efficiency*. Advanced Materials, 2018. **30**(43).
58. Raj, N., V. Breedveld, and D. Hess, *Fabrication of fully enclosed paper microfluidic devices using plasma deposition and etching*. Lab on a Chip, 2019. **19**(19): p. 3337-3343.
59. Raj, N., V. Breedveld, and D.W. Hess, *Flow control in fully enclosed microfluidics paper based analytical devices using plasma processes*. Sensors and Actuators B-Chemical, 2020. **320**.
60. Balu, B., et al., *Directional mobility and adhesion of water drops on patterned superhydrophobic surfaces*. Journal of Adhesion Science and Technology, 2011. **25**(6-7): p. 627-642.
61. Balu, B., V. Breedveld, and D.W. Hess, *Fabrication of "roll-off" and "sticky" superhydrophobic cellulose surfaces via plasma processing*. Langmuir, 2008. **24**(9): p. 4785-4790.

62. Balu, B., et al., *Tunability of the adhesion of water drops on a superhydrophobic paper surface via selective plasma etching*. Journal of Adhesion Science and Technology, 2009. **23**(2): p. 361-380.
63. Balu, B., et al., *Patterning of superhydrophobic paper to control the mobility of micro-liter drops for two-dimensional lab-on-paper applications*. Lab on a Chip, 2009. **9**(21): p. 3066-3075.
64. Jiang, L., et al., *Mechanical durability of liquid repellent coatings*. Surface & Coatings Technology, 2017. **328**: p. 182-191.
65. Stith, D., *The Tesla valve - A fluidic diode*. Physics Teacher, 2019. **57**(3): p. 201-201.
66. Truong, T.Q. and N.T. Nguyen, *Simulation and optimization of Tesla valves*. Nanotech 2003, Vol 1, 2003: p. 178-181.
67. Nguyen, Q.M., J. Abouezzi, and L. Ristroph, *Early turbulence and pulsatile flows enhance diodicity of Tesla's macrofluidic valve*. Nature Communications, 2021. **12**(1).
68. Johnson Michael, C. and V. Schultz Gary, *Papermaking felt having hydrophobic layer*. 2000, Appleton Mills: US.
69. Despault Marc, P. and S. Patterson Brady, *Press felt with improved dewatering capability*. 2006, AstenJohnson INC: US.
70. Despault Marc, P. and S. Patterson Brady, *Press felt with regenerated cellulosic scrim*. 2005, AstenJohnson INC: US.

71. Xu, J., R. Phillips, and D. Hedou, *The effect of press felt non-uniformity on sheet smoothness and dewatering*. J-for-Journal of Science & Technology for Forest Products and Processes, 2012. **2**(5): p. 6-11.
72. Diaz-Kotti, M., *Press felt with grooved fibers having improved dewatering characteristics*. 2001, Shakespeare CO: US.
73. Beck David, A., *Anti-rewet felt for use in a papermaking machine*. 2003, Voith paper patent GMBH: US.
74. Beck David, A., *Pressing apparatus having semipermeable membrane*. 2002, Voith Sulzer Papiertech patent: US.
75. Hansen Robert, A., *Anti-rewet press fabric*. 2004, Hansen Robert A.: US.
76. Girifalco, L.A. and R.J. Good, *A Theory for the estimation of surface and interfacial energies: Derivation and application to interfacial tension*. Journal of Physical Chemistry, 1957. **61**(7): p. 904-909.
77. Hansson, P.M., et al., *Robust hydrophobic surfaces displaying different surface roughness scales while maintaining the same wettability*. Langmuir, 2011. **27**(13): p. 8153-8159.
78. Olejnik, K., et al., *Optical measurement of the hydrophobic properties of paper products*. Measurement, 2018. **115**: p. 52-63.
79. Tang, Z.G., D.W. Hess, and V. Breedveld, *Fabrication of oleophobic paper with tunable hydrophilicity by treatment with non-fluorinated chemicals*. Journal of Materials Chemistry A, 2015. **3**(28): p. 14651-14660.

80. Schrader, M.E., *Young-Dupre revisited*. Langmuir, 1995. **11**(9): p. 3585-3589.
81. Farzaneh, M., et al., *Pore-Scale transport and two-phase fluid structures in fibrous porous layers: Application to fuel cells and beyond*. Transport in Porous Media, 2021. **136**(1): p. 245-270.
82. Karaman, M., et al., *Self-supporting superhydrophobic thin polymer sheets that mimic the nature's petal effect*. Applied Surface Science, 2012. **259**: p. 542-546.
83. Kim, A., C. Lee, and J. Kim, *Durable, scalable, and tunable omniphobicity on stainless steel mesh for separation of low surface tension liquid mixtures*. Surface & Coatings Technology, 2018. **344**: p. 394-401.
84. Mortazau, M. and K. Tajiri, *Liquid water breakthrough pressure through gas diffusion layer of proton exchange membrane fuel cell*. International Journal of Hydrogen Energy, 2014. **39**(17): p. 9409-9419.
85. Park, K.C., et al., *Optimal design of permeable fiber network structures for fog harvesting*. Langmuir, 2013. **29**(43): p. 13269-13277.
86. Su, C.L., et al., *Novel three-dimensional superhydrophobic and strength-enhanced electrospun membranes for long-term membrane distillation*. Separation and Purification Technology, 2017. **178**: p. 279-287.
87. Zhang, W.S., et al., *Structural design and environmental applications of electrospun nanofibers*. Composites Part A-Applied Science and Manufacturing, 2020. **137**.
88. Hensel, R., et al., *Wetting resistance at its topographical limit: The benefit of mushroom and serif T structures*. Langmuir, 2013. **29**(4): p. 1100-1112.

89. Jamali, M., H.V. Tafreshi, and B. Pourdeyhimi, *Penetration of liquid droplets into hydrophobic fibrous materials under enhanced gravity*. Journal of Applied Physics, 2019. **125**(14).
90. Jamali, M. and H.V. Tafreshi, *Studying droplet adhesion to fibers using the magnetic field: a review paper*. Experiments in Fluids, 2021. **62**(8).
91. Miao, D.Y., et al., *Continuous, spontaneous, and directional water transport in the trilayered fibrous membranes for functional moisture wicking textiles*. Small, 2018. **14**(32).
92. Tuteja, A., et al., *Designing superoleophobic surfaces*. Science, 2007. **318**(5856): p. 1618-1622.
93. Tuteja, A., et al., *Robust omniphobic surfaces*. Proceedings of the National Academy of Sciences of the United States of America, 2008. **105**(47): p. 18200-18205.
94. Young, *Philosophical Transactions of the Royal Society of London*. 1805: W. Bowyer and J. Nichols for Lockyer Davis, printer to the Royal Society.
95. de Laplace, P.S., *Traité de mécanique céleste*. 1805: Typ. Crapelet.
96. Gauss, C.F., *Principia generalia theoriae figurae fluidorum in statu aequilibrii*. 1830, Gottingae: Dieterichs. ii, 53 p.
97. Choi, W., et al., *Fabrics with tunable oleophobicity*. Advanced Materials, 2009. **21**(21): p. 2190-+.

98. Cottin, C., H. Bodiguel, and A. Colin, *Drainage in two-dimensional porous media: From capillary fingering to viscous flow*. Physical Review E, 2010. **82**(4).
99. Ferrand, L.A. and M.A. Celia, *The effect of heterogeneity on the drainage capillary-pressure saturation relation*. Water Resources Research, 1992. **28**(3): p. 859-870.
100. Rouquerol, J., et al., *Liquid intrusion and alternative methods for the characterization of macroporous materials (IUPAC Technical Report)*. Pure and Applied Chemistry, 2012. **84**(1): p. 107-136.
101. Cai, J.C., et al., *Generalized modeling of spontaneous imbibition based on Hagen-Poiseuille flow in tortuous capillaries with variably shaped apertures*. Langmuir, 2014. **30**(18): p. 5142-5151.
102. Zheng, Q.S., Y. Yu, and Z.H. Zhao, *Effects of hydraulic pressure on the stability and transition of wetting modes of superhydrophobic surfaces*. Langmuir, 2005. **21**(26): p. 12207-12212.
103. Moghadam, A., et al., *A new approach to modeling liquid intrusion in hydrophobic fibrous membranes with heterogeneous wettabilities*. Colloids and Surfaces a-Physicochemical and Engineering Aspects, 2018. **558**: p. 154-163.
104. Aaltosalmi, U., et al., *Numerical analysis of fluid flow through fibrous porous materials*. Journal of Pulp and Paper Science, 2004. **30**(9): p. 251-255.
105. Cimadoro, J., et al., *Wetting a superomniphobic porous system*. Soft Matter, 2019. **15**(42): p. 8621-8626.

106. Dodds, S., M. Carvalho, and S. Kumar, *Stretching liquid bridges with moving contact lines: The role of inertia*. Physics of Fluids, 2011. **23**(9).
107. Eggers, J., *Nonlinear dynamics and breakup of free-surface flows*. Reviews of Modern Physics, 1997. **69**(3): p. 865-929.
108. Rapp, B.E., *Chapter 23 - Plateau-Rayleigh instability, in microfluidics: Modelling, mechanics and mathematics*, B.E. Rapp, Editor. 2017, Elsevier: Oxford. p. 467-477.
109. Agraharam, S., et al., *Plasma chemistry in fluorocarbon film deposition from pentafluoroethane/argon mixtures*. Journal of Vacuum Science & Technology a- Vacuum Surfaces and Films, 1999. **17**(6): p. 3265-3271.
110. Jiang, L., et al., *Two-Step Process to create "roll-off" superamphiphobic paper Surfaces*. Acs Applied Materials & Interfaces, 2017. **9**(10): p. 9195-9203.
111. Jiang, L., et al., *Fabrication of highly amphiphobic paper using pulp debonder*. Cellulose, 2016. **23**(6): p. 3885-3899.
112. Jiang, L., et al., *Fabrication of non-fluorinated hydrophilic-oleophobic stainless steel mesh for oil-water separation*. Separation and Purification Technology, 2017. **184**: p. 394-403.
113. Ferain, E. and R. Legras, *Pore shape control in nanoporous particle track etched membrane*. Nuclear Instruments & Methods in Physics Research Section B-Beam Interactions with Materials and Atoms, 2001. **174**(1-2): p. 116-122.
114. Cassie, A.B.D. and S. Baxter, *Wettability of porous surfaces*. Transactions of the Faraday Society, 1944. **40**: p. 0546-0550.

115. Hubbe, M.A., et al., *Rate-limiting mechanisms of water removal during the formation, vacuum dewatering, and wet-pressing of paper webs: A review*. *Bioresources*, 2020. **15**(4): p. 9672-9755.
116. Dimic-Misic, K., et al., *Iso- and anisotropic etching of micro nanofibrillated cellulose films by sequential oxygen and nitrogen gas plasma exposure for tunable wettability on crystalline and amorphous regions*. *Materials*, 2021. **14**(13).
117. Li, L., V. Breedveld, and D.W. Hess, *Design and fabrication of superamphiphobic paper surfaces*. *ACS Applied Materials & Interfaces*, 2013. **5**(11): p. 5381-5386.
118. Li, L., et al., *Creation of low hysteresis superhydrophobic paper by deposition of hydrophilic diamond-like carbon films*. *Cellulose*, 2013. **20**(6): p. 3219-3226.
119. Gerullis, S., et al., *Plasma treatment of cellulose: investigation on molecular changes using spectroscopic methods and chemical derivatization*. *Cellulose*, 2022. **29**(13): p. 7163-7176.
120. Kolarova, K., et al., *Effect of plasma treatment on cellulose fiber*. *Cellulose*, 2013. **20**(2): p. 953-961.
121. Eid, K.F., M. Panth, and A.D. Sommers, *The physics of water droplets on surfaces: exploring the effects of roughness and surface chemistry*. *European Journal of Physics*, 2018. **39**(2).
122. Decker, E.L., et al., *Physics of contact angle measurement*. *Colloids and Surfaces a-Physicochemical and Engineering Aspects*, 1999. **156**(1-3): p. 177-189.

123. Gao, N. and Y.Y. Yan, *Modeling superhydrophobic contact angles and wetting transition*. Journal of Bionic Engineering, 2009. **6**(4): p. 335-340.
124. Hong, S.J., et al., *Droplet compression and relaxation by a superhydrophobic surface: Contact angle hysteresis*. Langmuir, 2012. **28**(13): p. 5606-5613.
125. Lam, C.N.C., et al., *Study of the advancing and receding contact angles: liquid sorption as a cause of contact angle hysteresis*. Advances in Colloid and Interface Science, 2002. **96**(1-3): p. 169-191.
126. Chen, H., T. Tang, and A. Amirfazli, *Liquid transfer mechanism between two surfaces and the role of contact angles*. Soft Matter, 2014. **10**(15): p. 2503-2507.
127. Chen, H.C., T. Tang, and A. Amirfazli, *Liquid Bridge and Drop Transfer between Surfaces*, in *Computational Methods for Complex Liquid-Fluid Interfaces*, M.T. Rahni, M. Karbaschi, and R. Miller, Editors. 2016. p. 453-465.
128. Weisstein, E.W., *Spherical Cap*. MathWorld. **Wolfram Online**.
129. Chen, H., et al., *How pinning and contact angle hysteresis govern quasi-static liquid drop transfer*. Soft Matter, 2016. **12**(7): p. 1998-2008.
130. Shi, D.L. and J.J. McCarthy, *Numerical simulation of liquid transfer between particles*. Powder Technology, 2008. **184**(1): p. 64-75.
131. De Souza, E.J., et al., *Capillary forces between chemically different substrates*. Langmuir, 2008. **24**(18): p. 10161-10168.

132. Kumar, S., *Liquid transfer in printing processes: Liquid bridges with moving contact lines*, in *Annual Review of Fluid Mechanics, Vol 47*, S.H. Davis and P. Moin, Editors. 2015. p. 67-94.
133. Al-Sharafi, A., et al., *Droplet stretching between hydrophobic and hydrophilic plates: Droplet fluid heating*. *International Communications in Heat and Mass Transfer*, 2021. **120**.
134. Akbari, A. and R.J. Hill, *Liquid-bridge stability and breakup on surfaces with contact-angle hysteresis*. *Soft Matter*, 2016. **12**(32): p. 6868-6882.
135. Chen, H., A. Amirfazli, and T. Tang, *Modeling liquid bridge between surfaces with contact angle hysteresis*. *Langmuir*, 2013. **29**(10): p. 3310-3319.
136. Li, L., V. Breedveld, and D.W. Hess, *Hysteresis controlled water droplet splitting on superhydrophobic paper*. *Colloid and Polymer Science*, 2013. **291**(2): p. 417-426.
137. Shi, Z., et al., *Dynamic contact angle hysteresis in liquid bridges*. *Colloids and Surfaces a-Physicochemical and Engineering Aspects*, 2018. **555**: p. 365-371.
138. Willett, C.D., et al., *Capillary bridges between two spherical bodies*. *Langmuir*, 2000. **16**(24): p. 9396-9405.
139. Wang, L.F., et al., *Capillary bridges and capillary forces between two axisymmetric power-law particles*. *Particuology*, 2016. **27**: p. 122-127.
140. Agarwal, P., et al., *Dynamic stretching of a liquid bridge*. *International Journal of Advances in Engineering Sciences and Applied Mathematics*, 2019. **11**(4): p. 238-243.

141. Bansch, E., C.P. Berg, and A. Ohlhoff, *Uniaxial extensional flows in liquid bridges*. Journal of Fluid Mechanics, 2004. **521**: p. 353-379.
142. Cabezas, G., et al., *Detection of liquid bridge contours and its applications*. Measurement Science and Technology, 2002. **13**(6): p. 829-835.
143. Montanero, J.M. and A. Ponce-Torres, *Review on the dynamics of isothermal liquid bridges*. Applied Mechanics Reviews, 2020. **72**(1).
144. Rabinovich, Y.I., et al., *Capillary forces between surfaces with nanoscale roughness*. Advances in Colloid and Interface Science, 2002. **96**(1-3): p. 213-230.
145. Zhao, J.Y., et al., *Study on stretching liquid bridges with symmetric and asymmetric surface wettability*. Physical Review Fluids, 2020. **5**(6).
146. Moghadam, A. and H.V. Tafreshi, *On liquid bridge adhesion to fibrous surfaces under normal and shear forces*. Colloids and Surfaces a-Physicochemical and Engineering Aspects, 2020. **589**.
147. Tsunazawa, Y., et al., *Contact force model including the liquid-bridge force for wet-particle simulation using the discrete element method*. Advanced Powder Technology, 2016. **27**(2): p. 652-660.
148. Yildirim, O.E. and O.A. Basaran, *Deformation and breakup of stretching bridges of Newtonian and sheer-thinning liquids: comparison of one- and two-dimensional models*. Chemical Engineering Science, 2001. **56**(1): p. 211-233.
149. Chen, Y.J. and P.H. Steen, *Dynamics of inviscid capillary breakup: Collapse and pinchoff of a film bridge*. Journal of Fluid Mechanics, 1997. **341**: p. 245-267.

150. Dodds, S., M.D. Carvalho, and S. Kumar, *Stretching and slipping of liquid bridges near plates and cavities*. Physics of Fluids, 2009. **21**(9).
151. Dodds, S., M.S. Carvalho, and S. Kumar, *The dynamics of three-dimensional liquid bridges with pinned and moving contact lines*. Journal of Fluid Mechanics, 2012. **707**: p. 521-540.
152. Dormann, M. and H.J. Schmid, *Distance-dependency of capillary bridges in thermodynamic equilibrium*. Powder Technology, 2017. **312**: p. 175-183.
153. Mehring, C., J. Xi, and W.A. Sirignano, *Dynamic stretching of a planar liquid bridge*. Physics of Fluids, 2004. **16**(3): p. 728-747.
154. Brulin, S., C. Tropea, and I.V. Roisman, *Pinch-off of a viscous liquid bridge stretched with high Reynolds numbers*. Colloids and Surfaces a-Physicochemical and Engineering Aspects, 2020. **587**.
155. Chen, H., T. Tang, and A. Amirfazli, *Fast liquid transfer between surfaces: Breakup of stretched liquid bridges*. Langmuir, 2015. **31**(42): p. 11470-11476.
156. Li, X.Q., et al., *Stretching and rupture of a viscous liquid bridge between two spherical particles*. Asia-Pacific Journal of Chemical Engineering, 2021. **16**(1).
157. Papageorgiou, D.T., *On the breakup of viscous-liquid threads*. Physics of Fluids, 1995. **7**(7): p. 1529-1544.
158. Chen, H., T. Tang, and A. Amirfazli, *Effects of surface wettability on fast liquid transfer*. Physics of Fluids, 2015. **27**(11).

159. Wu, J.T., M.S. Carvalho, and S. Kumar, *Effects of shear and extensional rheology on liquid transfer between two flat surfaces*. Journal of Non-Newtonian Fluid Mechanics, 2019. **274**.
160. Choi, W.T., et al., *Wettability control of stainless steel surfaces via evolution of intrinsic grain structures*. Journal of Materials Science, 2016. **51**(11): p. 5196-5206.
161. Zhang, J. and Y. Meng, *Stick–slip friction of stainless steel in sodium dodecyl sulfate aqueous solution in the boundary lubrication regime*. Tribology Letters, 2014. **56**.
162. Choi, W.T., et al., *Hydrophobicity and improved localized corrosion resistance of grain boundary etched stainless steel in chloride-containing environment*. Journal of the Electrochemical Society, 2017. **164**(2): p. C61-C65.
163. Jang, Y., et al., *Inhibition of bacterial adhesion on nanotextured stainless steel 316L by electrochemical etching*. ACS Biomaterials Science & Engineering, 2018. **4**(1): p. 90-97.
164. Kestin, J., M. Sokolov, and W.A. Wakeham, *Viscosity of liquid water in the range $-8\text{ }^{\circ}\text{C}$ to $150\text{ }^{\circ}\text{C}$* . Journal of Physical and Chemical Reference Data, 1978. **7**(3): p. 941-948.
165. Vogel, H., *The temperature dependence law of the viscosity of fluids*. Physikalische Zeitschrift, 1921. **22**: p. 645-646.
166. Vargaftik, N.B., B.N. Volkov, and L.D. Voljak, *International tables of the surface tension of water*. Moscow Aviation Institute, 1983.

167. Plateau, J.A.F., *Statique expérimentale et théorique des liquides soumis aux seules forces moléculaires*. 1873, Paris: Gauthier-Villars.
168. Rayleigh, L., *On the instability of jets*. Proceedings of the London Mathematical Society, 1878. **s1-10**(1): p. 4-13.
169. Qian, B.A. and K.S. Breuer, *The motion, stability and breakup of a stretching liquid bridge with a receding contact line*. Journal of Fluid Mechanics, 2011. **666**: p. 554-572.
170. Zandian, A., W.A. Sirignano, and F. Hussain. *Mechanisms of liquid stream breakup: Vortices and time and length scales*. 28th European Conference on Liquid Atomization and Spray Systems (ILASS). 2017.
171. Zhang, X., R.S. Padgett, and O.A. Basaran, *Nonlinear deformation and breakup of stretching liquid bridges*. Journal of Fluid Mechanics, 1996. **329**: p. 207-245.
172. Darabi, P., et al., *Modeling the evolution and rupture of stretching pendular liquid bridges*. Chemical Engineering Science, 2010. **65**(15): p. 4472-4483.
173. Eggers, J. and T.F. Dupont, *Drop formation in a one-dimensional approximation of the Navier-Stokes equation*. Journal of Fluid Mechanics, 1994. **262**: p. 205-221.
174. Zhang, X.G. and O.A. Basaran, *An experimental-study of dynamics of drop formation*. Physics of Fluids, 1995. **7**(6): p. 1184-1203.
175. McKinley, G.H. and T. Sridhar, *Filament-stretching rheometry of complex fluids*. Annual Review of Fluid Mechanics, 2002. **34**: p. 375-415.

176. Patterson, B. *Enhanced water removal pressing*. in *Annual meeting-Pulp and Paper Technical Association of Canada*. 2003.
177. Joyce, M.J., *Flow control within a press fabric using batt fiber fusion methods*. 2003, Google Patents.
178. Despault, M.P. and B.S. Patterson, *Press felt with improved dewatering capability*. 2006, Google Patents.
179. Gilfoil, W., *Smart Water Receiver for Use in the Wet Press Section of a Paper Machine*. 2005, Georgia Institute of Technology.